Alma Mater Studiorum · University of Bologna

School of Science
Department of Physics and Astronomy
Master Degree in Physics

Characterization of in-gap Electronic States in Two-Dimensional Single Crystal PEA_2PbBr_4 Perovskite for X-ray Detection

Supervisor:
Prof. Daniela Cavalcoli

Co-supervisors:
Dr. Giovanni Armaroli

Dr. Andrea Ciavatti

Dr. Lorenzo Maserati

Submitted by:
Vito Foderà

Academic Year 2021/2022

ABSTRACT

Hybrid Organic-Inorganic Halide Perovskites (HOIPs) include a large class of materials described with the general formula ABX_3, where A is an organic cation, B an inorganic cation and X an halide anion. HOIPs show excellent optoelectronic characteristics such as tunable band gap, high adsorption coefficient and great mobility lifetime. A subclass of these materials, the so-called two-dimensional (2D) layered HOIPs, have emerged as potential alternatives to traditional 3D analogs to enhance the stability and increase performance of perovskite devices, with particular regard in the area of ionizing radiation detectors, where these materials have reached truly remarkable milestones. One of the key challenges for future development of efficient and stable 2D perovskite X-ray detector is a complete understanding of the nature of defects that lead to the formation of deep states. Deep states act as non-radiative recombination centers for charge carriers and are one of the factors that most hinder the development of efficient 2D HOIPs-based X-ray detectors. In this work, deep states in PEA_2PbBr_4 were studied through Photo-Induced Current Transient Spectroscopy (PICTS), a highly sensitive spectroscopic technique capable of detecting the presence of deep states in highly resistive ohmic materials, and characterizing their activation energy, capture cross section and, under stringent conditions, the concentration of these states. The evolution of deep states in PEA_2PbBr_4 was evaluated after exposure of the material to high doses of ionizing radiation and during aging (one year). The data obtained allowed us to evaluate the contribution of ion migration in PEA_2PbBr_4. This work represents an important starting point for a better understanding of transport and recombination phenomena in 2D perovskites. To date, the PICTS technique applied to 2D perovskites has not yet been reported in the scientific literature.

Aristotle said a bunch of stuff that was wrong.
Galileo and Newton fixed things up.
Then Einstein broke everything again.
Now, we've basically got it all worked out, except for:
small stuff, big stuff, hot stuff, cold stuff,
fast stuff, heavy stuff, dark stuff, turbulence
and the concept of time.

— Zachary Weiner

CONTENTS

INTRODUCTION

Solid state direct X-ray detectors are critically important in a wide range of applications. The demand for increasingly sensitive, low cost, lightweight, large-area and flexible sensors has strongly increased in recent years. State-of-the-art of traditional inorganic materials, like Cadmium Zinc Telluride (CZT), show high X-ray stopping power due to their high atomic number and their density, however the possibility of these materials in large-area flexible applications is very low [1]. Organic semiconductors have appeared promising alternatives to traditional inorganic semiconductors, thanks to the enormous flexibility of these materials, however they show a low stopping power, restraining the detection of high-energy X-ray at low radiation doses [2]. The compromise between mechanical rigidity and high X-ray absorption therefore represents an interesting challenge to be faced for the development of new materials for X-ray detection.

In recent years, the research on new materials for direct X-ray detection has largely revolved around Hybrid Organic-Inorganic Halide Perovskites (HOIPs). HOIPs are proving to be a new generation of room temperature radiation detection materials thanks to their strong stopping power, high density, long diffusion carrier, defect tolerance and high mobility life-time product $\mu\tau$. Hybrid perovskites include a large class of different materials described with the general formula ABX_3, where A is an organic cation, B inorganic cation and X an halide anion. The main problem with HOIPs is their stability. HOIPs are extremely sensitive to environmental conditions and in the presence of humidity they degrade within days or even hours [3]. An alternative is provided by a subclass of these materials called *layered* or *two-dimensional* perovskites. We will refer to, for brevity, simply as 2D HOIPs.

2D HOIPs are a class of compounds that shared a peculiar crystal structure, in which one or more layers of inorganic material are superimposed on a layer of dielectric organic material. Their electronic structure is similar to a multiple quantum well. This structure gives these materials truly distinctive opto-electronic properties, making them excellent candidates in many technological applications. While traditional inorganic solid-state materials have been studied for decades and the charge transport properties and non-radiative recombination mechanisms are now well understood, very few literature studies refer to 2D HOIPs. The study of charge transport and the physical phenomena that lead to the formation of deep levels,

which can act as non-radiative recombination centers for charge carriers, are essential elements for increase efficiency in 2D HOIPs-based devices. The aim of my thesis work is to study deep levels that act as traps for charge carriers, through Photo-Induced Current Transient Spectroscopy (PICTS), a transient photocurrent measurement never applied in 2D HOIPs, that allows for deep states characterization in high resistivity materials.

In the present work, the material subject to study was PEA_2PbBr_4 which, in Hofstetter et al. [4] , proved to be one of the most stable materials to degradation among 2D perovskites. Traps states evolution under stressful events such as exposure to X-ray (the so-called Radiation Hardness) and also due to aging was evaluated. In support of these results, other charge transport characteristics were evaluated, such as the mobility life-time of the charge carriers and a preliminary study on the presence of ionic currents, a question currently much debated in the scientific literature, because it is considered at the basis of the degradation phenomena in 3D HOIPs. The following thesis work is divided into three parts. In the first part I present the theory underlying the physical events that characterize the phenomena of non-radiative recombination in the deep levels, I present the physical characteristics of HOIPs and the operating principles of an ionizing radiation detector, and how the efficiency of the latter is linked to recombination phenomena. The second part describes the main experimental techniques used during my work. From the synthesis of crystals, to the opto-electronic characterization and, with particular emphasis, the Photo-induced Current Transient Spectroscopy technique. In the third and last part I present the results of my work.

Part I

2D PEROVSKITES AS NOVEL MATERIAL FOR X-RAY DETECTION

Due to their peculiar optoelectronic properties, layered hybrid perovskites (2D HOIPs) are an interesting object of study in applications such as X-ray detectors. This family of perovskites, compared with 3D HOIPs, offers high resistance to crystal structure degradation. However, the transport and non-radiative recombination properties of charge carriers remain poorly understood within these materials.

1

DEFECT STATES IN A CRYSTAL LATTICE

The approach of physicists to the study of crystalline solids underwent major changes during the 20th century. The first effective model capable of describing the electrical properties of solids is due to Paul Drude, who in 1900 published a famous paper on the electrical properties of metals[5]. With contributions from J.J. Thomson and H. Lorentz, what is called Drude's model remains to this day the main classical reference model to the study of the electrical and optical properties of solids. In classical physics, a metal can be viewed as a gas of electrons confined within an isotropic, uniform atomic solid. The electrons are subject to thermal motion described by the Maxwell-Boltzmann statistic, and when an external potential difference is applied to the ends of, let's say, a conducting wire, drift motion occurs. In this drift motion, electrons collide with atomic ions from which a viscous motion ensues and from which it is possible to isolate a fundamental parameter of this model, namely "relaxation time", defined as the time elapsed between the collision of an electron with one atom and the other. Although we are now aware that the basic assumptions of Drude's model were fundamentally wrong, this model allows us to predict with good accuracy a whole range of opto-electronic properties of a wide variety of materials. This predictive ability is due, much to one's surprise, to a succession of errors in the estimation of certain physical quantities that incredibly offset each other by vanishing. Right away, however, it was clear that Drude's model was not sufficient to describe the physics of solids: the model could not explain the presence of positive charge carriers found in experiments, it failed in its predictions at low temperature, it could not explain why certain materials were conductors and others insulators, and it contradicted the experimental evidence for thermal transport phenomena.

The Drude's Model

Setting things right a bit was done by Arnold Sommerfeld, in 1927, with a paper that for the first time used the quantum approach to the study of the opto-electronic characteristics of solids[6]. Starting from the Schrodinger equation for free, non-interacting electrons and assuming that the underlying statistics were Fermi-Dirac statistics, Sommerfeld took solid-state physics to the next stage. In Drude's model, charge transport was due to a large number of slowly moving particles, but Sommerfeld's model showed a whole different picture: only a limited number of high-velocity particles, energetically distributed in a neighborhood of about $K_B T$ from the Fermi level, were responsible for charge transport. This approach solved some of the problems

The Sommerfeld's Model

of Drude's model regarding thermal phenomena, returned a more reasonable specific heat value, and worked almost always at low temperatures. He was still unable to explain, however, why there were materials in which the charge carriers were positive and what was the physical ingredient that made some materials conductors and others insulators. But it was not long before these problems were solved.

The Bloch's Theorem and the Semi-Classical Model

In 1928 Felix Bloch published his doctoral thesis on the *quantum theory of matter*. The basic assumption was quite simple: a crystalline solid can be schematized as a three-dimensional geometric structure that repeats itself in space. The electrons, then, while seen as not interacting with each other, cannot be defined as truly free, but are affected by a positive periodic potential given by the symmetrical and periodic arrangement of ions in space. By positing these boundary conditions, the wave functions that solve the Schrodinger equation are no longer mathematically described by planes waves, but by wave functions endowed with a periodicity determined by the crystalline potential. This, in a nutshell, is Bloch's Theorem. This model, characterized by particles with quantum behavior affected by classical potentials, is also called the semiclassical model. Unlike Drude's model where electrons move slowly, and Sommerfeld's model where they move at extremely high velocities, Bloch's electron velocity is defined by the periodic potential, which then determines their dynamics. This implies that the electron energy is no longer parabolic, as in the case of free electrons. From this fact emerges the most mind-blowing aspect of the semiclassical model: the electronic state is now characterized by the energy band in which the electron is located and the crystalline momentum. The electron is now confined to move within an energy band in phase space, barring scattering phenomena that result in its transition. Obviously there are as many bands as there are electrons in the material, but given the periodicity of the electron wave function it is possible to determine the global dynamics and properties of the system by studying the local properties of the smallest portion of the crystal that enjoys all the symmetry properties of the crystal lattice. This gives rise to what is known as the band theory or band structure of crystalline solids.

Now physics had a complete theory capable of describing electronic dynamics, predicting the presence of positive charge carriers called holes, correctly predicting the trend of specific heat, and explaining, thanks to band theory, not only the existence of insulating materials and conducting materials, but also predicting the existence of materials called semiconductors, the basis of all electronics and much of contemporary technology. Another extremely important result was the concept of effective mass: within the periodic potential, not only the velocity of the charge carrier, but also its mass is related

to the band, through the inverse of the second derivative of the energy tensor. Only one uncovered point remained: in a crystalline solid described as a periodic and infinite geometric lattice, the electron never undergoes scattering phenomena. In other words, the semiclassical model so far describes insulators as perfect insulators and conductors as perfect conductors (not to be confused with the concept of superconductor, which is not a perfect conductor but a perfect diamagnet). Not only does this fail to correctly describe some electrical properties of materials, but the model also fails to describe the mechanical properties of solids. What is missing is a handful of fundamental ingredients that differentiate real solids from their mathematical modeling.

1.1 DEFECT STATES ENERGY LEVEL

The underlying problem is easy to understand if we begin by noting the differences between a mathematical conceptualization of a crystalline material and a real crystal. First, a real crystal has finite dimensions. However, this fact, so glaring, can be overlooked when the dimensions of the material we are studying fall within ordinary everyday dimensions. Take, for example, a cube of any crystalline solid with an edge of one centimeter. Considering a lattice parameter of a few Å and a density of 10^{23} atoms per cm^3. It is easy to see that the edge contains around 10^8 atoms and the ratio of atoms in the bulk to atoms on the surface turns out to be about $1/10^8$. A whole other discussion would have to be opened when nano-structured materials are considered, but this is not the case here.

Knowing the crystalline defects to predict the physical behavior of condensed matter

What makes a material "real" and gives it many of the properties that do not naturally emerge from the band structure are precisely those conditions that interrupt the periodicity of the crystal structure. These features are commonly referred to as "crystalline defects" and can be divided into point, linear, surface and bulk defects. It is also easily demonstrated, for example, already from classical statistical mechanics, that a crystalline solid cannot exist in a thermodynamically stable configuration without a minimum amount of crystalline defects. I will not present the albeit easy demonstration of this fact, which can be found in any basic materials thermodynamics text [7]. The word "defect" is actually a misleading term. A defect is usually something inconvenient that needs to be removed. Here, actually, "defects" play a fundamental role in solid-state physics, and it is through the study, knowledge and engineering of them that contemporary technology thrives. In solid state physics, the study of defects plays such an important role that physicists define micro- and nanostructured materials as "the set of crystalline defects that characterize the properties of the micro- or nano-structure". Without necessarily having to bother with nanoscience, it has been clear for decades now

in *materials science* that it is precisely crystalline defects that characterize many properties of solids such as the hardness of steel, the thermal properties that make certain materials highly efficient insulators or that make rubies red and certain gems green. All this is due to the presence of defects in the crystal lattice. And it is precisely the knowledge and control of these crystalline defects that allows us to control the behavior of a material to have ever more efficient LEDs and solar cells, more powerful lasers and faster transistors.

Shallow and Deep energetic state due to lattice defects

Defects can be "puntual", like vacancies in the lattice that respect charge neutrality, such as Frenkel-type or Schottky-type defects. Or vacancies that are occupied by electrons. Or impurity atoms that replace atoms in the material hosting these impurities. When these impurity atoms are deliberately inserted into the material, this is called doping, a fundamental technique for modulating the opto-electronic properties of a semiconductor. It is beyond the scope of this thesis to go into more detail about the physical characteristics that distinguish the various crystalline defects. Those who are interested can delve deeper with any of the introductory books on solid-state physics[8]. Lattice defects relevant in the study of radiation detector properties are those defects that introduce charge-carrier-occupiable energy states within the energy gap of the semiconductor used as a detector. These states can be grouped into two categories: shallow state and deep state.

1.1.1 *Shallow states*

When the energy state due to the crystalline defect is near the valence band or the conduction band, it is called a shallow defect or shallow state. These states are usually due to point defects such as dopants and impurities . It is very easy to verify how the energy value of these defects is in the tens of meV range. Let's take a simple Hydrogenic model. We can write the quantized energy in the common way

$$E_n = -\frac{m_e e^4}{2(4\pi\epsilon_0\hbar)^2 n^2} = -13.6\,\frac{eV}{n^2},$$

where m_e is the electron mass, e is the elementary charge and n is a positive integer bigger then zero. By substituting m_e with the electron effective mass m^*, ϵ_0 with the dielectric constant of the semiconductor $\epsilon = \epsilon_0\epsilon_r$, with same simple algebra one can find that the ground state energy of a shallow state could be written as

$$E_1 = -13.6\,\frac{m^*}{m_e {\epsilon_r}^2},$$

and by putting $\frac{m^*}{m_e} \approx 1/10$, $\frac{1}{{\epsilon_r}^2} \approx 1/100$ that are common value for a wide range of semiconductor, one can easily find $E_1 \approx 10^{-2}$eV.

With the same approach we can see that the Bohr radius of a shallow impurity can be written as a function of hydrogen Bohr radius a_b:

$$a_S = -\frac{m_e a_b \epsilon_r}{m^*} \approx 100 a_b \approx 5\text{nm},$$

implying that shallow states are delocalized. To conclude, at common temperature shallow states are thermally inactive and delocalized, so do not constitute recombination centers for charge carriers and don't affect the properties and performance of radiation detectors[9]. Things change when energy states go deep into the band gap.

1.1.2 *Deep states*

As we will see shortly, unlike shallow states, deep states act as recombination centers for charge carriers, and are all the more efficient the closer they are to the Fermi level. It is for this reason that deep states are commonly called trap states. When a high energy photon reaches the sensitive part of a detector, a cascade of charge carriers occurs. These charge carriers will become a measurable current if and only if they can reach the electrodes. Trap states prevent this process, limiting the efficiency of the detector. There is no simple model to describe the effects of deep defects on crystal properties as we have seen for shallow states. What we do have, however, is a statistical approach developed complementarily and independently in 1952 by W.Schottky and W.T. Read[10] and R.N Hall[11] and takes the name of SRH model, from the initials of the three physicists.

The Schottky-Read-Hall Recombination Model

1.2 SRH MODEL FOR DEEP STATES

Let us imagine that we have a trap state with energy E_t falling within the band gap of a semiconductor, as shown in Figure 1. Only four

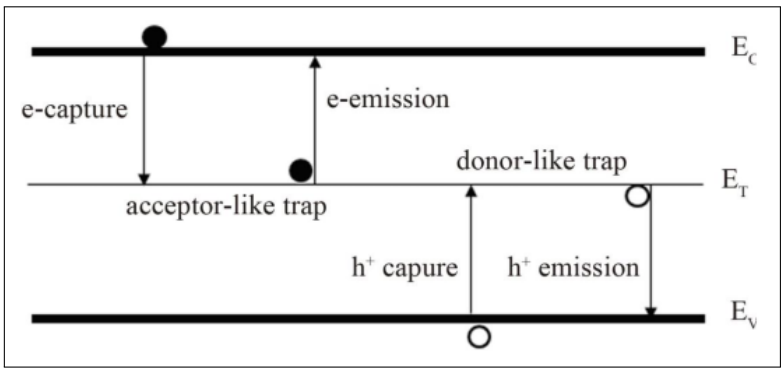

Figure 1: If a defect introduces an energy level E_t into the band gap, four physical processes can occur: capture or emission of an electron by the trap, capture or emission of a hole by the trap.

interaction processes are possible between the charge carriers and the trap. Capture of an electron by the trap, emission of an electron by the trap, capture of a hole by the trap, and emission of a hole by the trap. These processes can be represented mathematically through the following four equations:

$$\begin{aligned} C_e &= V_{thn}\sigma_n n N_t(1-f_t) \\ E_e &= e_n f_t N_t \\ C_p &= V_{thp}\sigma_p p N_t f_t \\ E_p &= e_p(f_t-1)N_t, \end{aligned} \tag{1}$$

where $V_{thn(p)}$ is the electron (hole) thermal velocity, $\sigma_{n(p)}$ is called *capture cross section* for electron (hole), $f_t = 1/(1+\exp(E_t - E_f))$ is the Fermi-Dirac statistics for the trap, $e_{n(p)}$ is the thermal emission rate for electron (hole) by the trap, $n(p)$ is the electron (hole) density and N_t is the trap density with energy E_t. These equations represent the probability of an electron to be captured or emitted by a trap and the probability of an hole to be captured and emitted by a trap, respectively. f_t represents the probability that a trap is occupied by an electron.

Written in this way, it is easy to see that the electron capture rate is directly proportional to the trap density, the electron density, and the probability that the trap is empty (which is equivalent to say that it is occupied by a hole). In contrast, for a hole the capture rate is proportional to the hole density, trap density and the probability that the trap is occupied by an electron. Necessarily, the trapping processes must depend on the thermal velocity of the charge carriers, since by their nature (related to Fermi-Dirac statistics) they are thermally activated phenomena. The capture process is characterized by a capture cross section, σ, analogous to the concept employed in nuclear physics. We will see later the importance of this parameter in determining the physical nature of the trap. Placing ourselves in a situation of thermodynamic equilibrium, $C_e = E_e$ and $C_p = E_p$ must hold, from which we get

$$\begin{aligned} V_{thn}\sigma_n n N_t(1-f_t) &= e_n f_t N_t \\ V_{thp}\sigma_p p N_t f_t &= e_p(f_t-1)N_t. \end{aligned} \tag{2}$$

Electron or Hole Thermal Emission Rate from a Trap State

From here, with some simple algebra we can extract the general formula for electron (hole) thermal emission rate

$$e_{n(p)} = V_{thn(p)}\sigma_{n(p)}N_{C(V)}\exp\left(\pm\frac{E_T - E_{C(V)}}{K_b T}\right) \tag{3}$$

with $N_{C(V)} = 2\left(\frac{m^*_{e(h)}K_b T}{2\pi\hbar}\right)$, where m^* is the effective mass. $N_{C(V)}$ is the electron (hole) density at the edge of the conductance (valence) band. Equation 3 is a very important equation that, as we will see in

the next chapters, is able to link theoretical model and experimental measurements in current transient spectroscopy. Let us now assume that we are very close to equilibrium and in a stationary condition in intrinsic semiconductor. This condition hold for low injection carrier and for $n = p$, so the intrinsic charge carrier density is ${n_i}^2 = np = n^2 = p^2$. The net recombination rate can be evaluated by assuming $V_{thn}\sigma_n = V_{thp}\sigma_p$. One find

Net Ricombination Rate for a Deep State

$$r_{Bi} = C_e - E_e = \frac{V_{th}\sigma N_T(pn - n_i^2)}{n + p + 2n_i \cosh\left[(E_T - E_F)/K_b T\right]} \tag{4}$$

where n_i is the intrinsic carrier concentration. It's easy to see that recombination rate have a minima for $pn = {n_i}^2$, so for intrinsic semiconductor and have a maximum when $E_T = E_F$. The closer a trap is located to the center of the band gap the higher the recombination rate will be. Let us now go into a little more detail. Let us place a p-type semiconductor (the same considerations can be made for a n-type semiconductor) in a low injection situation, that is, $n << p$ and $n_i << p$, and consider a trap placed very close to the fermi level such that the recombination rate is maximum. We can then rewrite

$$r_{Bi} \approx \frac{V_{th}\sigma N_T(pn - n_i^2)}{n + p + 2n_i} \approx \frac{V_{th}\sigma N_T(pn - n_i^2)}{p}.$$

In this condition, for slightly change from equilibrium, we can write charge carrier density as $p = p_0 + \delta p$ and for low injection $p \approx p_0$, ${n_i}^2 = n_0 p_0$ and recombination rate becomes

$$r_{Bi} \approx \frac{V_{th}\sigma N_T(p_0 n - p_0 n_0)}{p_0} = V_{th}\sigma N_T(n - n_0) = V_{th}\sigma N_T \Delta n = \frac{\Delta n}{\tau_n},$$

where we have defined *minority carrier lifetime*

Minority carrier lifetime

$$\tau_n = \frac{1}{V_{th}\sigma N_T} \tag{5}$$

For p-devices, minority carrier lifetime coincide with electrons lifetime, for n devices with hole. This is another very important result of SRH model: in a semiconductor, majority carrier are trapped by deep states and the limiting factor is the minority carrier lifetime. We just found a link between minority carrier lifetime, trap density and capture cross section.

1.3 THE LINK BETWEEN DEEP STATES AND MOBILITY-LIFETIME

We discussed how deep states act as traps for charge carriers and obtained a key time parameter, a limiting factor, that links recombination rate to capture cross section and trap density. Similarly, we reiterated in previous paragraphs that the performance of a direct radiation detector depends on the ability of charge carriers, created

in the crystal after interaction with photons, to reach the electrodes. To now, these two ways of looking at things seem independent of each other. In this section we will try to understand the connection between them. Since the limiting factor governing the recombination of charge carriers in a semiconductor is the lifetime of the minority carriers, let us imagine generating electrons in a p-type semiconductor and study their diffusion within the material. It doesn't matter how these minority carriers are generated: just assume we are applying optical excitation to the device with electromagnetic radiation of energy greater than the band gap. For simplicity we can imagine that the semiconductor has a cylindrical shape and that the injection of charge carriers occurs at one of the two ends, where we will place the zero of our reference system. We call Δn the charge created in $x = 0$. It's easy to see that we can consider $J = \frac{dn}{dt}$ as the diffusion flux along x axis, so we can simply write the first Fick's law as

First Flick's Law for Minority Charge Carrier

$$\frac{dn}{dt} = -D_n \frac{d\Delta n}{dx} \tag{6}$$

where

$$D_n = \frac{K_b T}{q} \mu_n$$

is the Nernst-Einstein equation for diffusion, where q is the charge, K_b the Boltzmann constant and μ_n the electronic mobility. If we consider small steps along x, that is from x and x+dx, and by placing $\frac{dn}{dt} = \frac{\Delta n}{\tau_n}$, we can rewrite the Fick's equation as

$$D_n \left(\left. \frac{d\Delta n}{dx} \right|_{x+dx} - \left. \frac{d\Delta n}{dx} \right|_{x} \right) = \frac{\Delta n}{\tau_n} dx$$

from wich we can write

$$D_n \frac{d^2 \Delta n}{dx^2} = \frac{\Delta n}{\tau_n}. \tag{7}$$

The solution of this equation is, considering a semi-infinite semiconductor

$$\Delta n = \Delta n(0) \exp\left(-\frac{X}{L_n}\right) \tag{8}$$

Diffusion Lenght for Minority Charge Carrier

where

$$L_n = \sqrt{D_n \tau_n} = \sqrt{\frac{K_b T}{q} \mu_n \tau_n}. \tag{9}$$

L_n is the diffusion length of minority charge carriers, which in turn is related to the lifetime of the carriers. The performance of a detector is closely related to this parameter, because it is an average index of the distance a charge carrier can travel before recombining. The factor within, $\mu\tau$, is called the mobility-lifetime of charge carriers and is an experimentally accessible parameter, as I will show in later chapters. We will see that mobility-lifetime is a key parameter in determining the performance of an ionizing radiation detector.

2

HYBRID ORGANIC-INORGANIC PEROVSKITES (HOIPS)

For decades, since the invention of the first diode and transistor in the 1950s, modern electronics has relied on semiconductor materials of an inorganic nature, such as silicon and germanium. Even today, industry and most of the technologies we use are still based on inorganic-type semiconductor materials. The current state of the art in X-ray commercial detectors is in fact based on inorganic semiconductors. But the scientific community of solid-state physicists and materials scientists have been studying the optical and transport properties of organic materials for some decades now. Specifically, over the past fifteen years there have been many papers investigating the properties of organic semiconductors as materials sensitive to ionizing radiation. It is an ever-evolving field that has achieved many successes in terms of devices with high detectivity and sensitivity, but also shows severe limitations mainly due to the limited stopping power of these materials. In a parallel manner, another type of material has been re-discovered in the last year: hybrid perovskites. I use the word re-discovered because there are strong indications that hybrid perovskites had already been synthesized in 1882, only to be forgotten [12] and to be re-discovered in 1978 [13]. Only in the last two decades, however, we finally understood the potentially application of hybrid perovskites. But let us go in order.

Inorganic, organic and hybrid material in contemporary technology

2.1 CONVENTIONAL HOIPS

There would be much to say about the vicissitudes that have distinguished the history of perovskites from their discovery to the central role they now play in a variety of solid-state physics fields, from the development of white-light LEDs to high-efficiency solar cells to radiation detectors. Their name is an honorific to Russian Count Lev Perovski given by German crystallographer Gustav Rose, who first discovered this particular mineral with the formula $CaTiO_3$ in the Ural Mountains in 1839[14] and to whom he wished to dedicate them. The perovskites constitute a variegated and numerous family of materials that share the same crystalline structure, with properties that range throughout the knowledge of solid state physics. A complete description of the entire family, all its physical properties and all its current applications would require a whole book. Below is a brief description of the main physical properties as a corollary of my thesis and which concern only the so-called hybrid halide perovskites.

Metal-Halide Hybrid Organic-Inorganic Perovskites (HOIPs)

2.1.1 *Crystal Structure*

In general today we refer to perovskites as the class of materials with chemical formula ABX_3 where A and B are two cations and X is an anion. The structure is typically cubic but as a function of temperature it tends to deform and solid-solid phase transitions can occur. It is usual to introduce two dimensionless factors to determine the structure of perovskites. These are the t-factor [15] [16] introduced by Goldschmidt in 1926 defined as

t and μ factor

$$t = \frac{r_A + r_X}{\sqrt{2}(r_B + r_X)}$$

where r_A and r_B and r_X are the atomic radii of components A,B and X, and the octahedral factor

$$\mu = r_B / r_X$$

which defines an additional parameter for establishing perovskite stability. The perovskites we refer to in this paper are commonly referred to as Metal-Halide Hybrid Organic-Inorganic Perovskites, commonly abbreviated as HOIPs. HOIPs are crystal structures that can occur with three-dimensional, two-dimensional, one-dimensional or zero-dimensional electronic degrees of freedom [17]. We can simply say that HOIPs can exists as bulk material, bidimensional-like material, nanowires and nanodots. Structures of the first type will have the label 3D in front of the initials, those of the second type 2D while the last two will not be discussed in this paper.

Crystal structure of 3D HOIPs

In Figure 2 is shown the geometrical structure of 3D HOIPs. Chemical species for cation B are organic molecule, A is a metal cation and X is an halide ions. The crystal structure is formed by a network of AX_6 octahedra, within which resides a type B cation, which share an X-type anion in the vertices. Eight of these octahedra enclose within the interstitial site, cuboctahedral in shape, an organic molecular cation B. The term hybrid will indicate the presence of organic and inorganic components in the same material. As we have already said, HOIPs represent a large family of materials that share the same crystalline structure. In literature [1][18], the most studied class of HOIPs have methylammonium or formamidinium in B-site. The most common cation in A-site are Pb, Sn and, possibly, other isovalent metals. The anion in X-site is an halide chosen between Cl, Br, I. For $t - \mathtt{factor}$ close to one we have an ideal cubic structure. In general ones have a stable cubic hybrid perovskite structure for $0.9 \leqslant t \leqslant 1$ and a distorted cubic structure for $0.7 \leqslant t \leqslant 0.9$. Stable halide-based perovskite compounds can form where $0.81 \leqslant t \leqslant 1.1$ and $0.44 \leqslant \mu \leqslant 0.9$ [17]. Figure 3 shows octahedral factor μ versus tolerance factor t.This graph illustrates the range of compositions sta-

bilized in the cubic perovskite structure for HOIPs. The yellow area shows the most stabilized cubic structure zone.

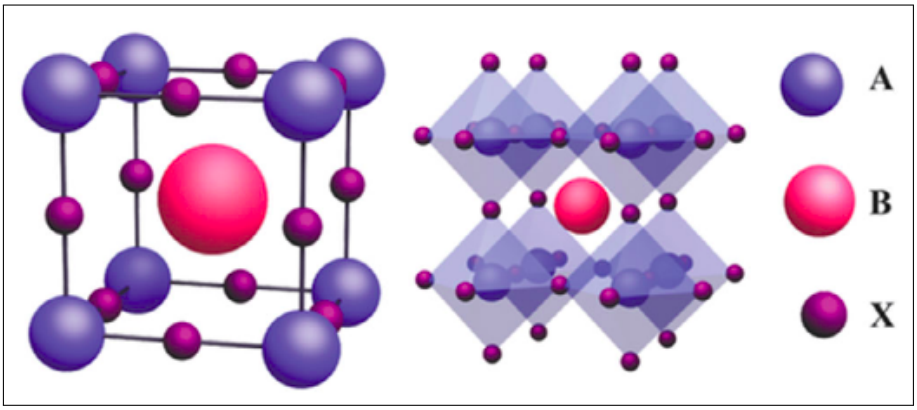

Figure 2: Unit cell of Hybrid Organic-Inorganic cubic perovskite crystal (left). Extended perovskite crystalline structure (right). From Maggiora et al.[19].

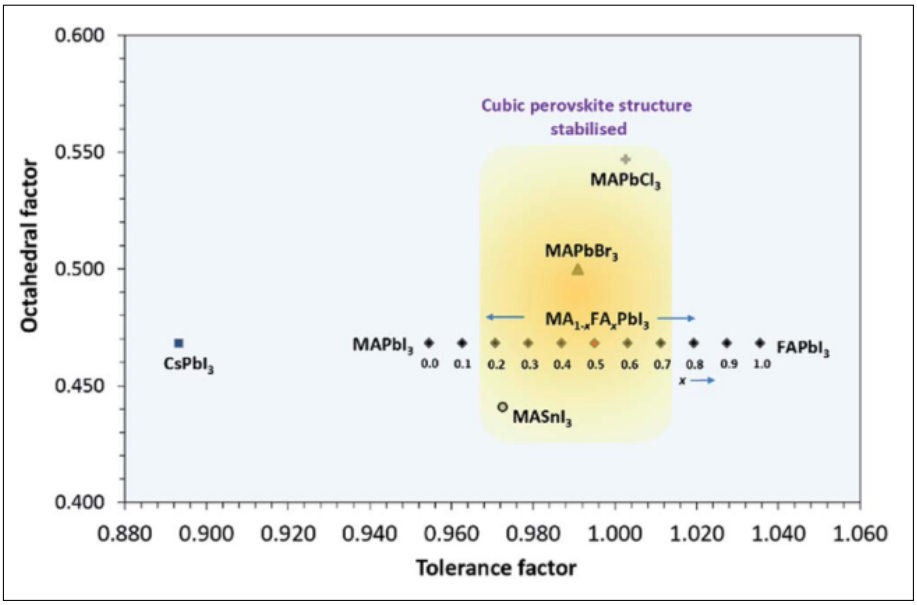

Figure 3: ν-factor vs t-factor: in yellow the range of stability in cubic structure[20]

2.1.2 *Transport and Optical Properties*

3D HOIPs are direct bandgap semiconductors. The absorption coefficient is in the order of $10^4 - 10^5 cm^{-1}$. A very interesting property of HOIPs is the possibility of extending the bandgap by simply creating a mixture of halides, for example $I_{3-x}Cl_x$, or by varing A, B and X atoms. Through this method it is possible to obtain a bandgap that extend optically from the near infrared to the near ultraviolet.

Single crystal OIHPs have the advantage of not presenting morphological disorder and grain boundaries. Carrier diffusion length is on the order of $10^1 - 10^2 \mu m$ and mobility on the order of $10^2 cm^2/Vs$ in single crystal, while in the polycrystalline material they are 1-2 orders of magnitude lower. These values differ slightly from study to study and the trend is that they are constantly increasing over time, a sign of the fact that the quality of the crystals made can be rapidly improved[21]. The resistivity of 3D HOIPs typically fluctuates around the value of $10^7 \Omega cm$, depending on its composition. There is some experimental evidence in the literature indicating that charge transport in 3D HOIPs is due to both electronic and ionic transport [22] [23].

2.1.3 *Critical Issues*

The problem of degradation

3D HOIPs are very unstable materials when exposed to normal environmental conditions and can degrade, losing their optical, mechanical, electrical and morphological characteristics, within days or even hours if exposed to environmental conditions where high humidity is present. Other factors such as exposure to heat, light, and electric fields also speed degradation [22]. This characteristic makes practical applications of this new family of materials difficult, although many advances have been made in recent years. Precautions such as encapsulation of the material to protect it from external conditions make it possible to extend its life, although we are still a long way from achieving the stability exhibited by inorganic semiconductors. This is one of the biggest challenges the scientific community is facing regarding 3D HOIPs. To date there is not a complete understanding regarding the physical factors at the root of this rapid degradation, but some work suggests that it is precisely the low ion activation energy that causes the easy migration of atoms and molecules that reassemble to create compounds that go on to define crystalline defects [23].

2.2 TWO-DIMENSIONAL HOIPS

The study of 2D perovskites immediately attracted attention because these systems can be considered natural multiple quantum wells in which the inorganic material acts as a potential well and the insulating organic layers act as potential barriers. The electron confinement occurs over subnanometric distances and induces the generation of stable room temperature excitons, with high binding energy and a Bohr radius that extends beyond the boundaries of individual layers. It seems that the stability of the exciton does not derive from the the dimensional boundary only, but organic layer plays an important role by modulating the dielectric properties of the material[24]. Even

more attractive is the stability of the physical properties shown by these materials compared to 3D HOIPs.

2.2.1 *Crystal Structure*

When the organic molecule inside the cage formed by the eight octahedral structures increases in size, the shape of 3D HOIPs deforms. When a RNH_3 structure is added to the organic molecule, that is, a large aliphatic or aromatic alkylammonium spacer cation (e.g., 2-phenylethylammonium (PEA) and n-butylammonium (n-BA)), the organic molecule causes the inorganic layers to split along the same direction but in opposite verses, perpendicular to the organic plane. What is obtained is a compound with chemical formula

$$(RNH_3)2A_{n-1}M_nX_{3n+1}.$$

In this formula A is a monovalent organic cation, typically $CH_3NH_3^+$ (i.e. MA^+) or $HC(NH_2)_2^+$ (i.e. FA^+), M is a divalent metal cation, X is a halide anion, and n = 1, 2, 3, 4... represents the number of octahedral layers $[MX^6]^{4-}$ within each quantum well [25]. In Figure 4 it is possible to observe the structure of these layered perovskites as n vary. From this point of view, a 3D HOIPs is nothing more than a layered structure with n tending to infinity. In 3D perovskites, each octahedral layer formed by $[MX_6]^{4-}$ is connected with six nearby halogen atoms. Conversely, 2D perovskite crystals can be considered as n layers of $[MX_6]^{4-}$ sandwiched octahedral sheets from two layers of large organic spacer cations, giving rise to natural multi-quantum-well structures, in which the inorganic plane act as potential "sinks" while the organic layers function as potential barriers. We are therefore faced not with a single material, but with a family of compounds

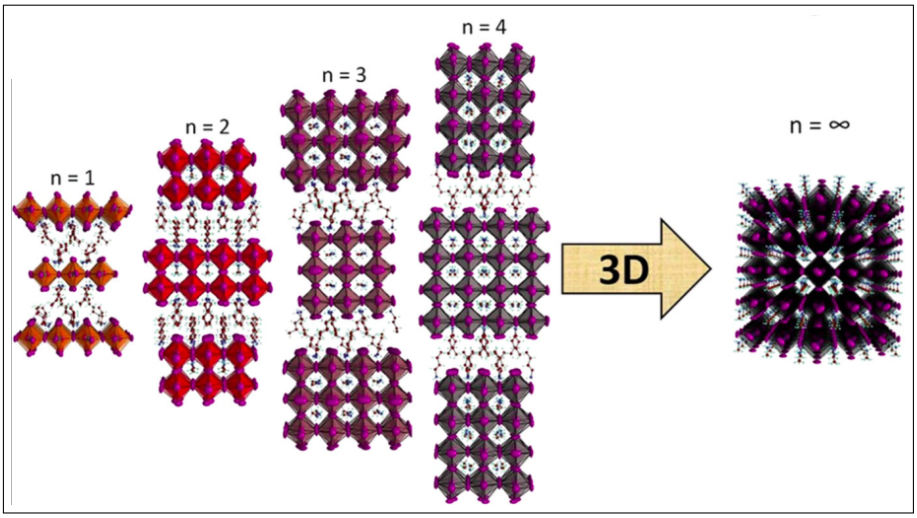

Figure 4: Crystal structures of layered perovskites, extending from n = 1 to n = ∞.[24]

that share the same crystalline structure. The adjective 2D, used very often in literature, is in fact wrong to describe these materials. We are not talking about spatially two-dimensional materials, such as graphene, but about three-dimensional materials where the electronic degrees of freedom are confined between organic layers. These layers can be close enough to each other that the confinement has quantum characteristics. When n is greater than one, it is usually referred to as quasi-2D perovskites. It would therefore be more correct to use the adjective *layered* perovskites. In order not to add heaviness to the debate, also in this work we will follow the nomenclature suggested by the literature and we will indicate these materials both as 2D or layered. The 2D HOIPs studied in this thesis is PEA_2PbBr_4, a layered perovskite with n = 1.

2.2.2 *Transport, Optical and Stability Properties*

The complex layered structure of 2D perovskites naturally self-assembles during the synthesis process. This structure, combined with the organic properties of the potential barrier, leads to the formation of stable excitonic states even at high temperatures. The possibility of being able to modify the variety of the organic molecule, of the metal and of the halogen, means that the band gap of these perovskites can be finely tuned in a wide range that goes from visible to ultraviolet. In 2D perovskite, ion migration can be suppressed by the interlayer cations [26], even if the debate is still open. Compared to traditional high-temperature-prepared inorganic semiconductors, 2D HOIPs can be prepared by solvent evaporation at room temperature, which creates few defects in crystals. In addition, 2D perovskites have low sensitive to defects, and are therefore a good candidate for high performance photodetectors with high reactivity and low dark current. Because of excellent stability and exceptional optoelectronic properties, 2D layered perovskites performed better in photodetectors than their 3D counterparts [27]. The photoluminescence quantum efficiency makes 2D perovskites excellent candidates not only as X and γ ray detectors, but also as active components in photovoltaic cells and white light LEDs [28]. The biggest problem when we talk about 3D perovskites is their poor stability and easy deterioration [29] [30]. 2D perovskites, on the other hand, show great stability, in comparison. Stability with respect to humid environments, with respect to large electric fields, with respect to light, aging, vacuum and ionizing radiation [31] [32] [4]. The presence of large organic molecules in the crystal structure also offers stability with respect to phase transitions, which instead often occur in 3D HOIPs as solid-solid transitions [33].

3

X-RAY DETECTOR

It is a common feeling among physicists not to worry about the usefulness of the object of their study. Whether they are theoretical or experimental physicists, the history of physics is peppered with amusing anecdotes about it. Perhaps the most famous anecdote concerns Michael Faraday, one of the most famous experimental physicist of the 19th century, who, seeking funding from the British government, invited the then crown minister of finance to visit his laboratory, at that time one of the world's technological jewel. Bewildered, the minister asked him "but what is it exactly the object of your studies?" and Faraday unhesitatingly replied "I don't know, but I'll bet you can put a tax on it someday". Another amusing anecdote concerns Heinrich Hertz, who in 1886 congenized an experiment that led to the experimental demonstration of the existence of electromagnetic waves that a few years earlier were theorized by James Clerk Maxwell. Pressed by the press, when asked what the technological implications of his discovery were, he reply dryly "It's of no use whatsoever".

The dicovery of X-rays

These just described, of course, are simple more than little stories that professors pass on to physics students or that can be read in some famous popular science texts. The reality of things is obviously very different. Among the most mind-blowing counter examples of how research in basic physics has revolutionized the technological scenario and influenced dozens of other disciplines in a very few year, a post of honor belongs to Wilhelm Conrad Röntgen with the discovery of X-rays. In November 1895, while accelerating electrons inside prototypes of what would shortly become cathode ray tubes, the physicist noticed that a fluorescent screen placed far away and not aligned with the produced electron beam glowed faintly. Within a month, Röntgen presented a paper to the then nascent medical physics community his work on what he called X-rays, where he showed the first X-ray-image in history, that of his wife's hand, who lent herself as a test subject. Within a few months, the first radiology departments and diagnostic imaging medicine were born. Today, a little more than a century later, x-rays are being used in a very wide variety of applications, so wide that it would take a separate thesis just to describe their vast use: from medicine, restoration, industrial applications, civilian security systems, military applications, basic sciences, astrophysics, materials study, just to list a few. This implies constant and increasing research in x-ray-sensitive materials to create increasingly sensitive and high-performance detectors.

3.1 HOW A SOLID STATE X-RAY DETECTOR WORKS

The physical mechanism behind a solid-state X-ray detector is very simple to understand. When a high-energy photon interacts with the sensitive material of which the detector is made, the photon energy is transmitted to the crystal, which generates a response that can be electrical (a current or potential difference at its ends) or optical. The former are called direct detectors and the latter indirect detectors.

Direct X-rays detectors

In a direct X-ray detector, the high-energy photon interacts with the sensitive material, creating a response that results in either a current pulse (current mode operator) or a potential difference (voltage mode operator). Since the physical process is the same, we will consider detectors of the first type. When the photon interacts with the crystal, it generates an high-energy electron, which in turn interacts with the surrounding creating a cascade of electron-hole pairs through photoelectric effect and Compton scattering phenomena. If a potential difference is placed at the ends of the crystal, the charge carriers separate and go toward the electrodes, generating a current. The intensity of this current depends on a variety of factors, of which I will list the most important ones [34].

Some important figures of merit for X-rays detectors

STOPPING POWER: To protect ourselves from ionizing radiation, we typically use lead plates, because we know that the higher the atomic density of the material that the radiation has to pass through, the greater the stopping power. This simple observation is also valid when we talk about X-rays detectors. The radiation-sensitive material must be strongly interacting with the high-energy photons in order for it to have good sensitivity. The intensity pattern of a radiation flux within a material can be expressed as

$$I = I_0 e^{-\mu_c l}$$

where μ_c is the linear attenuation coefficient. μ_c is related to the mass coefficient α and the density material ρ by the simple relation $\mu_c = \alpha\rho$. So, efficient X-rays detector material have high mass coefficient and high density.

MOBILITY-LIFETIME: mobility lifetime $\mu\tau$, which characterize the carrier drift length and describe the capability to extract the charge from detector crystal, and therefore the capability to have a strong signal. Larger the $\mu\tau$ product, better the charge collection efficiency. In Section 1.3 I demonstrated the relation between $\mu\tau$ parameters and sensing-material crystal defects. In

fact, we saw that there is a relation between the diffusion length of generated charge carrier and the $\mu\tau$ product:

$$L_D = \sqrt{\frac{K_B T}{q}\mu\tau},$$

where K_B is the Boltzmann constant, T is the temperature, q the charge of the carrier, μ the mobility and τ the carrier lifetime. L_D is a length expressing the average path taken by a charge carrier before being recombined. Obviously, the higher the value of L_D, the greater the fraction of generated charge carriers that will reach the electrodes.

DARK CURRENT: Dark current is the current flowing at the ends of a semiconductor, given a potential difference, in the complete absence of incident radiation. It is apparent that a good X-ray detector should have the lowest possible dark current. If, as we have said, a detector is a transducer that transforms the energy of incident photons into a current, the presence of a current in the absence of photons actually constitutes a source of noise. It is not possible to completely eliminate the dark current, but the search for materials with very low dark current is crucial in the development of increasingly high-performance devices.

In general, the parameters described so far are not the only ones that can be found in the literature, but they are considered among the most important. Specifically, they are also those that were evaluated in the course of this experimental work.

Indirect X-ray detectors

In an indirect X-ray detector, the absorbed photon generates a cascade of events leading to the re-emission, by the detector itself, of photons at lower energy than the absorbed one, usually in the visible or ultraviolet range, which are subsequently in turn detected by a photodiode. These device are called *scintillators* and are widely used in a very vast variety of fields. Many figures of merit of scintillators are shared with those described in the section on direct detectors, but much more would be said for this type of device. The core of the research of the team with which I have had the pleasure to work with at the Department of Physics at the University of Bologna - the Semiconductor Group- concerns the study of novel materials for direct X-rays detectors, so I will not dwell further in describing in detail how scintillators work. Just know that there exist.

3.2 DEEP STATES AS LIMITING FACTOR IN X-RAY DETECTION

At the end of this long discussion on deep states, their role as recombination centers, and the link between defects and the diffusion length of charge carriers, it should now be easy to understand how these energy states are closely related to the performance of any radiation detection device, and specifically for X radiation. To further emphasize the causal link, let us look at Figure 5. As I have already pointed out in the section on the operation of X-rays detectors, when a high-energy photon interacts with the crystal it triggers a succession of physical events that leads to the creation of a number of electron-hole pairs. If a potential difference is present at the ends of the device, the pairs separate and begin their journey to the electrodes. If we were to consider the material as an ideal crystal, along their path the charge carriers would encounter no crystalline defect, hence no strongly localized deep state acting on the charge carrier as a non-radiative recombination center.

All charges, in essence, would reach the electrodes. However, the efficiency of the device would not be equal to one. First, not all high-energy photons would interact with the crystal. We have seen that this depends on the density of the sensing material and the atomic mass number. In addition, some of the photon energy would inevitably go to excite phonon states. Nevertheless, these unavoidable effects contribute only partially to determining the efficiency of our detector. It is the unavoidable presence of the crystalline defects that disturbs the path of the charge carriers.

When the carriers, say electrons for simplicity, encounter a deep state, they interact with it and have a certain probability of recombining and not reaching the electrodes. This results in a final current that is only a fraction of what was initially generated by the cascade of electron-hole pairs. With this last explanation we can close the first part of this thesis. I hope the reader is now well aware of the role that deep states play in limiting the performance of a radiation detector. The study and characterization of deep states is only the first step. This information, in many cases, allows techniques to be used to limit or passivate the effect that these recombination centers have on charge carriers, enabling the creation of increasingly sensitive and high-performance devices.
The study of deep states and recombination phenomena has practical implications that many times escape even to physicists that works in different branches. Suffice it to bring up the example of the efforts of the scientific community of solid-state physicists to develop increasingly efficient LEDs, which led to the 2014 Nobel Prize win by Isamu Akasaki, Hiroshi Amano and Shūji Nakamura "for the invention of

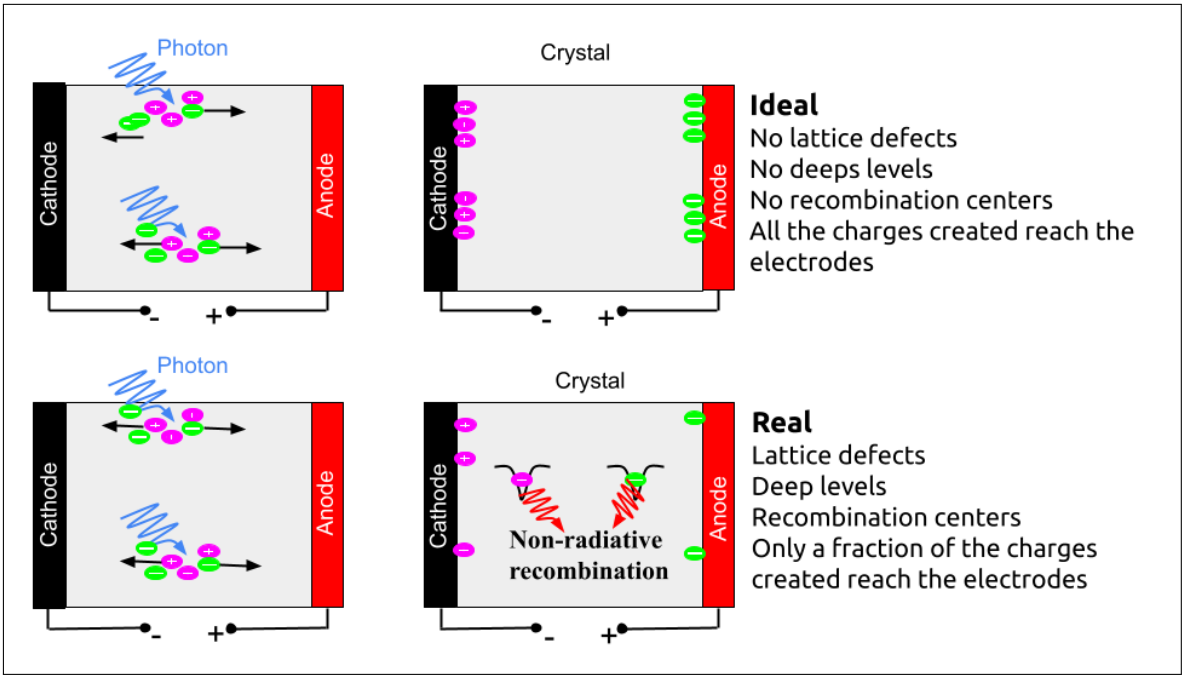

Figure 5: The deep states act as non-radiative recombination centers, affecting the efficiency of radiation detection devices.

the high-efficiency blue LED, which made possible the production of energy-saving white light sources". It is therefore no exaggeration to say that the study of crystal defects and recombination phenomena has very important implications for everyday life, often in ways that are difficult to predict.

Part II

METHODS AND EXPERIMENTAL TECHNIQUES

Photo-Induced Current Transient Spectroscopy (PICTS) is the technique of choice for studying deep states in highly resistive ohmic materials. Combined with the study of temperature-dependent resistivity and mobility life-time measurements, these techniques offer a fairly complete picture that can describe transport and recombination phenomena in 2D HOIPs

4

SINGLE CRYSTAL GROWTH TECHNIQUES

4.1 PEA_2PbBr_4 SYNTHESIS

The synthesis of PEA_2PbBr_4 follows a simple slow and controlled evaporation process. Starting from the precursors PEABr and $PbBr_2$ the following stoichiometric formula is obtained:

$$2PEABr + PbBr_2 \longrightarrow PEA_2PbBr_4 \tag{10}$$

The precursors are then mixed in the right stechimetric proportions and dissolved in DMF (N,N-Dimethylformamide). Solutes and solvents are combined to form a 1.3 molar solution (slightly above the supersaturation value of the solute in the solvent), and remains overnight in a closed container inside which a stirrer is inserted which mixes the liquid. Then the solution is passed through special 0.22 μm filters and placed in a beaker. The beaker is covered with a waxy film to which four holes with a diameter of about one millimeter are made. On the one hand, this process reduces any impurities that can act as nucleation centers and on the other hand reduces the evaporation rate. The driving force of the seeded growth from a solution is the supersaturation state of the solute in the solvent, which can be achieved by solvent evaporation. The success of the synthesis process depends mainly on the speed with which the solution evaporates, which must be as slow as possible. The solution is left to rest in the beaker, for a period during which the evaporation of the solvent causes the molarity to drop below the saturation threshold. After about three weeks, nucleation phenomena occur which lead to the formation of crystals with an approximately rectangular shape with sides ranging from a few millimeters to about one centimeter. This process can be expressed through the steady-state nucleation growth rate at the crystal surface [35]

$$J = \Gamma^* \exp\left(-\frac{\Delta G}{K_b T}\right) \tag{11}$$

where Γ^* is a pre-exponential term that vary very weak compared with the exponential term, ΔG is the Gibbs free energy change for the nucleus formation, K_b is the Boltzmann constant and T is the temperature. According to the equation, there is a critical supersaturation level, below which the nucleation rate is practically zero and beyond which it increases sharply.

5

TRANSIENT SPECTROSCOPY

5.1 GENERAL ASPECTS

In the first chapter I show how deep states act as recombination centers for charge carriers and how these are all the more efficient at acting as traps the closer the state is to the middle of the band gap. We started by making the assumption that if a trap state is present, then only four interaction processes are possible between the trap and the charge carriers (capture or emission of an electron and capture or emission of a hole). We have easily extracted an equation, Equation 3, which relates the emission rate of charge carriers by a trap state, with the capture cross section of the trap itself and its activation energy. Many simplifications have been made in the form presented there, which in any case do not invalidate the model. But let's go a little further and find a more complete formulation. We first assumed that each deep state can only trap one charge carrier, but this is an understatement. In reality we must bear in mind the possibility of degenerate states. Furthermore, we assumed that the capture cross section was a constant that intrinsically depends only on the physical characteristics of the trap itself. While this latter observation continues to hold true, experience shows that capture cross section could be actually highly temperature dependent, of the form of

$$\sigma_T = \sigma_\infty exp\left(-\frac{\Delta E_\sigma}{K_b T}\right). \tag{12}$$

It is therefore usual, in literature [36] [37], to find the emission probability rate write as

$$e_i(T) = \gamma T^2 \sigma_{ia} exp\left(-\frac{E_{ia}}{K_b T}\right) \tag{13}$$

where i = n for electron and i = p for hole, $\sigma_{ia} = (g_0/g_1)\sigma_\infty$ is the so called electron/hole apparent capture cross section, with g_0 and g_1 respectively empty trap energy degeneracy and occupied trap energy degeneracy; K_b is the Boltzmann constant, T is the temperature, E_{ia} is the apparent trap activation energy, γ is a constant of the form

$$\gamma = 2\sqrt{3} M_c (2\pi)^{\frac{3}{2}} K_b{}^2 m^* h^{-3}$$

with M_c the number of conduction band minima for electrons and the number of valence band maximum for holes, m^* is the effective mass and h is the Planck constant. γ can be easily calculated once the band structure of the material is known. Often these data are readily

available in the literature from experiments or ab initio calculations, as in the case of the present work. At this point one can say that we aren't able to extract the correct value for energy activation and capture cross section, but with the help of some thermodynamic concepts we can correct interpreted them. Let us start with an important observation: the band gap and the Fermi level are not constant but are a function of temperature. In a constant temperature experiment we would have no problem but we are talking about thermally activated phenomena and the techniques we are discussing are thermal spectroscopies. Let's go back to equation 3 and review it from another point of view.

Since, by definition, the energy gap of a semiconductor is the sum of the chemical potentials necessary for the formation of an electron hole pair [38], in the same way we can define the energy level of a defect as the difference in chemical potential for the formation of a free charge carrier and an ionized defect [39]. Recalling that the chemical potential is closely related to Gibbs free energy, it is possible to rewrite equation 3 as [40] (for simplicity I use notation for electron, but the same dissertation is valid for hole):

$$e_n(T) = \langle \nu_n(T) \rangle \sigma_n(T) N_C(T) exp\left(-\frac{\Delta G(T)}{K_b T}\right) \tag{14}$$

where $\langle \nu_n(T) \rangle$ is the average thermal velocity of the carrier and $\Delta G(T)$ is the Gibbs free energy. All the quantity involved are function of temperature, as one aspect. $\Delta G(T)$ must be equal to the separation of the energy level of the state from the appropriate band edge at each temperature, so we can write that $\Delta G(T) = E_C(T) - E_t(T)$. Remembering that for definition $\Delta G(T) = \Delta H - T\Delta S$, Equation 14 become

$$e_n(T) = \chi_n \langle \nu_n(T) \rangle \sigma_n(T) N_C(T) exp\left(-\frac{\Delta H}{K_b T}\right), \tag{15}$$

where $\chi_n = \exp(\Delta S/K_b)$. Returning to the definition of the capture cross section given by Equation 12 we can finally write

$$e_n(T) = \chi_n \sigma_\infty \langle \nu_n(T) \rangle \sigma_n(T) N_C(T) exp\left(-\frac{\Delta H + E_\sigma}{K_b T}\right) \tag{16}$$

and comparing this with the Equation 14 for the trap signature we see that the apparent activation energy of $e_n T^{-2}$, E_{na}, and the apparent capture cross section, σ_{na}, represent the quantities

$$E_{na} = \Delta H + E_\sigma$$

and

$$\sigma_{na} = \chi_n \sigma_\infty.$$

By making explicit the temperature dependence of $N_c(T)$ and $\langle \nu_n(T) \rangle$ we find the form of Equation 13. We have just seen that the activation energy of the thermal emission rate is not necessarily equal to the energy separation of the trap from the edge band and the same can be said of the capture cross section. These are parameters that represent a fingerprint of the defects of a material, although sometimes you have to be content with extracting the apparent values. Usually the question is overcome by combining different spectroscopic techniques and finally merging all the data. These are processes that involve different study groups and require years of work. In this thesis, given the practically absence of literature concerning the deep defects in $(PEA)_2PbBr_4$, it was not possible to have the amount of data necessary to uniquely define the energies and the capture cross section. The data that we will see, therefore, must be taken as apparent values of the parameters in question. This nevertheless makes the presented results less important in understanding the phenomena of recombination in 2D perovskites. It is a first, necessary, step.

Thermodynamically, the activation energy is an enthalpy while the energy level $(E_c - E_t)$ is a Gibbs free energy. They differ in the amount of $T\Delta S$, where ΔS is the change in total entropy. These differences can be important when describing the properties of a deep state and one must be adopted the correct terminology, in particular to make a clear distinction between an activation emission energy and the energy level of the trap. The energy level can be temperature dependent and can only be calculated by combining measurements of $e_n(T)$ and $\chi_n(T)$, or it can be measured in an optical experiment at a fixed temperature. However, the activation energy retains its significance as a quantity that characterizes the trap signature. The differences between the activation energy and the energy level (Ec - Et) can be even greater if the the capture cross section depends on the temperature and it is often difficult to understand how much these values differ.

Let us now consider a semiconductor in which there are N_t deep states, of which n_t are occupied. Imagine that through a certain physical process, be it optical or electrical, n free electrons are generated with a thermal velocity $\langle v_n \rangle$. Keeping in mind the Equation 1, we can write a completely general formula that describes the net rate of change of electron occupancy:

$$\frac{dn_t}{dt} = (c_n + e_p)(N_t - n_t) - (e_n + c_p)n_t, \tag{17}$$

i.e., the variation in occupied traps depends on the difference between the probability of electron capture (or similarly hole emission) by an empty trap and electron emission (or similarly hole capture) by an occupied trap. $e_n(p)$ is the electron (hole) thermal emission rate we found in Equation 3. For now, we doesn't matter of the mathematical

form of $c_{n(p)}$. Simply keep in mind it is the electron (hole) capture rate probability. Assuming $c_n + e_p = a$ and $e_n + c_p = b$ and assuming that at time $t = 0$, $n_t = n_t(0)$ is valid; then we can write the solution of the differential equation above as:

$$n_t(t) = \frac{a}{a+b}N_t - \left(\frac{a}{a+b}N_t - n_t(0)\right)\exp\left(-(a+b)t\right) \tag{18}$$

In the case of steady state, $\frac{dn_t}{dt} = 0$ hold and solution for $t = \infty$ become

$$n_t(t) = \frac{a}{a+b}N_t = n_t(\infty) \tag{19}$$

and Equation 17 could be written as

$$n_t(t) = n_t(\infty) - [n_t(\infty) - n_t(0)]\exp\left(t/\tau\right) \tag{20}$$

where $\tau = (a+b) = e_n + c_n + e_p + c_p$. Equation 20 tell us that if the occupancy is momentarily perturbed it then relaxes exponentially to the steady state occupancy with a rate constant (a + b) which is the sum of the rates of all the operative processes both emission and capture. The initial occupancy is usually set by the experimental conditions, though there are two situations in particular which are frequently encountered: when the state is initially fully occupied ($n_t = N_t$) or completely empty ($n_t = 0$). For our purpose, we consider only the former. In the presence of an optical or electrical excitation that generates as minority charge carrier electron, for example, the return to equilibrium implies a rate emission of electrons from the traps that can be described as:

$$\frac{dn_t}{dt} = -e_n n_t(t), \tag{21}$$

which solution can be simplified to

$$n_t(t) = n_t(0)e^{-e_n t}, \tag{22}$$

The same consideration could be done for hole. Therefore, as I sad in Section 1.1.2, the electron (hole) emission thermal rate turns out to be a fundamental physical quantity for studying the deep states in a semiconductor material. It is a theoretical quantity that gives us access to the capture cross section and the activation energy of the trap. The purpose of transient spectroscopy is to find a link between measurable physical quantity, let's say a current, with the emission probability rate. There are many transient spectroscopy techniques. Each of these techniques tries to link the thermal emission rate to a measurable macroscopic physical quantity such as capacitance, impedance, current and more. I don't want to go into detail in this text. For further information I recommend the text by P. Blood and J.W.Orton [9].

We can just say that these techniques are mainly divided into two categories: techniques applicable to semiconductor with a depleted region and techniques applicable to semiconductor without a depleted region. In the first case, probably the most used technique is the Deep Level Transient Spectroscopy DLTS. This technique is able to link capacitive transients (measurable) to the thermal emission rate of the traps, and through an elaborate data analysis is able to return the activation energy, the capture cross section and the density of the traps of a semiconductor. This technique is extremely useful when the sample being analyzed is a pn or Schottky junction and you can have access to a depletion zone. On the other hand, when dealing with highly resistive materials and in the presence of an ohmic junction, DLTS cannot be used and it is preferred to adopt another technique called Photo-Induced Current Transient Spectroscopy PICTS

5.2 PHOTO-INDUCED CURRENT TRANSIENT SPECTROSCOPY PICTS

A PICTS experiment can be summarized with the following two steps: charge carriers are produced through an optical excitation and fill the traps; the optical excitation is switched off and the transient of the electric current is measured, which carries with it information about the thermal emission from the traps. These two steps are repeated during a temperature scan. The acquired signal is therefore a collection of current transients as a function of temperature. Subsequently, through an elaborate data analysis, it is possible to experimentally access the thermal emission rate e_n (or e_p for hole), and therefore measure the capture cross section, the activation energy and, possibly, the concentration for each trap present in the material. This last point is much debated in the literature and one must be very careful with the interpretation of the data.

5.2.1 *Filling the traps*

The rate of creation of electron-hole pairs due to the optical excitation of a semiconductor with an electromagnetic radiation of energy greater than the band gap depends on the absorbed flux and by the absorption coefficient of the semiconductor and can be expressed as:

$$G(x) = (1 - R)\alpha(\nu)\Phi_0 e^{-\alpha(\nu)x} \tag{23}$$

where R is the reflectivity, $\alpha(\nu)$ is the absorption coefficient, Φ_0 is the incoming flux and obviously we are considering an electromagnetic wave moving on the x axis. We have already derived a formula describing the diffusion of charge carriers in a medium, equation 7. In that case the charge carriers were created at the time $t = 0$ and then the external excitation was turned off. If we consider instead the ma-

terial exposed to a continuous flow of photons the equation can be modified as

$$D_n \frac{d^2 \Delta n}{dx^2} - \frac{\Delta n}{\tau_n} = G(x). \tag{24}$$

For high resistivity material $\Delta n \gg n_0$ and $\Delta p \gg p_0$ where n_0, p_0 are equilibrium electron/hole density. Furthermore $\Delta n = \Delta p$ because charge carriers are produced in pairs. This equation is very difficult to solve and is not practical in experiment. It is practically difficult the measure of Φ_0 and R, and it is not usual to calculate the concentration profile of injected carriers during the trap filling process. We need another approach. Considering a slightly p-type semiconductor, in the presence of Δn free electrons per unit volume moving with a certain thermal velocity, a deep centre is exposed to a flux of $\Delta n \langle \nu_n \rangle$ electrons per unit area per unit time. The number of electrons captured by the $(N_t — n_t)$ unoccupied states in a further short time interval Δt is

$$\Delta n_t = \sigma_n \langle \nu_n \rangle \Delta n (N_t - n_t) \Delta t. \tag{25}$$

Now, we can define the electronic capture rate by unoccupied states as the number of states that are occupied in a given time interval divided by the number of free states, i.e.

$$c_n = \frac{\Delta n_t / \Delta t}{(N_t - n_t)} = \sigma_n \langle \nu_n \rangle \Delta n. \tag{26}$$

Likewise, in the hole case we have

$$c_p = \frac{\Delta (N_t - n_t)/\Delta t}{n_t} = \sigma_p \langle \nu_p \rangle \Delta p. \tag{27}$$

From equation 5,8 and 9 one can see that these equation are strictly related to the diffusion length of the charge carriers. We can now find the equation that determines the concentration of filled traps. If the intensity of the incident radiation is large enough to allow for a capture rate greater than the emission rate, then the concentration of traps filled by the photogenerated charge carriers at the steady state condition $t > (c_p + c_n)^{-1}$, i.e. $t \to \infty$, can be expressed as (from equation 17)

$${n_t}^{ph}(\infty) = \frac{\sigma_n \langle \nu_n \rangle \Delta n}{\sigma_n \langle \nu_n \rangle \Delta n + \sigma_p \langle \nu_p \rangle \Delta p} N_t. \tag{28}$$

For $\Delta n = \Delta p$, $\langle \nu_n \rangle \approx \langle \nu_p \rangle$ we can write

$${n_t}^{ph}(\infty) = \left(1 + \frac{\sigma_n}{\sigma_p}\right)^{-1} N_t. \tag{29}$$

This condition is independent by Φ_0, but the time to reach steady state decrease with increasing incoming flux. Equation 26 and 27

gives us some important information: the total density of traps coincides with the density of traps occupied during the illumination of the sample if and only if $c_n \gg c_p$ or (equivalently) the capture cross section of the traps is the same for electrons and holes. This is not a trivial condition and we will return to it when we discuss how to calculate the trap concentration in the next paragraphs.

5.2.2 *Modeling the Current Transient*

The SRH model tells us that it is possible to access the values of the activation energy and capture cross section of the traps (at least the apparent values) if we know the thermal dependence of the emission rate of the traps. The PICTS technique allows to experimentally find this link with the current transient that occurs when the external radiation is turned off. Initially the plateau reached by the photocurrent drops abruptly, but a current transient remains, due to the thermal emission rate of the traps that are emptying. Figure 6 schematizes the processes described so far. We have said that the PICTS technique is applied to highly resistive material with ohmic junction. We can then say if our sample is subjected to a potential difference, the cur-

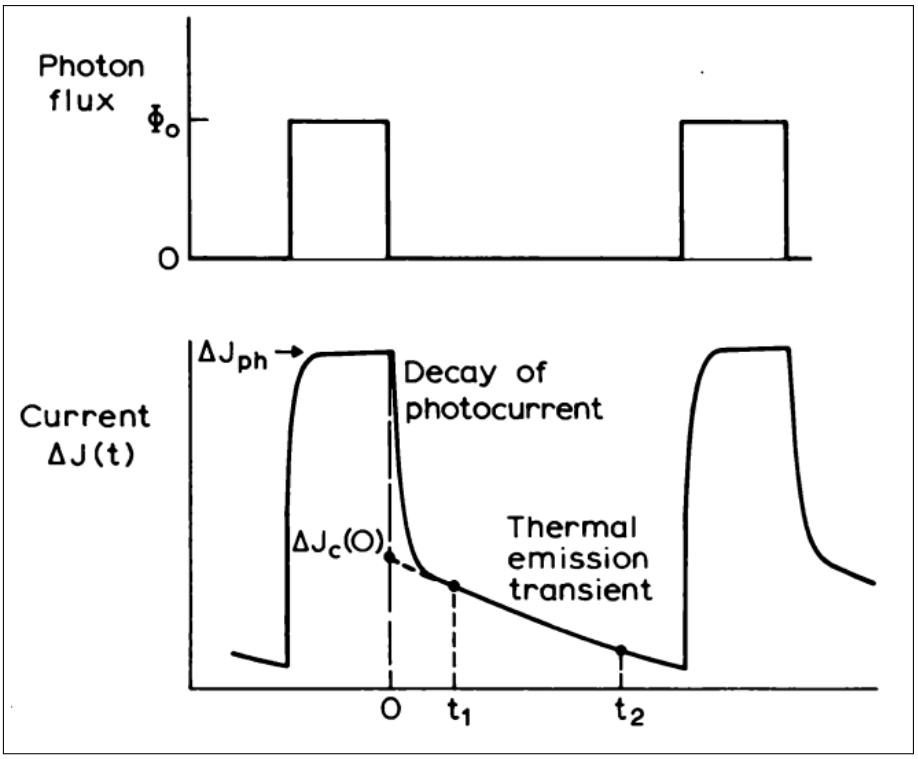

Figure 6: In this image the current response due to the irradiation of a sample with electromagnetic radiation of appropriate energy is schematised. When the external radiation is turned off, the value of the current collapses, but a few moments later there is a thermal transient due to the emptying of the traps [9].

rent density is proportional to the electric field at the extreme of the junctions according to the relation

$$\vec{J} = \sigma\vec{\mathcal{E}} \tag{30}$$

where this time $\sigma = ne\mu_n + pe\mu_p$ is the conductivity, e is the elementary charge, n and p are the electrons/holes density and μ_n and μ_p are the electrons/holes mobility. We can assume that the dark current is negligible respect the photocurrent, so in absence of illumination we can assume that $\mathcal{E}$ is zero. If Δn are the excess charges produced during illumination and we consider the thermal emission of electrons from the traps to be the dominant phenomenon (but an identical treatment can be assumed for the holes) the variation of charge carriers during the thermal transient can be expressed as

$$\frac{d\Delta n(t)}{dt} = e_n n_t(t) - \sigma_n \langle \nu_n \rangle \left(N_t - n_t(t)\right) \Delta n(t) - \frac{\Delta n(t)}{\tau_n}, \tag{31}$$

where the first term is the detrapping rate by the full traps, the second term is the retrapping rate by the empty traps and the third term is the recombination rate r_{Bi} found in Section 1.2. This equation does not yet have an easy solution. We need to simplify the model. The second term, that is the retrapping rate, is negligible compared to the other two because during the illumination the number of available traps is small compared to the number of full traps, provided that the sample has been illuminated with a sufficient flux. Furthermore we can consider the third term, the recombination rate, the fastest and dominant process, such that we can consider the thermal emission slow compared to the recombination rate, which is like saying that we are in a quasi-stationary state, that is, we can put the derivative to zero. Under these conditions we can rewrite

$$\frac{\Delta n(t)}{\tau} = e_n n_t(t). \tag{32}$$

Substituting into Equation 33, setting $\mu_n \gg \mu_p$, $n = \Delta n(t)$, $\tau = \tau_n$ and making use of Equation 22, the current transient in a field $\mathcal{E}$ for an electron trap is

$$J(t) = -e\mathcal{E}\mu_n \tau_n n_t(0) e_n \exp\left(-e_n t\right). \tag{33}$$

An identical equation hold for holes. We now have an experimental value through which we can access the thermal emission rate of the trap e_n. As we see, the transient also strictly depends on the mobility-lifetime $\mu\tau$. The result we have obtained makes use of many simplifications and therefore very stringent conditions, but it is widely used in the PICTS literature. What we have assumed at a microscopic level is that there is a linear relationship between n_t and Δn, that the recombination time is constant (τ does not depend on time) and that $\Delta n(t)$ varies slowly over time respect to all other phenomena

involved, which is equivalent to saying that $\tau e_n \ll 1$. The analogous from an experimental point of view is that the sample being analyzed is highly resistive and that the current in the sample varies linearly with the potential difference. Retrapping have to be neglected and the effective recombination rate have to be faster than thermal emission rate and independent of trap density.

5.2.3 *The PICTS spectrum*

Let's consider a real sample on which interdigitated contacts have been evaporated. For simplicity, the shape of the sample will be that shown in Figure 7. L, l and d are three geometric parameters that respectively indicate the length of the contacts, their distance and d is the active depth of the channel, i.e. the maximum depth with respect to the surface in which there is the production of electron hole pairs created by the absorption of the incident light. From the expression of the current density given by the Equation 33, we can now write the current transient as [41] [42]

$$I(t) = \frac{Ld}{l} qV\mu\tau n_t(0) e_n e^{-e_n t} \tag{34}$$

where q is the elementary charge, V the applied voltage, $n_t(0)$ the initial trapped carrier density, t the time, e_n the thermal emission rate and $\mu\tau$ the mobility-lifetime.

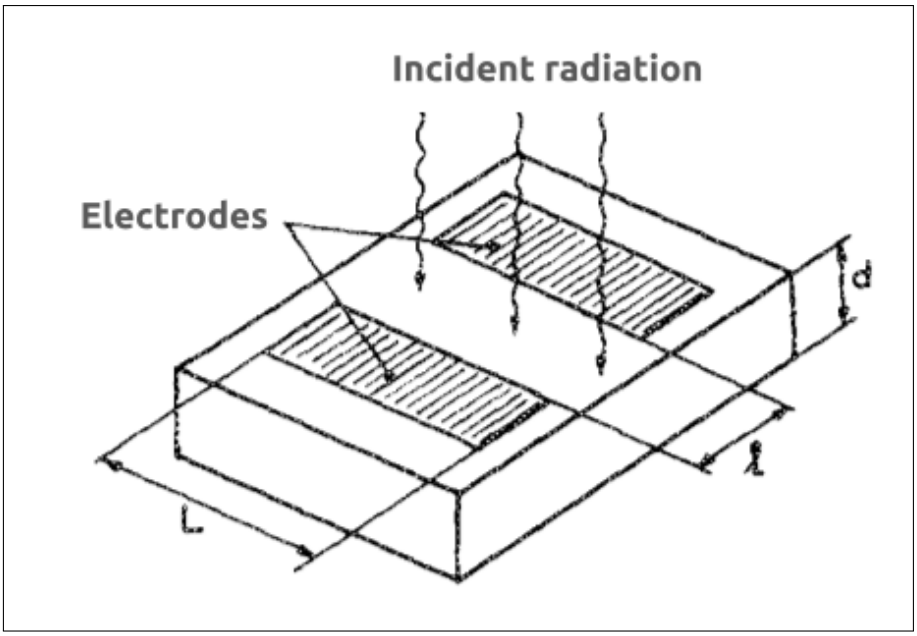

Figure 7: Geometry of interdigitated contacts on a sample, from Tapiero et al. [41].

The Double-Gate Method and the concept of Rate Window

Now that we have a model capable of describing the trend of the current transient as a function of time and which has as a parameter the thermal emission rate of the trap, we can build our PICTS signal. The basic idea is similar to many other transient spectroscopy techniques and is based on the "rate windows" concept. The rate windows is an arbitrarily chosen time interval from where we go to measure the difference in the current value. Referring to Figure 8, the istant $t = 0$ coincide with the LED turned off. Once the time instant in which the transition to thermal emission occurs has been defined in the electrical transient (we can call this instant t_0), we choose two successive instants $t_1 > t_0$ and $t_2 > t_1$ and express the PICTS signal as the difference in the value of the currents in these two instants:

$$S(T; t_1, t_2) = i(t_1) - i(t_2) = \frac{Ld}{l} q V \mu \tau n_t(0) e_n (e^{-e_n t_1} - e^{-e_n t_2}) \quad (35)$$

If there was no thermal emission from the traps, the current difference between the two fixed points would simply be a constant as the decay of the transient would not be perturbed by the emptying of the traps. If a trap is present, however, we expect the thermal emission to reach a maximum at a certain temperature T_m, and therefore also the difference in the PICTS signal will be characterized by a maximum exactly at the point where the thermal emission from part of

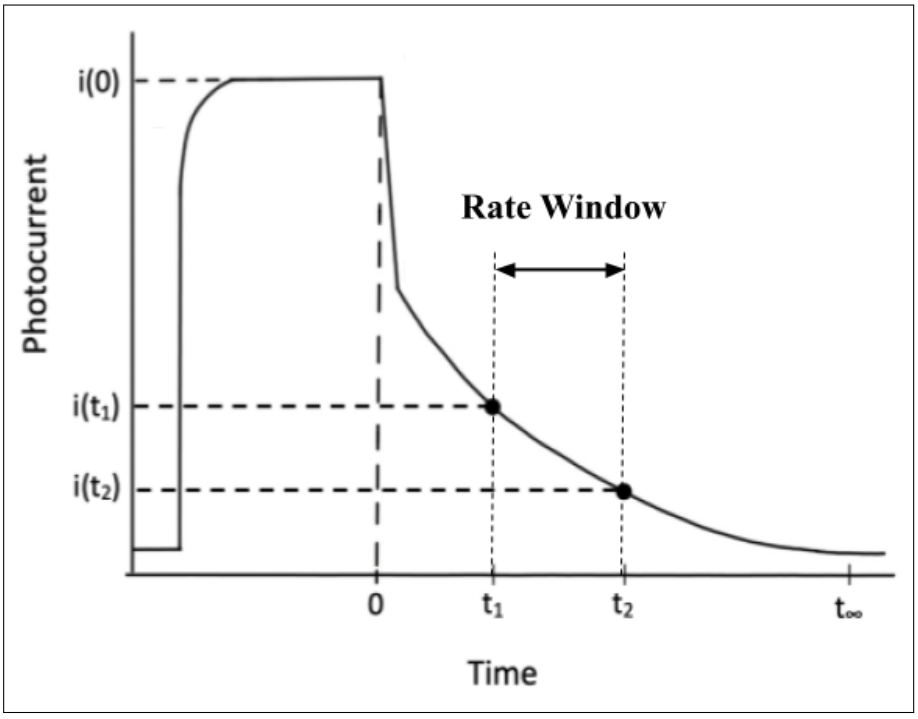

Figure 8: A typical photo-induced current transient. t1 and t2 represent two instants of time chosen to measure the PICTS signal. These instants of time are called *Rates Window*.

the trap is maximum. Mathematically, we can write the maximum of $S(T; t_1, t_2)$ as

$$\frac{dS}{dT} = \frac{dS}{de_n}\frac{de_n}{dT} = 0. \tag{36}$$

By considering Equation 33 and Equation 13, the solution brings to

$$e_n(t_1 - t_2) = \ln\frac{1 - e_n t_2}{1 - e_n t_1} \tag{37}$$

This is a transcendental equation and must be solved numerically via software analysis. Ideally, considering a semiconductor in which there is only one trap state, and chosen two time instants t_1 and t_2, therefore, we obtain a function $S(T; t_1, t_2)$ which will show a peak at a certain temperature T_m. By imposing the derivative of $S(T; t_1, t_2)$ to zero, we obtain the transcendental Equation 37 that tells us what is the value of the thermal emission rate e_n we are scanning given t_1 and t_2. By changing values of t_1 and t_2, that is, by changing rate window, we obtain a curve $S'(T; t_1', t_2')$ identical to the previous one but shifted, since now the value of e_n and T_m differ from the previous one. Therefore, by choosing a collection of values t_1 and t_2 it is possible to obtain a collection of values e_n as a function of T_m. By recalling the link between e_n and T

$$e_n(T_m) = \gamma T^2 \sigma \exp\left(-\frac{E_a}{K_b T_m}\right)$$

we can obtain an Arrhenius plot of the form

$$\ln\left({T_m}^2/e_n(T_m)\right) = \gamma\sigma + \frac{E_a}{K_b T_m} \tag{38}$$

and by fitting them, we can extract the activation energy and the capture cross section of the trap. One inconvenient feature of transient measurements compared with depletion current measurements is the presence of the temperature dependent $\mu\tau$ pre-exponential term in equation for i(t). This term is not included in standard calculations of T_m and the peak of $S(T; t_1, t_2)$ and the form of its temperature dependence is not necessarily known. It could introduces a temperature dependence into the sensitivity of the system so similar peak heights at different temperatures do not necessarily correspond to similar trap concentrations, and the peak height from the same trap changes as the peak temperature changes with different rate window settings. To deal with this problem the PICTS signal is normalized to the magnitude of the photocurrent during the illumination period [43].

5.2.4 *Traps concentration*

There are many spectroscopic techniques that allow you to directly measure the density of the trap states in a semiconductor: PICTS, unfortunately, is not one of them. This is due to the fact that in the equations we have described in the previous paragraphs, the density of traps N_t never appears. The only parameter we encounter is $n(0)$, which is the density of traps filled during the period of illumination. So the question is: is it possible to prove that under certain conditions $n(0) = N_t$ holds? The answer is no, we cannot be sure. In the literature it is possible to find cases in which the estimate of the density of traps calculated with the PICTS technique, compared with other spectroscopic techniques, turns out to be correct and cases in which it is not. Recalling Equation 28 and by the relations expressed by equations 24 and 25, one can write

$$n(0) = N_t(1 - e^{-(c_p+c_n)t}). \tag{39}$$

The trend is shown in Figure 9. Therefore $n(0) = N_t$ hold if and only if the illuminance time $t_I \approx 1/(c_n + c_p)$. Experimentally these values are difficult to access. What we can assume is that these times, both those of capture and of emission, are comparable to each other and a

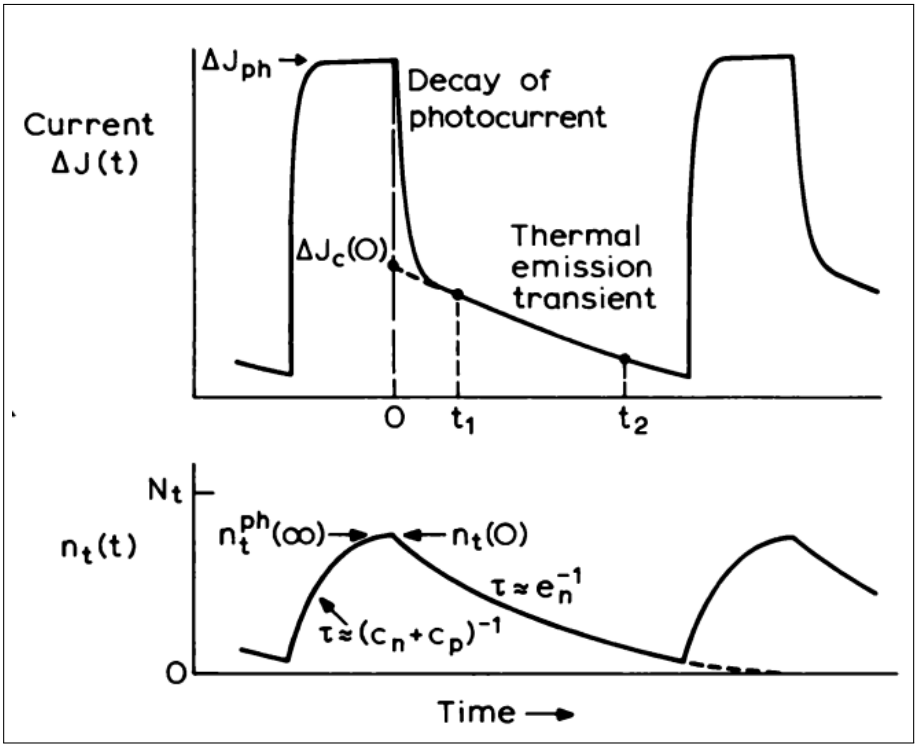

Figure 9: Comparing the trend of the current transient (above) with the concentration of filled traps (below). [9]

rough experimental estimate is possible by calculating the characteristic decay time of the electrical transient. As we will see in the results session, the illumination time during our experiment has always been equal or greater than the characteristic time of the transient. It is therefore possible to provide an estimate of the trap concentrations. This estimate must be considered qualitative rather than quantitative, and certainly provides a lower limit to the density of traps. The method for calculating the trap concentrations that I will show in this section was proposed by Tapiero et al. in 1988 [41]. It is based on two assumptions:

- the lighting time is long enough to allow the traps to be filled, so $n(0) \approx N_t$.
- The $\mu\tau$ value does not depend on the temperature at least in the range in which the trap is present.

If the delay times are chosen so that $t_2 \approx 4t_1$, then the condition $e_n \approx {t_1}^{-1}$ hold and one can write the PICTS signal at the maximum T_m as

$$S(T_m, t1) \approx \frac{Ld}{l} qV\mu\tau N_t e_n e^{-e_n t_1} = \frac{Ld}{l}\frac{qV}{et_1}\mu\tau N_t \tag{40}$$

hence

$$N_t = \frac{l}{Ld}\frac{et_1}{qV}\frac{1}{\mu\tau} S(T_m, t1) \tag{41}$$

where q is the elementary charge and e is the Euler's constant. This is the simplest, but also the most approximate, way to access to trap concentrations. As we will see in the results section, this approach is sufficient for the purpose of this work. Although the value found through this process is more qualitative than quantitative, it provides important information on the evolution of the number of deep defects in the crystal due to natural degradation processes or the consequences of x-ray exposure.

5.2.5 *Experimental Setup*

The schematic of the set-up used to perform the measurement is presented in Figure 10. The illumination source is a LED of higher energy than the sample bandgap, modulated by a rectangular wave, placed in the front of a transparent window of a cryostat chamber. The sample sits inside the cryostat, subjected to a constant potential difference, and is inserted so that it is aligned with the LED. The cryostat chamber is under high vacuum, at a pressure of about 10^{-4} mbar, through a rotating pump. The temperature is controlled by two sensors, a diode, located on the cold finger of the cryostat, which monitors the temperature of the sample, and a thermocouple which regulates the

PID feedback control of the temperature controller. The sample is brought to the temperature of liquid nitrogen and a thermal ramp is initiated that in a couple of hours brings the temperature to a fixed value, 350K in my experiment. At regular temperature intervals (every half kelvin) a transient is collected. The raw data then consists of a series of transients as a function of temperature. The signal is collected with a BNC cable, amplified by a current-voltage amplifier that also provides bias power to the sample, and collected by a data acquisition board (DAQ). The latter is managed by the LAbVIEW software installed on the laboratory computer.

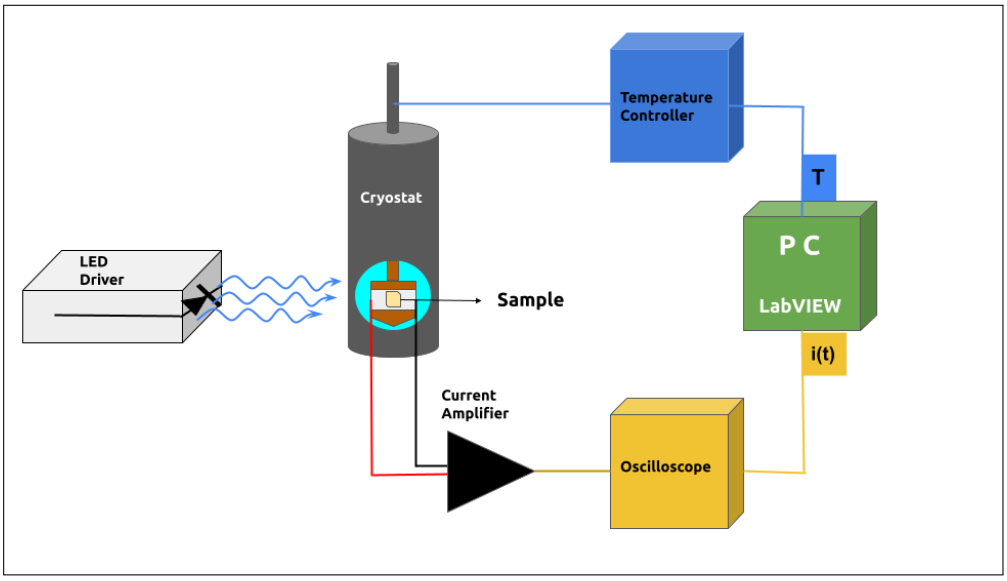

Figure 10: Typical PICTS experiment setup.

5.2.6 *PICTS in practice*

What has been explained so far may be difficult to understand on the first try. For this reason to fix the ideas I will show in sequence the steps that lead from a collection of transients as a function of temperature to the values of activation energy and capture cross section of the traps. The spectrum is taken from a sample used during the calibration of the equipment, but the purpose of the following is regardless of wanting to obtain any physical information. The only purpose is to accompany the reader in a deeper understanding of the PICTS technique. Let us consider the Figure 11. We can see some of the transients collected between 79 K and 340 K. Every thirty second the system collected a current transient. These are the raw data that the experimental setup allows to collect: a collection of current transients as a function of temperature. The colors are arranged so that purple corresponds to the lowest temperatures and red to the highest. In the box it can be observed in detail how the transient changes

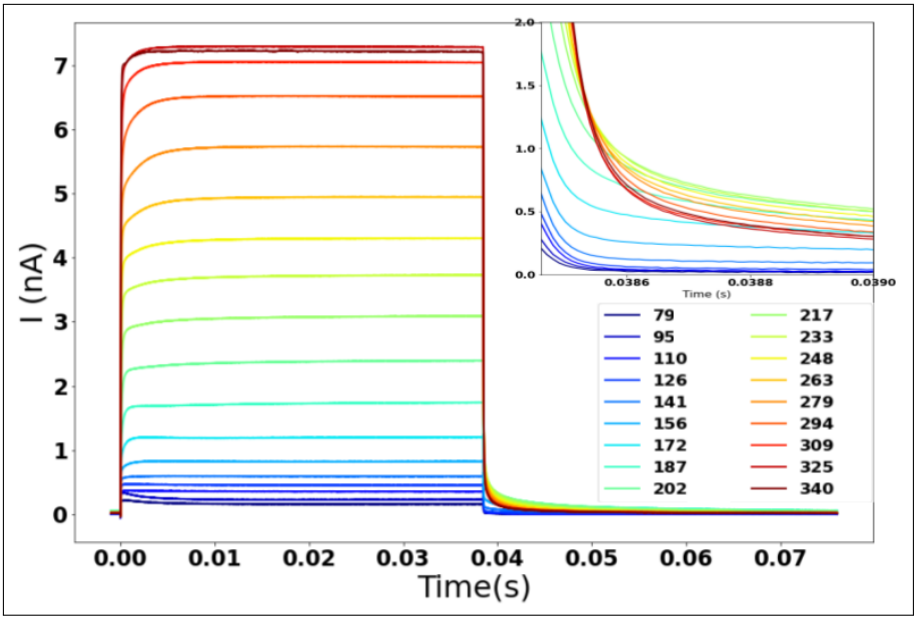

Figure 11: Real data acquired from the Au01 sample. They are current transients acquired at various temperatures between 79 K and 340 K. In the box the detail of the thermal transient.

as the temperature varies. Looking at these transients it is already possible to observe that the characteristic decay time increases when the temperature is between 150K and 220K, and then decreases again. This is already a rough indication that there are traps in that area that reach a peak of emission. The next step is to obtain the PICTS spectrum described by Equation 35 and the Arhenius plot of Equation 38.

A PICTS spectrum is shown in Figure 12 a). The signal consists of what appears to be several shifted copies of the same curve, but as mentioned in the previous paragraph what we are observing is the same spectrum at different rate window values, which in the image is expressed in Hertz and coincides with the value of $(t1 - t2)^{-1}$. In particular in the box, the pairs of values of t_1 and t_2 are reported. Each pair is represented by the same color. As you can see, there is a maximum between 150K and 200K, where previously we had noticed the maximum shift of the transient decay. The shape of the PICTS spectrum around the maximum is not predictable by the theory, therefore the identification of the maximums is in this case obtained through a Gaussian fit. We preferred to follow this path for several reasons, which I try to list. Starting from the fact that the PICTS spectrum is not a continuous line but a discrete series of points, and often the signal is also very noisy, especially at low temperatures, take advantage of a function optimization algorithm (i.e. find the maxima through the derivatives) not lends itself to being a viable choice.

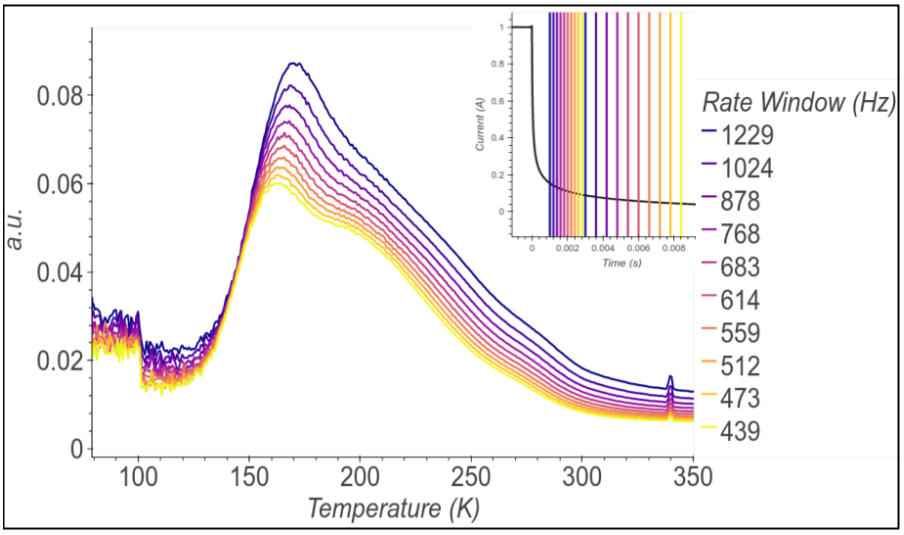

(a)

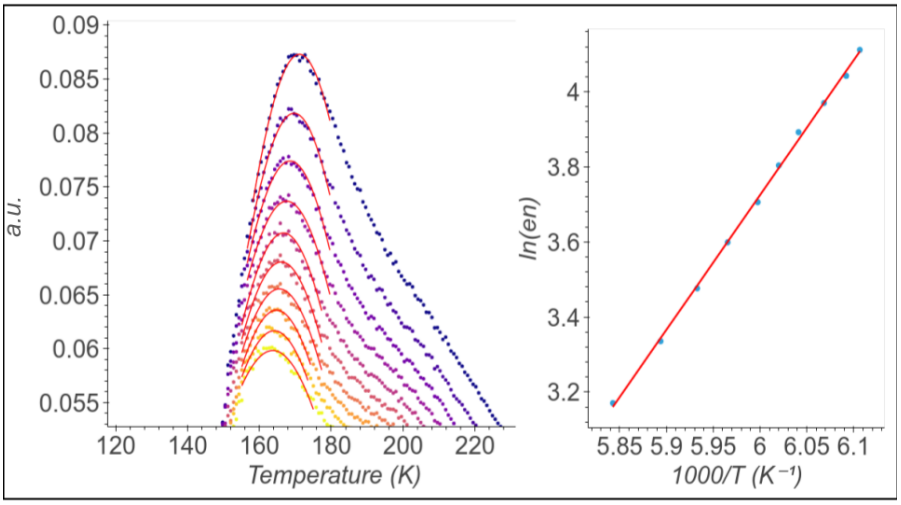

(b)

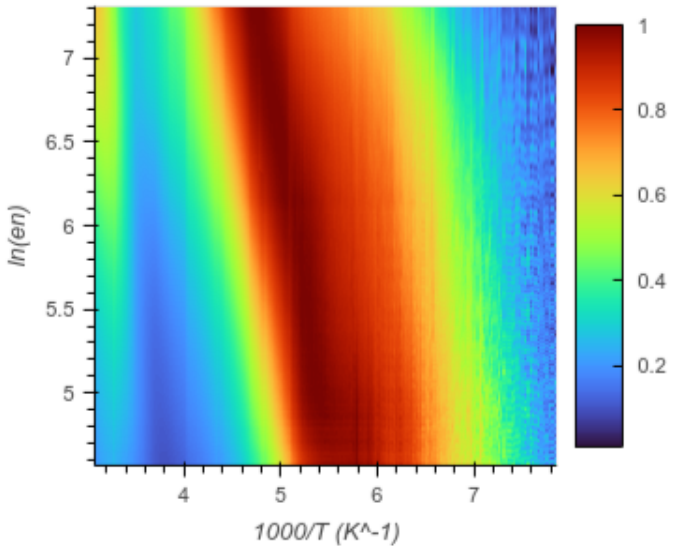

(c)

Figure 12: In a): A PICTS spectrum for several rate window. In b): Detail of the above PICTS spectrum with the Arrhenius plot. In c): Another way to view a PICTS spectrum: a map.

You could smooth the function first and only then apply an optimization algorithm, but any smoothing algorithm can introduce artifacts in the graph. The application of a simple Gaussian fitting near the maximum was found to be the best choice in terms of the quality of the data analysis. In Figure 12 b), the procedure for obtaining the Arrhenius plot is shown. The curves are fitted in the maximum zone to obtain, for each peak, a pair of values (e_n, T_m). These points are then inserted in a semilogarithmic graph where they appear, in fact, as straight lines. Through the slope it is thus possible to obtain the value of the activation energy and from the intercept the capture cross section. You can also go a step further to better observe the traps. If instead of generating, as in this case, a handful of rate windows we proceed to generate a large number of them, it is possible to obtain a two-dimensional map of $\ln(e_n)$ as a function of the temperature. This process is shown in Figure 12 c). As you can see now the trap is clearly seen. These graph, called map, are very useful for qualitatively comparing the shape of deep levels in samples.

6 TRANSPORT AND OPTICAL PROPERTIES

6.1 I-V CHARACTERISTIC AS A FUNCTION OF TEMPERATURE

The information that can be extracted from a current-voltage characteristic (I-V from now on) is manifold. What is of interest for this work are mainly two things: verify that the sample inserted in its sample holder and including contacts has an ohmic trend, and verify if ionic currents are present, possibly measuring the ionic activation energies. In the first case the speech is extremely simple. A material is said to be ohmic when the ratio between the current flowing inside the sample and the potential difference across, it remains constant. This quantity is called conductance. In Figure 13 are shown the two typical types of behavior that usually sound familiar: that of metals, purely ohmic, and that of Schottky or pn junctions, also called "rectifying".

But these are just two of the many behaviors that conductance can have. The typical physical quantity of reference in these cases is not the conductance itself, which also depends on geometric factors, but the electrical conductivity, which instead is an intrinsic quantity of the material and is usually a function of temperature. A link can be found between electrical conductivity and the activation energy of ion currents within a material. It has now been demonstrated that charge transport in 3D perovskites also occurs through ionic currents [44] [45]. The little literature present suggests that it is not the same for 2D analogues [44]. Let's try to understand how ionic motion can be observed through electrical conductivity. Let us consider a solid

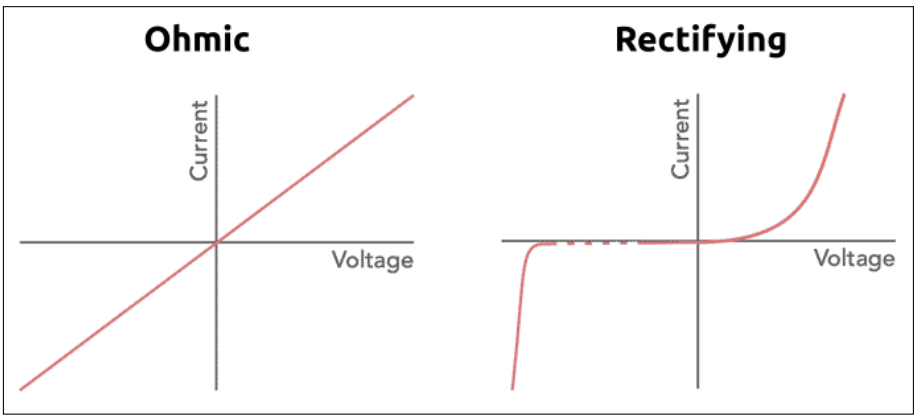

Figure 13: Two typical types of behavior for I-V. To the left that of metals, purely ohmic, and to the right that of Schottky or pn junctions.

in which we know that it is possible to have charge transport also through ionic diffusion. We apply a uniform and constant electric field to the ends of this solid. We know that two equations must be valid. On the one hand, the relationship between electrical conductivity and mobility that can be extracted from the Drude or Sommerfeld model

$$\sigma(T) = nq\mu(T), \tag{42}$$

where q is the charge, n is the charge density and μ the mobility. On the other hand, the general Nernst-Einstein equation must hold for the diffusion of charged particles in a solid

$$D(T) = \frac{K_b T}{q}\mu(T) \tag{43}$$

where K_b is the Boltzmann constant. Combining the two expressions and remembering that diffusion can be expressed in relation to the Boltzmann-Maxwell statistic as

$$D(T) = D_0 e^{-\frac{E_a}{K_b T}} \tag{44}$$

where E_a is an energy, we obtain

$$\sigma(T) = \frac{\sigma_0}{T}\exp\left(-\frac{E_a}{K_b T}\right). \tag{45}$$

The latter expression is also normally called, in semiconductor physics, the Nernst-Einstein equation, although in reality it is a consequence of the aforementioned equation and its relationship with electrical conductivity. We, however, will follow this nomenclature, that is typical to find in literature. It is not always possible to easily obtain the necessary geometric information to extrapolate electrical conductivity, as in the case of $(PEA)_2PbBr_4$. The shape of the crystal was too complex to obtain reasonable geometric values to derive conductivity, but we can review everything from another point of view. Placing the usual Ohm relation for resistance

$$R(T) = \frac{1}{\sigma(T)}\frac{L}{A} = \frac{\alpha}{\sigma(T)}$$

where $\alpha = L/A$ is the ratio between length and area of the sample. Inverting one have

$$\frac{1}{R(T)} = \left(\frac{\alpha\sigma_0}{T}\right)e^{-E_a/K_b T}$$

from which we can write

$$\ln\left(\frac{T}{R(T)}\right) = \ln(\alpha\sigma_0) - \frac{E_a}{K_b}\frac{1}{T}. \tag{46}$$

In this way, by measuring the electrical resistance of the sample as the temperature varies and plotting the related Arrhenius plot, it is possible to experimentally access, if they exist, the ion activation energy values.

The experimental setup for I-V in function of temperature is shown in Figure 14. The sample is in vacuum inside the cryostat. The sample is cooled to liquid nitrogen temperature and through a Source Measurement Unit, controlled by LabVIEW software, an I-V curve is acquired as the temperature is brought back to ambient value or beyond. Through a LED, it is possible to acquire the I-V curves even during irradiation.

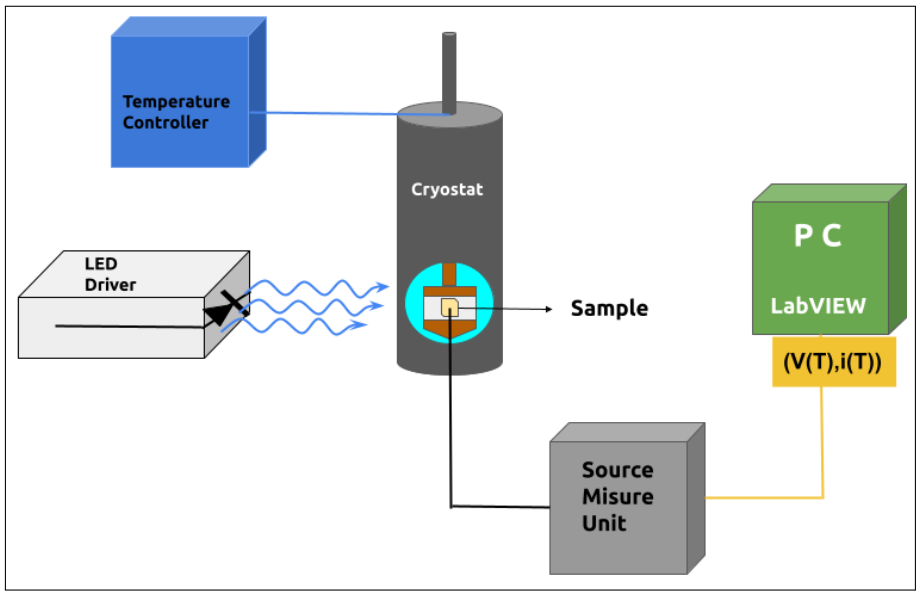

Figure 14: This setup allows you to collect various I-V curves as the temperature changes.

6.2 PHOTOCURRENT SPECTROSCOPY

Photocurrent spectroscopy is one of the simplest experimental techniques to trace the band gap of a semiconductor material. It is based on the idea that, in a semiconductor, only the incident radiation with a wavelength less than a critical wavelength is absorbed, promoting an electron from the valence band to the conduction band, thus generating a current. Therefore, taking a source of white light and breaking it down into its fundamental components, it is possible to evaluate the photocurrent as a function of the wavelength. Having identified the critical wavelength, remembering the relationship between the speed of light and its frequency and substituting in the famous Einstein

equation for the energy of a photon, we find that the band gap is equal to

$$E_{gap} = \frac{hc}{\lambda_c}$$

where h is the Planck constant, c is the speed of light and λ_c is the critical wavelength. In practice, to determine the energy gap of direct band gap semiconductors, as in the case of HOIPs, a modified version of the Tauc equation is used, a method better known as Tauc Plot [46]. We start from the assumption that it is possible to express the relationship between the absorption coefficient α and the energy gap E_g as

$$(\alpha h\nu)^{1/\gamma} = B(h\nu - E_g) \tag{47}$$

where h is the Planck constant, ν is the photon's frequency, B is a constant. The γ factor depends on the nature of the electron transition and is equal to $1/2$ or 2 for the direct and indirect transition band gaps. Therefore, considering the case of direct transitions, the expression will simply become

$$\alpha h\nu = A(h\nu - E_g)^{1/2}$$

where A is a constant. In a graph in which the x-axis is the photon energy, the direct bandgap value can be extrapolated by fitting a straight line to the linear segment to intersect the x-axis from the plot of $(\alpha h\nu)^2$ versus $E = h\nu$. This is possible because from the theory of transitions in two-state systems, as well as the optical transitions from the valence band to the conduction band, we know that there is a direct proportionality relationship between α and the photocurrent circulating in the crystal. This means that, although the absorption coefficient is not known, the fit of the linear zone is equal and independent and intersects the energy axis precisely in the value of the optical band gap. The experimental setup is shown in the Figure 15. The white light, produced by a special lamp, first passes through a chopper which modulates its on and off frequency (modulation which is passed to the lock-in in order to discriminate the photocurrent signal and eliminate the noise) and then enters a monochromator, able to open the optical spectrum in all its components. A power supply generates a bias across the sample. In this way, a scan of the photocurrent at the ends of the sample is made as a function of the frequency of the incident light, a signal that is amplified by the lock-in. Everything is managed by LabVIEW software.

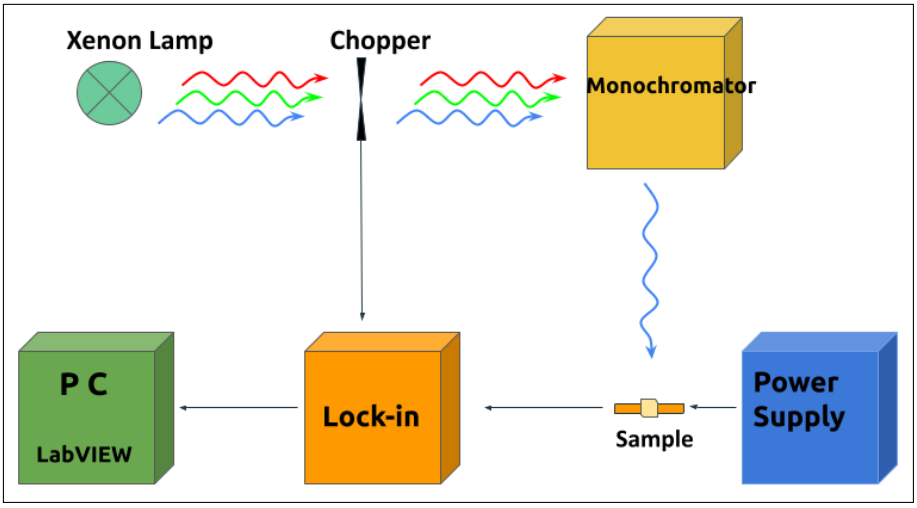

Figure 15: A typical setup for photocurrent spectroscopy measurements.

6.3 CHARGE CARRIER MOBILITY LIFE-TIME

The charge carrier mobility μ and carrier lifetime τ product, the so called $\mu\tau$ product or *mobility life-time*, determines the average carrier drift distance per unit electric field, and thus the charge collection efficiency of a photodetector, as we saw in Section 1.3. The higher $\mu\tau$, the higher charge collection efficiency of a detector. One of the most widely used techniques to measure mobility life-time makes use of the modified Hecht equation [18][47], according to which the photocurrent of a semiconductor can be expressed as

$$I = \mu\tau\frac{V}{L^2}\left[\frac{1-\exp\left(-\frac{L^2}{\mu\tau V}\right)}{1+\frac{Ls}{\mu V}}\right] I_{sat} \tag{48}$$

where L is the inter-electrode spacing, I_{sat} is the saturated photocurrent, V is the applied bias and s is the surface recombination velocity. The experimental setup is shown in Figure 16. The source that induces the photocurrent can be electromagnetic radiation with energy higher than the band gap, or in the frequencies of ionizing radiation or, if it is not possible to obtain easily the saturation of the photocurrent, it is possible to use a source of alpha particles. The radiation hits the sample while the bias at its ends passes from zero to an appropriate maximum value. This value must allow the photocurrent to reach a plateau.

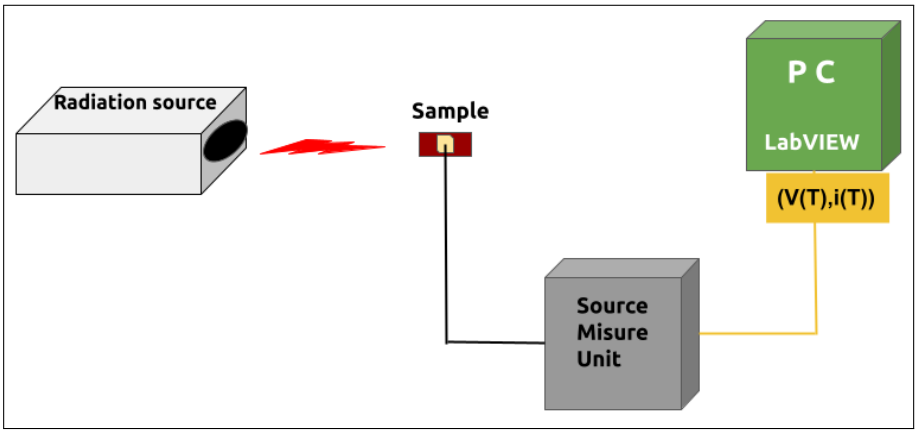

Figure 16: Ref alfa

Part III

RESULTS AND DISCUSSION

PEA_2PbBr_4 shows a low concentration of deep states and in small numbers. This material shows excellent radiation hardness, and measurements on one-year-old samples show the robustness to deterioration of this perovskite. From the results of this study, 2D HOIPs, compared with 3D HOIPs, do not show ionic transport phenomena that can deteriorate the crystal structure.

7

RESULTS AND DISCUSSION

Two samples were initially synthesized to which interdigitated contacts were evaporated. Since there are no indications in the literature regarding which materials would allow a better ohmic behavior of the sample, a necessary condition for PICTS measurements, two materials with different work functions, gold and chromium, were chosen. Figure 17 a) show a scheme of the samples and its substrate. $(PEA)_2PbBr_4$ single crystal were fixed on a substrate of mica, a material that allows a good thermal transport but at the same time is a good electrical insulator. Copper contacts have been placed on the sides of the mica base. Through gold wires the sample was connected to the copper bases. In Figure 17 b) a picture of the sample is shown.

Figure 17 c) shows an image of the crystal under an optical microscope under polarized light. Polarized light allows us to observe whether grain boundaries are present, as each crystalline domain has different atomic orientations and is able to create diffraction patterns that appear in the form of different colors if more than one crystalline domain is present. As can be seen, the crystal appears homogeneous

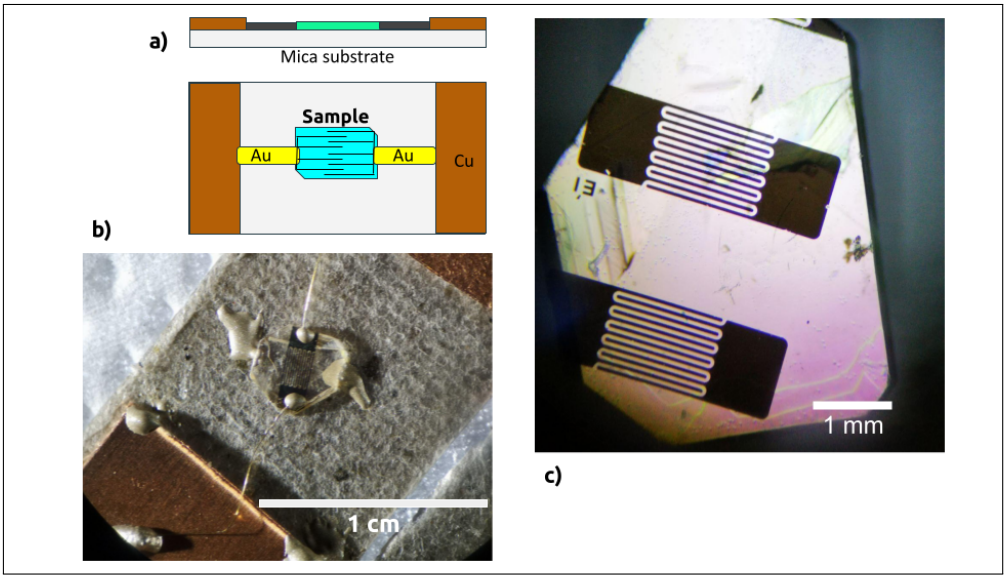

Figure 17: a): Schematic representation of the sample mounted on its support structure. b): A photo of the sample in which you can also see the contacts through the gold wires that arrive on the copper plates. c):A polarized light optical microscope image of a PEA_2PbBr_4 crystal. The homogeneity of the diffuse color indicates that we are looking at a single crystal.

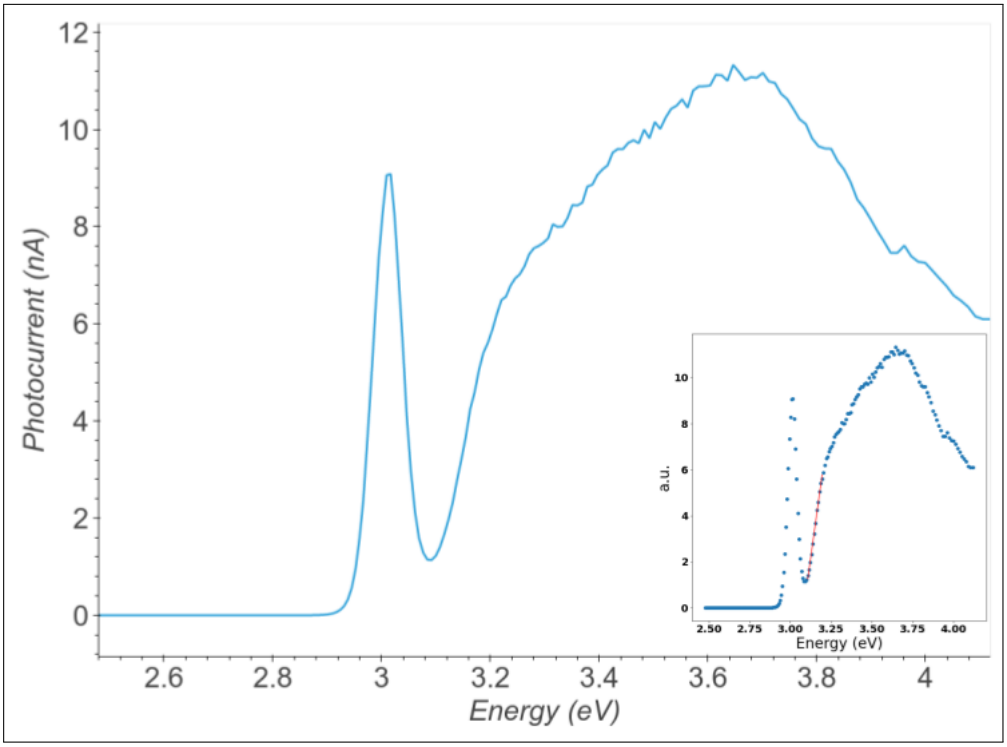

Figure 18: Photocurrent spectroscopy for PEA_2PbBr_4 perovskite

in color, without grain boundaries. The photocurrent spectrum allows to calculate both the crystal energy gap and the excitonic binding energy. Figure 18 shows the photocurrent spectrum obtained and, in the box, the Tauc plot for direct gap semiconductors with the relative fit. The energy gap is (3.08 ± 0.02) eV. An UV LED with 365 nm light emission was therefore chosen as the light source. It must be clarified that in the case of semiconductors with large excitonic states such as 2D perovskites, the excitonic state can slightly shift the true value of the band gap, therefore the Tauc plot is not the best choice. The correct method for estimating the energy gap in these cases can be found in Armaroli et al. [48]. Unfortunately, the Tauc plot is almost always reported in the literature, and given that the photocurrent spectrum with its excitonic peak is a fingerprint of perovskite, and we needed to ascertain that the material we had synthesized was exactly what we intended to synthesize, we used the same method currently followed by the majority of research groups.

For both samples I studied the trend of the current as a function of the applied voltage and of the temperature. This allows both to verify that the behavior of the material is ohmic and to verify if there are traces of ionic activation. In Figure 19 a) the I-V in function of temperature of the Au01 sample can be seen. What is observed is a symmetrical current trend, approximating an ohmic trend. For temperatures above 300K there is a sharp increase in the temperature of

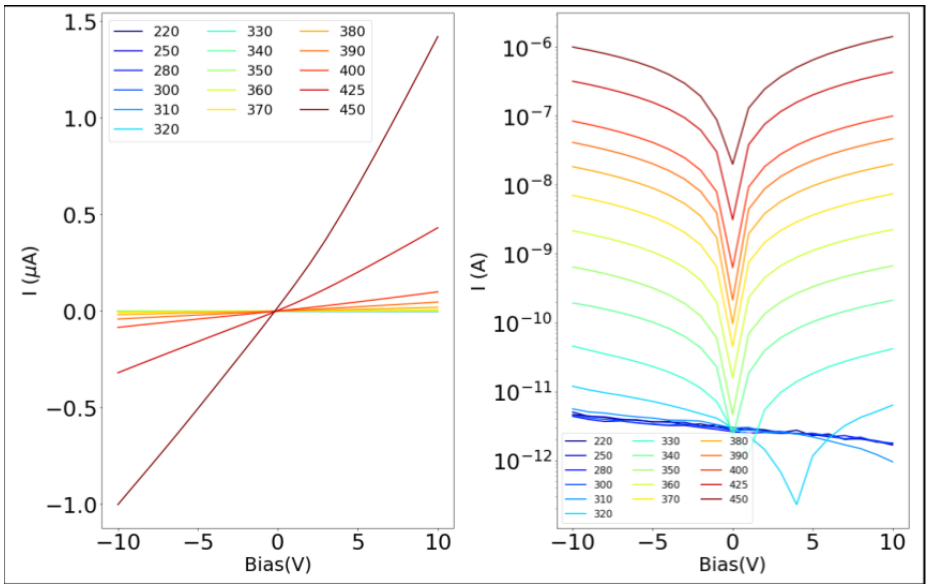

(a)

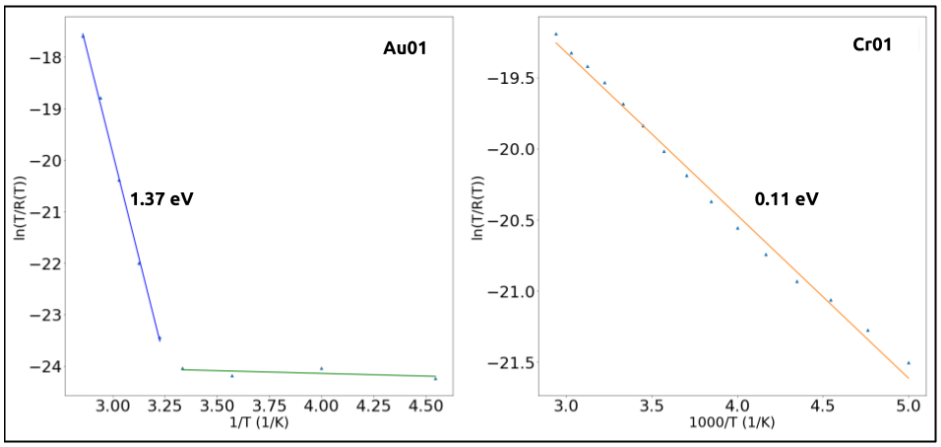

(b)

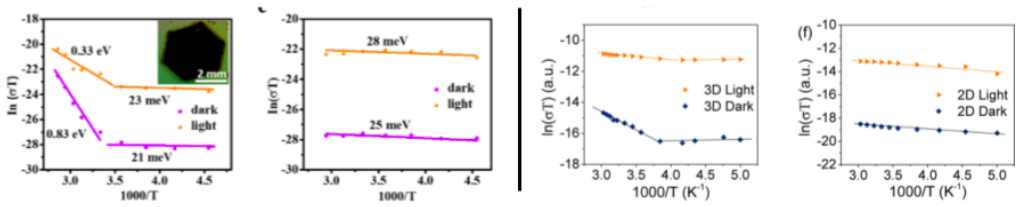

(c)

Figure 19: a): I-V for the gold interdigitates contacts sample. In logarithmic scale on the right. b): the Nernst-Einstein equation applied to PEA_2PbBr_4. c) From literature (left: Xiao et al. [44]; right: Lin et al. [26]). 3D perovskites show ionic activation, while 2D does not seem to indicate ionic activation.

dark current, an index of ionic activation. From the Nernst-Einstein equation, as we saw in Section 6.1, ionic diffusion in material could be verified. In Figure 19 a) it is possible to observe the I-V for the gold interdigitates contacts sample. As you can see, the range of current values changes significantly as the temperature varies, passing from pico Amperes to micro Amperes within a few tens of Kelvin. Specifically, there is a critical temperature around 300K from where the current increases sharply. From the literature it is evident that already at low temperatures the 3D perovskites show ionic activation, while for the 2D the little literature present does not seem to indicate ionic activation, as you can see in Figure 19 c). For each I-V measurement, the resistance value was obtained from a simple linear fit, for both samples. What is observed is shown in Figure 19 b). In the case of gold interdigitates contacts sample, an ionic activation energy of (1.37 ± 0.03) eV is observed at a temperature just over 300 K. The same phenomenon is not observed for the chromium interdigitated contact sample.

Other measurements were carried out on other samples, always with interdigitated gold contacts, always observing an activation energy around 1.3eV/1.4eV. To go even deeper we contacted some samples simply with silver paste on the sides, along the conductor planes. Also in this case we have observed the same activation energy. Unfortunately it is difficult to make a comparison with the literature. In Figure 19 c), for example, if we observe the conductivity trend as a function of temperature for 2D perovskites, it is clear that no activation energy is present; but other considerations can be made regarding the fact that gold and silver used as metals to contact the samples are adsorbed, creating ionic compounds that can diffuse inside the material [49]. We have not come to the head of the problem, which still remains an open question, but we will return to the question in the next paragraphs.

To complete, in Figure 20 the dark and light currents are shown, on the left in the case of a sample without interdigitated contacts and on the right the same but for Au01. As it is possible to see also the light current shows a good ohmic trend, necessary to carry out PICTS measurements. The use of interdigitated contacts was necessary because, as can be seen from the image of the sample without interdigitated contacts, the resistance in the $(PEA)_2PbBr_4$ in a crystal of a few millimeters of side are tens of TΩ, with dark currents in the order of the femto Amps and light current of a few tens of pico Amps, too small to have a good signal to noise ratio with the equipment at our disposal. Charge carrier Mobility life-time was evaluated and is shown in In the Figure 21 a). We performed $\mu\tau$ measurements under UV illuminance, x-ray and alpha particles. In the case of UV and

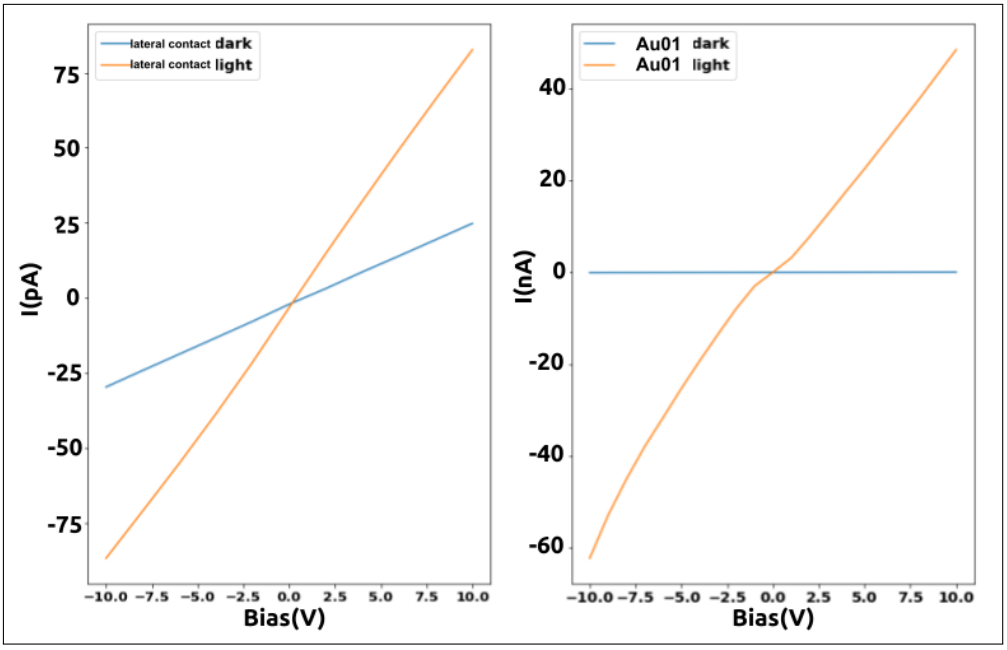

Figure 20: I-V at room temperature for lateral contacted sample (left) and gold interdigitated contacts sample (right).

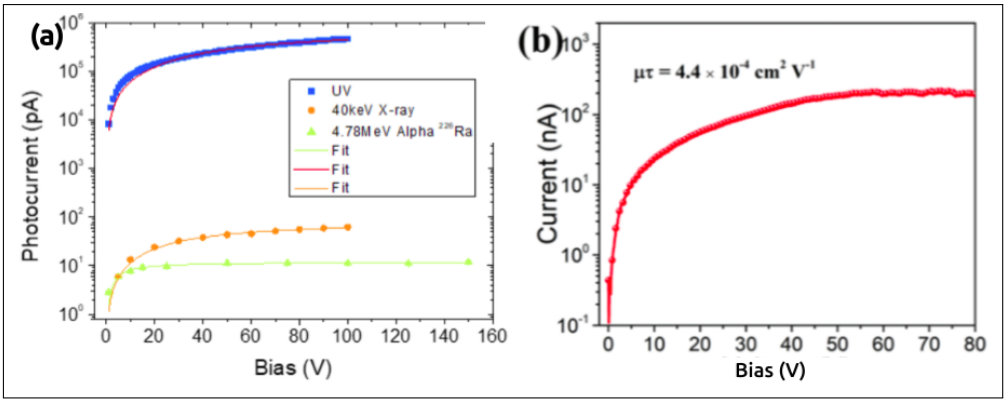

Figure 21: a): mobility life-time measurements at our laboratories. In the image it is possible to see how only with alpha particles it is possible to reach a plateau in the photocurrent. b): the measure of Zhang et al. [18] with UV rays.

x-ray illumination, the photocurrent never reaches a plateau, unlike what is shown Figure 21 b) from Zhang et al. [18]. Only under bombardment of alpha rays it was possible to obtain the correct trend of the Etch equation, from which it was possible to obtain a $\mu\tau$ value equal to $(3.2 \pm 0.3)10^{-6}$ cm^2V^{-1}. There is in the literature a reference value measured by Zhang et. al [18] but the experimental value shown (Figure 21 b)) was in contrast with the value of our samples. Once all this information was obtained, it was possible to proceed with the PICTS technique. In the literature, to date, there is no information regarding the deep states in any 2D perovskites and specifi-

cally the PICTS technique had not yet been applied. The purpose of my thesis was not only to evaluate deep defects through transient spectroscopy, but also to explore the evolution of these deep states when the crystal was subjected to high doses of x-ray (the so-called radiation hardness, an important stability parameter for X-ray detector's sensitive material) and the evolution of defects due to the aging of the material, to evaluate the stability by the time of $(PEA)_2PbBr_4$. The only reference in the literature gave a qualitative indication of the stability over humidity and resistance to X-ray of various types of 2D perovskite, and $(PEA)_2PbBr_4$ was the most promising of all the 2D perovskites studied in terms of stability [4]. But the study focused only on simple repeated I-V measurements after the samples were exposed to either low doses of X-radiation or very humid environments. These results, although indicative of a certain trend, were weak. So, the two samples underwent two different treatments which are schematized in Figure 22. In the case of the sample with interdigitated gold contacts, Au01, the hardness radiation was evaluated. Three close measurements were made in time. Between the first two a time of about a month has elapsed to assess the repeatability of the measurements. The sample was then bombarded with a total X-ray dose of 200 Gy and tested again with the PICTS technique. For the sample with chromium interdigitates, Cr01, degradation over time was instead evaluated. Three scans were done in a total time period of one year. Both samples were stored under normal environmental conditions for all the duration of the work. Figure 23 shows the laboratory instrumentation and specifications.

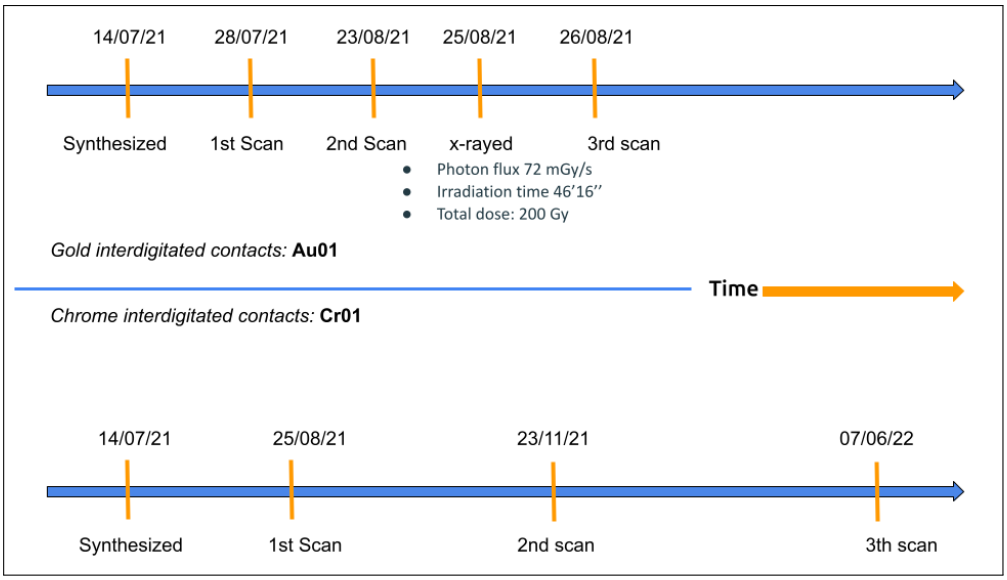

Figure 22: Timeline.

7.1 DEFECT STATES IN PEA_2PbBr_4

Figure 23 shows the instrumentation and parameters used during PICTS measurements. The measurements were performed trying to always maintain the same experimental conditions. First we compare the deep defect values obtained for the Au01 and Cr01 samples. PICTS spectra and maps are shown in Figure 24. As can be seen, two traps, T1 and T2, are clearly visible in both samples, while a third trap T3 appears lighter at higher temperatures. The graphs are not completely overlapping simply because they are viewed at different rate windows and on different thermal scales, but the maps on the right clearly show that the same traps are present in both samples. Care must be taken when looking at maps. The x axis goes as 1000/T, so from left to right the trap T3 will appear first, then the T2 and finally the T1. This choice is simply due to following the standard that is proposed in the literature. T3 is hardly visible. It can be seen by paying attention to the upper left part of the map. In fact T3 is a trap that appears at high temperatures and high rate window frequencies. The values of the activation energies and of the capture cross section are shown in Table 1. In the case of chromium it was not possible to evaluate T3. The visual proof of the belonging for the traps to the same family is given by grouping the Arrhenius plots in a single graph. This way of looking at traps is not unusual in the literature. Nobody expects to see exactly overlapping Arrhenius plots. Since there is an exponential relationship between the thermal emission rate and the activation energy, small variations due to normal random errors during data collection can lead to even important line deviations. What

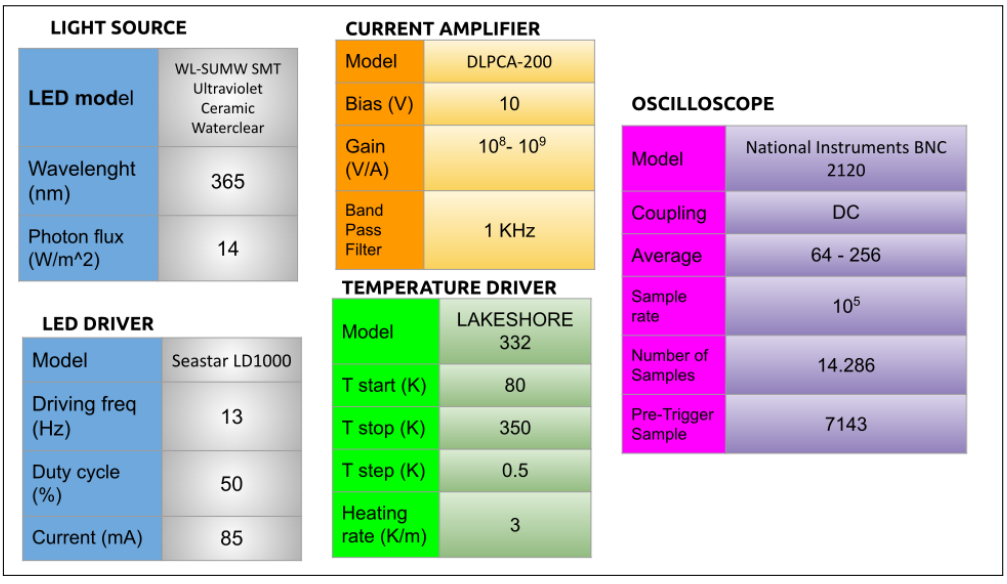

Figure 23: A resume of the instrumentation used during PICTS measurements and some experimental parameters.

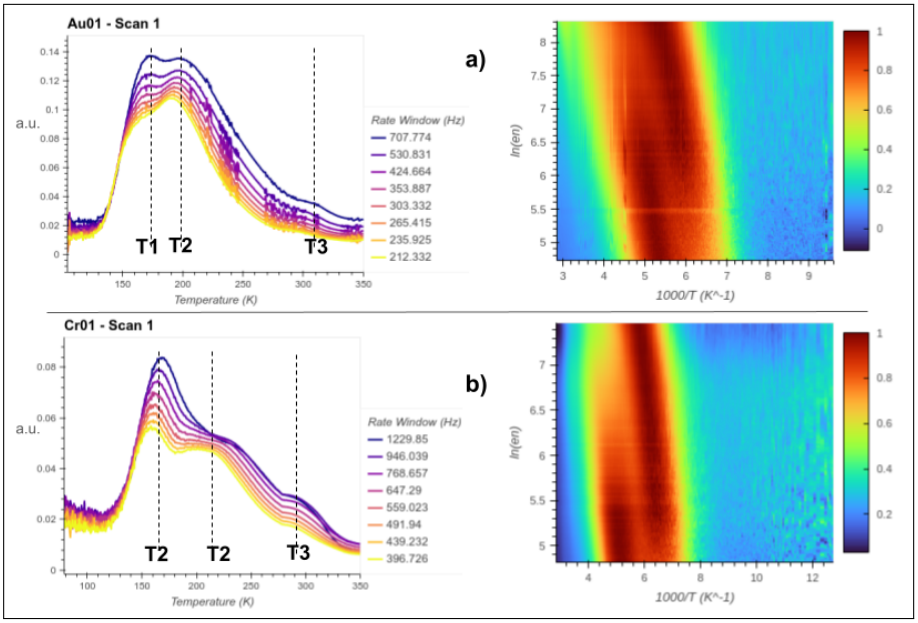

Figure 24: a): PICTS spectrum and PICTS map of the first scan on the AU01 sample. b): PICTS spectrum and PICTS map of the first scan on the Cr01 sample

is of interest in the literature is that the Arrhenius plots form groups. At that point it is possible to establish which trap belongs to which group, and each group represents a defect state. In Figure 25 it is possible to observe for the first time the deep states in the $(PEA)_2PbBr_4$. The image shows the Arrhenius plots for Au01 and Cr01. As you can see, it is possible to divide the graph into three zones, one for each trap. The reproducibility between the two samples is really satisfactory. The Arrhenius for T1s are thermally slightly distant, but this is a condition that can occur for complex spectroscopic techniques such as PICTS, but it could also be due to surface phenomena due to the diversity of interdigitated contacts. T2, on the other hand, appears perfectly overlapped in the two samples.

SAMPLE	T_1	T_2	T_3
Au01			
E_a (eV)	0.33 ± 0.05	0.40 ± 0.05	0.52 ± 0.08
$\sigma(cm^2)$	$(1.0 \pm 0.5)10^{-12}$	$(1.3 \pm 0.6)10^{-13}$	$(3.4 \pm 0.6)10^{-14}$
Cr01			
E_a (eV)	0.31 ± 0.05	0.38 ± 0.05	-
$\sigma(cm^2)$	$(2.5 \pm 0.1)10^{-13}$	$(1.4 \pm 0.4)10^{-14}$	-

Table 1: activation energy and capture cross section for traps in Au01 and Cr01

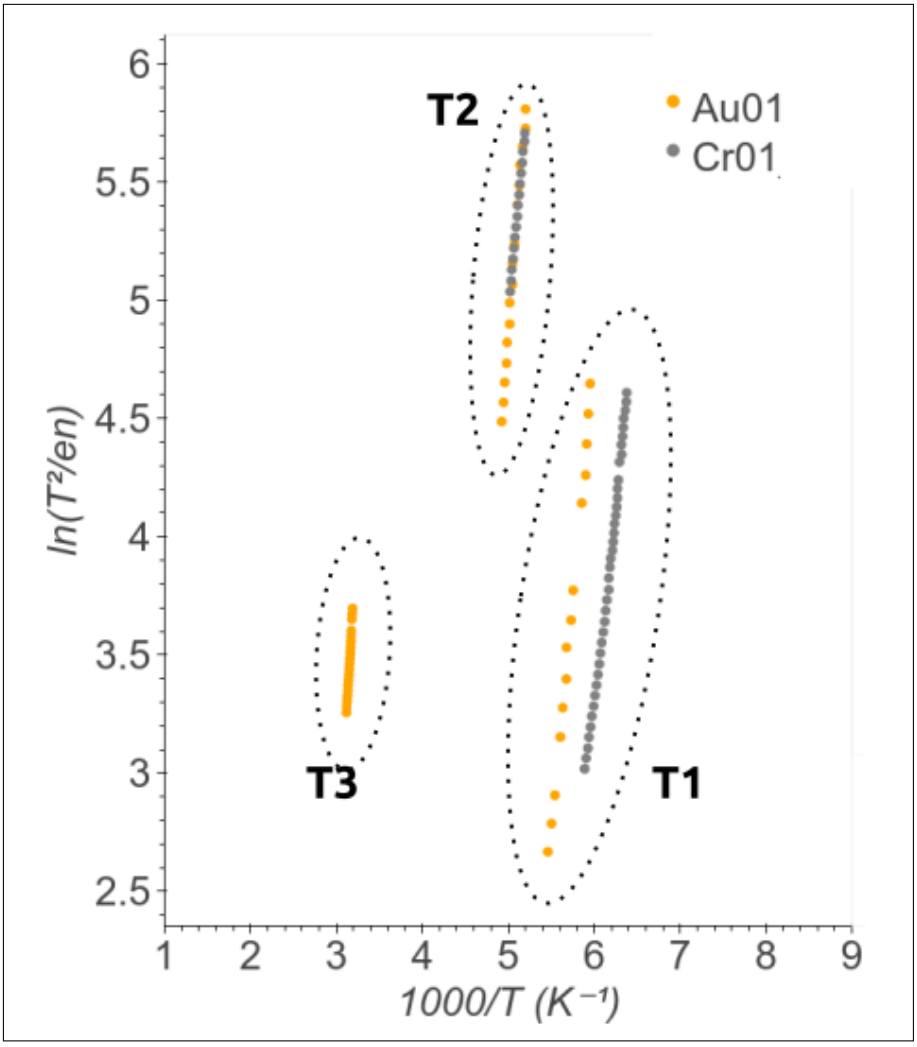

Figure 25: Comparison of Arrhenius plots between Au01 and Cr01 samples.

7.2 RADIATION HARDNESS

As previously mentioned, three scans were performed on the Au01 sample to evaluate the resistance of PEA_2PbBr_4 to ionizing radiation, the last of which after a prolonged dose of X-ray. The maps and the PICTS spectra at fixed rate windows are shown in Figure 26. As can be seen from the image, the reproducibility of the data is excellent. In the first row the PICTS spectra are shown, while immediately below it is possible to observe the maps. The two dominant traps, T1 and T2, are clearly seen. It may be more difficult to identify the third trap, which appears at the top left of the maps, at high temperatures and high emission rate. All the three PICTS spectra have the same rate window. As can be seen, the shape of the spectrum changes as the rate window vary. This is completely normal, because different traps have different thermal emission rate peak, therefore looking at a PICTS spectrum at a certain rate window a trap could be absent,

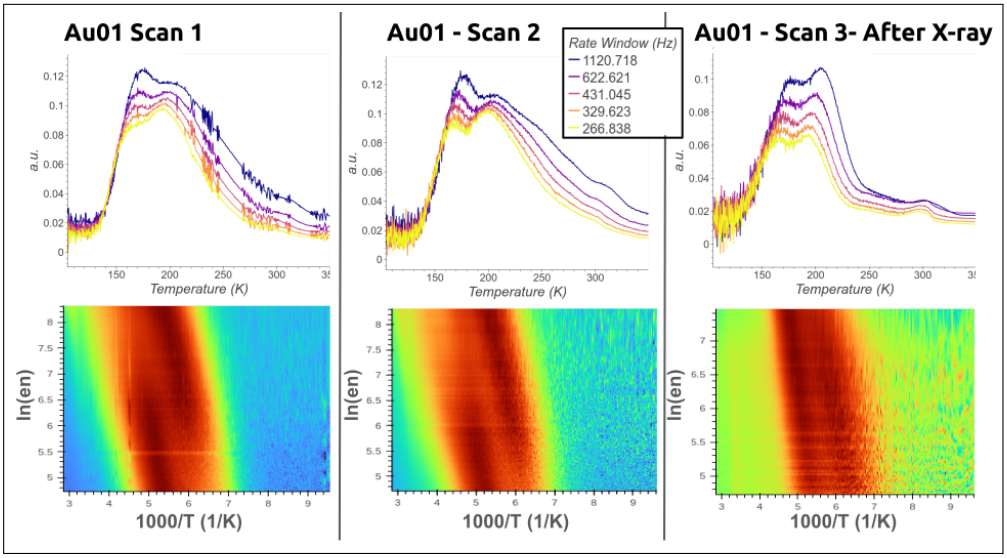

Figure 26: In the first row the PICTS spectra are shown, while immediately below it is possible to observe the maps. From left to right: the first scan on pristine sample, the second scan after two weeks and the third scan after a dose of 200 Gy of X-ray.

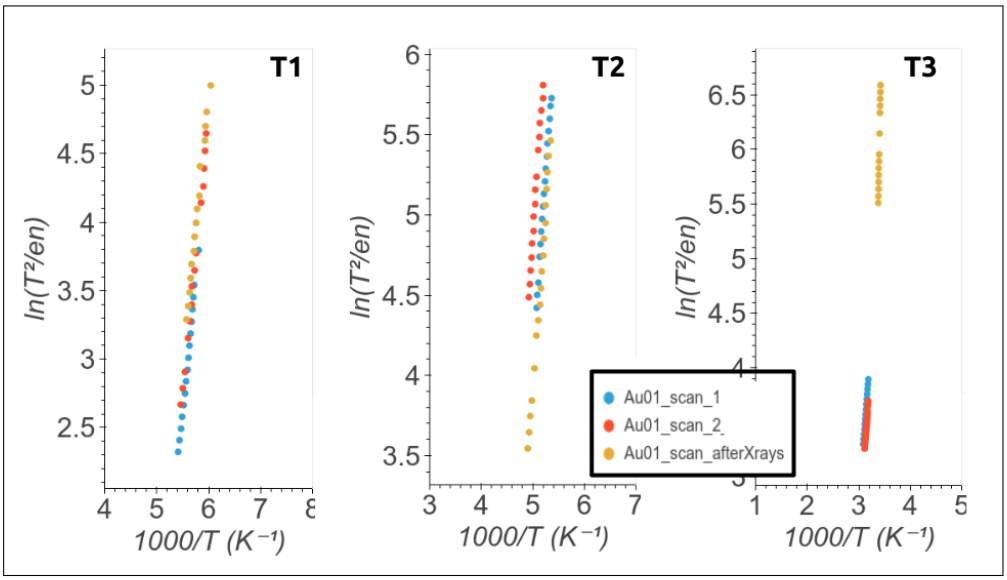

Figure 27: Arrhenius plot for the three traps in the three scans. T1 and T2 are well superimposed in all three scans. T3 appears to have undergone some changes.

while changing the rate window could even become dominant. Despite the high X-ray dose, 200Gy, the sample map after the third scan is in line with the previous two. If we look at Figure 27, the Arrhenius plots are reported separately for each of the three traps in the three scans. It is evident that the T1 and T2 traps form two separate families which each represent a defect and no significant change happens in the three scan, while T3 is varied. In Table 2 all the data are

AU01	T1	T2	T3
Scan 1			
E_a (eV)	0.33 ± 0.05	0.40 ± 0.05	0.52 ± 0.08
$\sigma(cm^2)$	$(1.04 \pm 0.5)10^{-12}$	$(1.3 \pm 0.6)10^{-13}$	$(3.4 \pm 0.6)10^{-14}$
Scan 2			
E_a (eV)	0.35 ± 0.05	0.40 ± 0.05	$0.62 \pm 0.0.8$
$\sigma(cm^2)$	$(2 \pm 1)10^{-12}$	$(8 \pm 5)10^{-13}$	$(2.5 \pm 0.9)10^{-12}$
Scan 3			
E_a (eV)	0.35 ± 0.05	0.39 ± 0.05	2.2 ± 0.3
$\sigma(cm^2)$	$(3 \pm 2)10^{-12}$	$(1.2 \pm 0.7)10^{-12}$	—

Table 2: activation energy and capture cross section for traps in Au01 in each scans.

reported. If we were to stop the data analysis here, we could say that after irradiation with X-ray, the defect that was called T3 is vanished, perhaps passivated by some physical phenomenon due to the interaction with ionizing radiation, while another trap has appeared in its place, which has another activation energy and a different thermal activation. Appearances can be deceiving. We will see in the following paragraphs that we are actually seeing the same defect.

7.2.1 *Evolution of trap concentrations*

We can now observe the evolution of trap concentrations. In the previous paragraphs we underlined that the calculation of the trap concentrations is possible if and only if the illumination time is at least of the same order of magnitude as the characteristic decay time of the transient. Looking at Figure 28 at two temperatures, one in which we are in the full peak of traps T1 and T2 and one in which we are on trap T3, it is possible to see that the above condition is satisfied. Using the technique explained in the previous chapter, what is obtained is shown in the Figure 29. The data regarding T1 are not present because in the non-normalized PICTS spectrum, which is used to calculate the concentration of traps, the maximum of T1 is covered by T2, therefore it is not measurable. What is noticed first of all is the concentration of traps, which appears to be in the order of 10^{12} cm^{-3} for the first two scans. This value has a very strong physical meaning and is in line with what is the current literature on 2D perovskites. DFT ab-initio simulations indicate that deep states are present. These deep states are due to point defects such as vacancy or substitional atoms. The high energy of formation of these defects results in a low concentration of traps [50]. The result that left us a bit stunned is

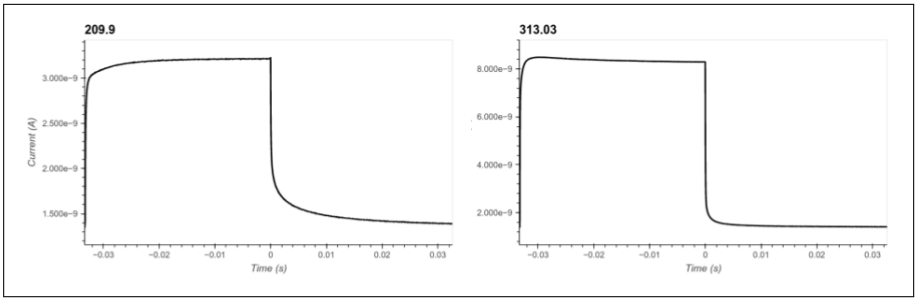

Figure 28: Detail of current transients at peak emission temperatures for T2 and T3 traps. As can be seen, the illumination period is greater than the characteristic decay time of the transient.

what happens to trap concentrations after X-ray bombardment. What we would have expected was an increase in trap concentrations, but what we saw was what appears to be a slight decrease in trap concentrations. Nothing striking, but significant in being able to quantitatively observe the robustness of perovskites at high radiation doses. To corroborate this result we resorted to a technique used to estimate the relative concentration of traps in a material [51] [52]. This technique allows, under certain conditions, to evaluate the relative variation of trap concentrations in the same sample after the sample

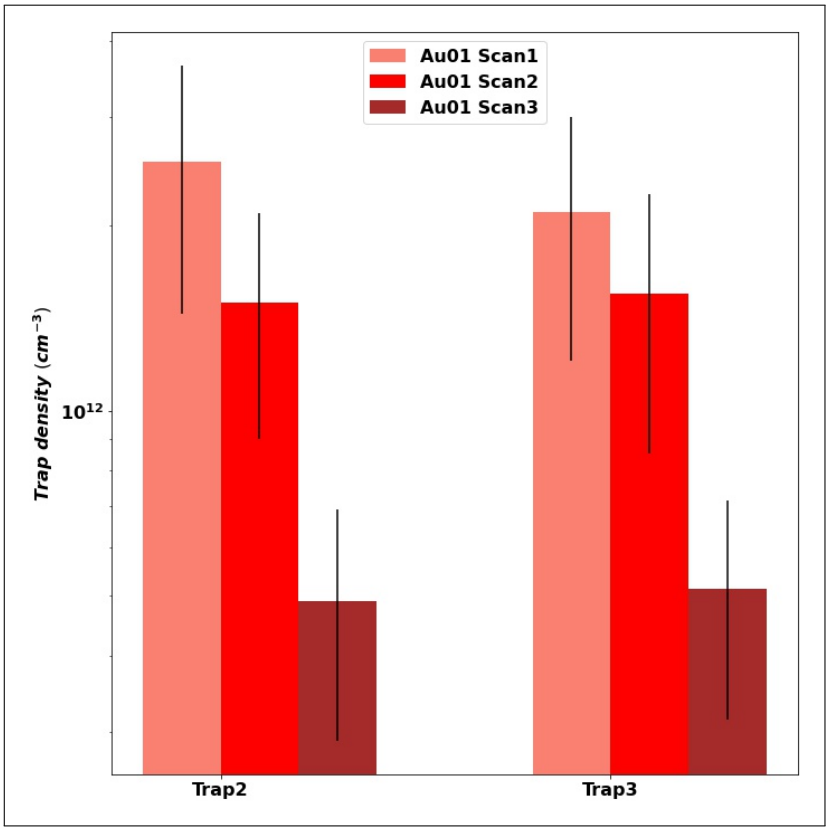

Figure 29: Evolution of the traps concentrations in the three scans.

has undergone certain treatments, such as x-ray exposure. In short, if the experimental conditions remain the same, i.e. the incident light radiation is always the same, the bias is always the same, etc., then normalizing the PICTS spectra of the samples as a function of the value of the photocurrent and comparing them with each other it is possible to observe how the density of traps has evolved. What we observe is shown in Figure 30 a). The spectra have been normalized to 1 to make the percentage variation more accessible. As can be seen, the spectra of scans 1 and 2 are substantially superimposable, while the PICTS spectrum of the sample subjected to X radiation appears

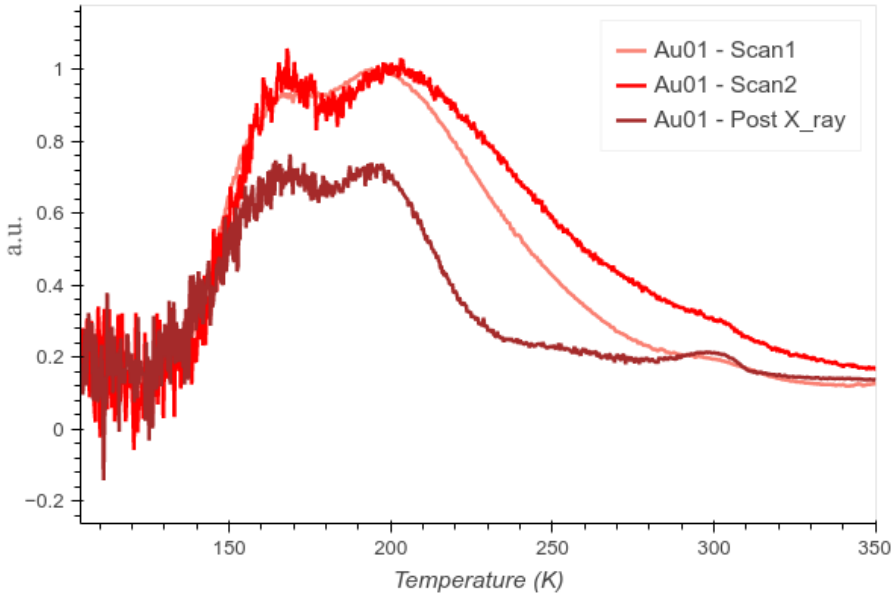

(a)

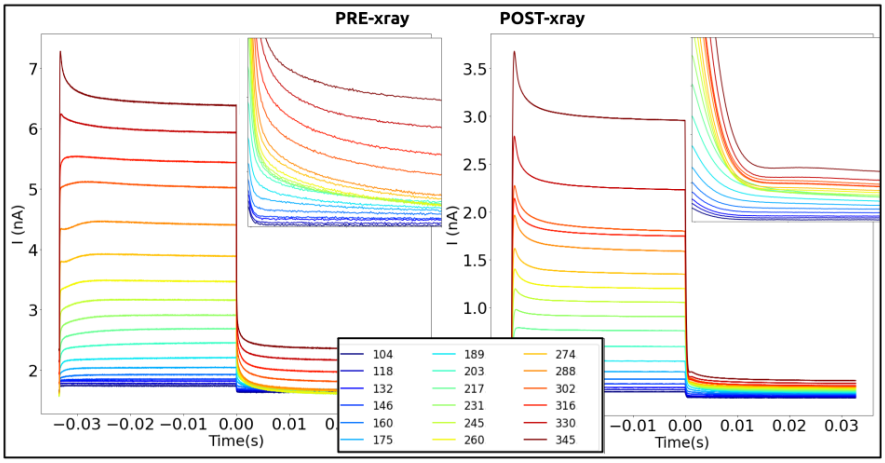

(b)

Figure 30: a): normalized relatives traps concentration. b): Collection of current transients as the temperature changes, compared before X-ray exposure and after X-ray exposure

to have a lower relative concentration of traps, confirming what has been seen previously. It is emphasized that the two techniques are independent. Another really interesting aspect has been reported in Figure 30 b). What we are observing is the comparison of the current transients of the Au01 sample at different temperatures, before and after X-ray exposure, therefore scan 2 and scan 3. As can be clearly seen, the rise velocity of the current has significantly increased in the sample subjected to radiation. Not only that, even the thermal emission has significantly decreased, especially at high temperatures, as can be seen from the trend of the transient.

7.3 AGING

Despite the excellent opto-electronic properties, 3D perovskites have the big problem of degrading within a few days or less, unless they are encapsulated and protected from the external environment. The problem seems to be the ionic diffusion inside the material that creates deep defective states. Also for this reason the 2D perovskites are attracting a lot of attention. It is known at a qualitative level that this family of perovskites is able to maintain its opto-electronic properties even after months and even if exposed to ionizing radiation. For the first time, it is possible to observe how deep states degrade according to the age of the material. The PICTS spectra of the three measurements, the maps and the Arrhenius plots of the traps are shown in Figure 31. The sample with chromium interdigitated contacts proved

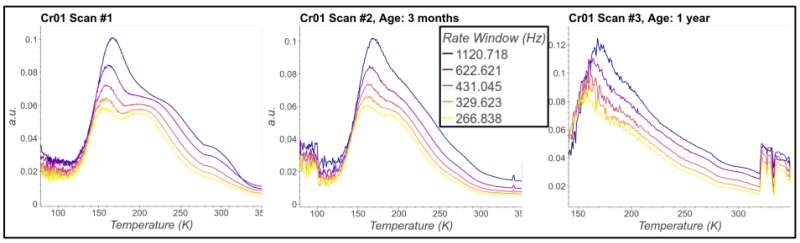

(a) Fig a)

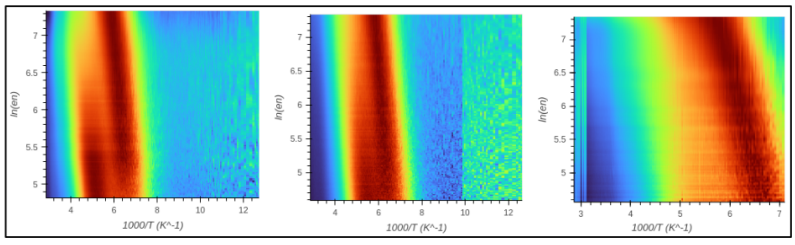

(b) Fig b)

Figure 31: a): PICTS spectra for Cr01 respectively on pristine sample, after three months and after one year. b): Corresponding maps respectively, from left to right, pristine sample, after three month and after one year.

more difficult to analyze. Although from the point of view of optical and electrical characteristics there are no substantial differences with the sample with interdigitated in gold and even the PICTS spectra are well superimposed, the processing of the data to obtain the Arrhenius plots did not allow the analysis of all the traps. Observing the spectra and the maps what we can say is that even after three months the sample has not suffered any signs of degradation due to environmental exposure. The scan made after a year is instead noisier and with patterns that do not seem to come from the sample itself but from a degradation of the interdigitated contacts over time. The sharp jump observed around 300K is not due to any physical process of the material. Repeating the measurements, it is thought that what is observed is due to the expansion and electrical interaction between the chromium contact and the gold wire, covered with a particular silver epoxy paste as a fixative, which has been degrading over time. Despite this, at low temperatures, albeit noisy, the PICTS spectrum is comparable with the other two. The Arrhenius plots is shown in Figure 32. The values of the extracted traps are only those of the T1 and T2 trap for scan 1, and only of the T1 trap for the other two (as you can see well from the maps). Traps T2 and T3 are also visible in the last two scans, but the data analysis does not allow the extraction of the physical values of the traps.

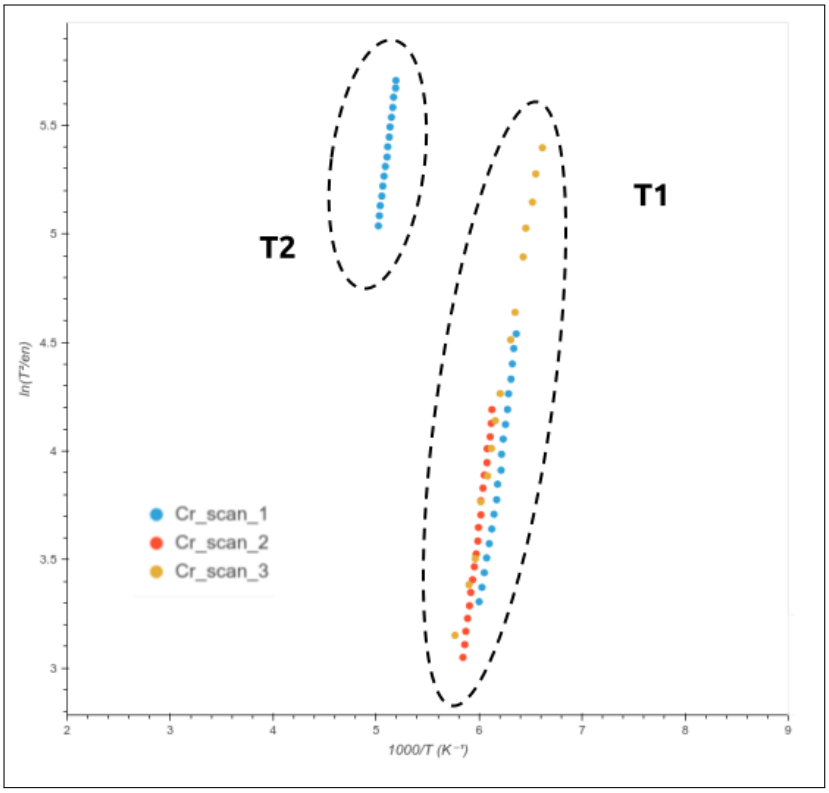

Figure 32: Arrhenius plot for the three scans. T1 traps are well superimposed in all three scans.

7.3.1 *Evolution of trap concentrations*

Let's see how trap concentrations change in one year. In Figure 33 the evolution of normalized relative traps concentrations is shown. While for the first two scans there are no particular differences, despite the fact that three months have passed between one measurement and another, in the case of the third scan there is an evident increase in concentrations, although these remain at internal of the same order of magnitude. This result is astounding, as it demonstrates a great robustness of the material with respect to environmental conditions and aging, obviously within the family of hybrid crystals. In this way what used to be an intuition, a qualitative estimate, now has numbers that validate the hypothesis. Unfortunately, the deterioration of the hypoxy paste used to contact the sample did not allow us to investigate further, as we could not calculate even quantitatively the trap concentrations one year later. As the paste deteriorated, it not only added a strong noise to the signal but also created a disturbance in the spectrum when the temperature reached room temperature, as can be seen from the image. This noise did not allow a sufficiently valid evaluation of the lifetime mobility value and thus a quantitative assessment of traps concentrations.

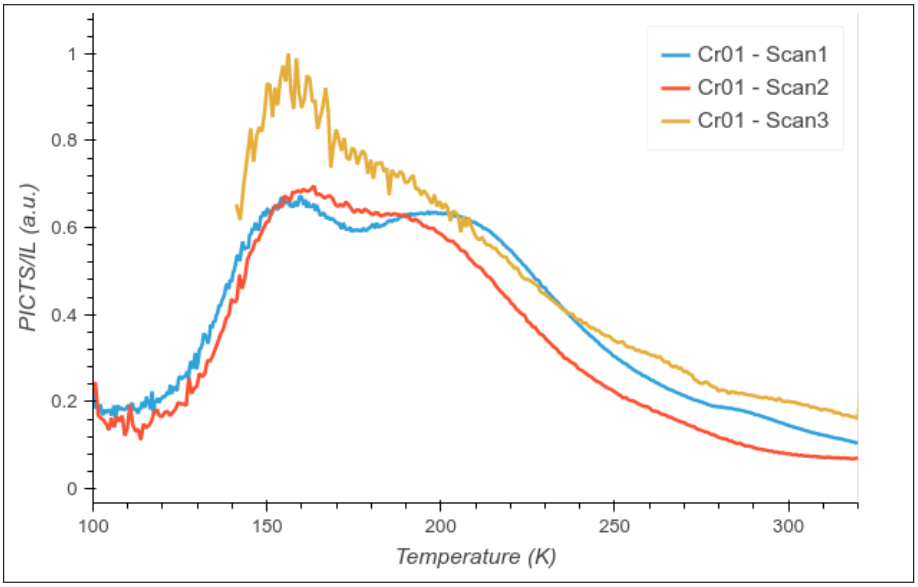

Figure 33: evolution of normalized relative traps concentrations with aging.

7.4 THE ROLE OF WATER

As described in Chapter 4, the synthesis of PEA_2PbBr_4, although the procedure does not have particular difficulties, is extremely slow and from the moment of preparation of the precursors in solution to the precipitation of the crystals, a period of time that is around three

weeks passes, but it can also be longer. The first syntheses took place during the summer and the synthesized crystals were excellent when compared with those obtained by the other research groups in literature [35]. With the change of season, however, the synthesis started to go wrong. The synthesis solution crystallized, but crystals were too small, thin and brittle to handle. Trying to put environmental variables under control and reviewing the entire synthesis process to avoid any errors made during the process, we realized that the variability in the morphological characteristics of the crystals was due to environmental humidity.During the summer, the relative ambient humidity in the synthesis laboratory reached values between 60% and 70%. During the winter, the relative humidity in the synthesis laboratory dropped to around 20%. The hypothesis was that, given the long synthesis period, the DMF solution absorbs a certain amount of water present in the environment and this water plays a fundamental role both in terms of nucleation of the crystals and in terms of the correct morphological structure.

To test our hypothesis, we calculated the absolute humidity present in the air in summer and winter. Assuming that in conditions of dynamic equilibrium, the concentration of water in the atmosphere coincides with the concentration of water in the DMF solution, the volume of water present in the solution in the summer period was 15 nL more for every 1 mL of solution. We therefore added the water in solution and the synthesis of the crystals is significantly improved. To go deeper into the role of water in PEA_2PbBr_4 crystalline defects, we prepared a solution in which we added about 150 nL of water, about ten times more than the theoretical value found. The crystals grew regularly. Two samples, called Au03 and Au04, was created, interdigitated gold contacts were evaporated and the values of the excitonic states, the band gap and the I-V characteristic were identical to the Au01 sample. Figure 34 a) shows the I-V as a function of the temperature for the sample Au04 in both dark and light and in b) the ion activation energy as a function of temperature. Also in this case an ionic activation energy around 1.3 eV was measured. In Figure 35 a) a comparison can be observed between the transients in the samples Au01 (dry from now on) and au04 (wet from now on). In Figure 35 b) the comparison between the PICTS spectra and maps is shown. It is clear that the main difference in the PICTS spectra turns out to be T3, while T1 is now not very visible and in the image it can only be seen as the left shoulder of T2. It is therefore natural to ask ourselves now what the role of water in the process of forming the defects that lead to those well-defined energy levels. Looking at the trend of transients at various temperatures, it can be observed that the characteristic times of rise and fall of the current have significantly increased, a sign of a greater concentration of traps. An interesting phenomenon can be

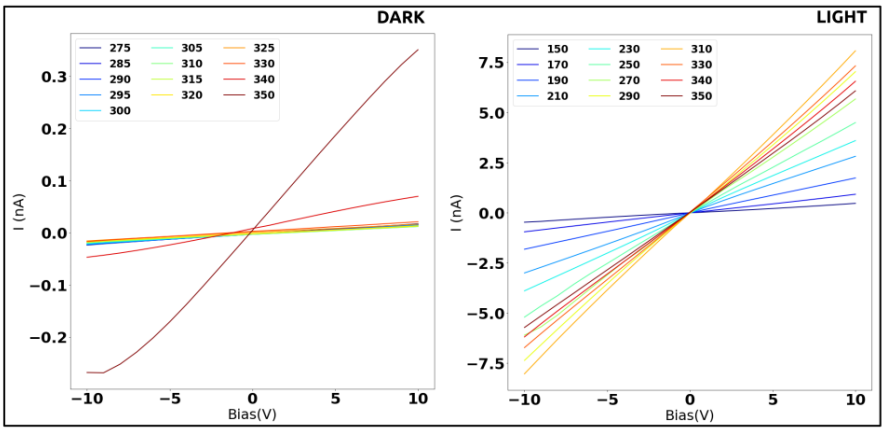

(a))

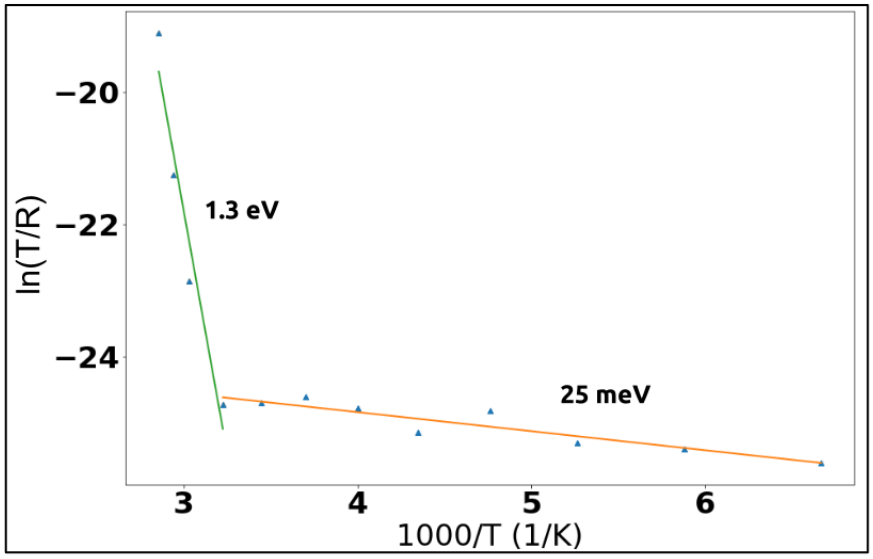

(b)

Figure 34: a): Trend of dark current and light current for different temperatures. b) Ion activation energy in the Au04 sample.

observed in Figure 35 c). Both traps present do not show a single linear trend. The thing is more evident with T3: it is clear that it can be divided into two energetic zones. This characteristic of change in energetic activation and capture cross section of the traps is a symptom of complex physical processes, difficult to argue with the data at our disposal. What we can say is that water does not introduce new defects but exacerbates those already present. This generates defects with complex dynamics, which are significantly affected by the variation in temperature. If we look at the Arrhenius plots of the traps in Figure 36, some important details can be observed. First, T1 and T2 traps in the WET and DRY samples clearly belong to the same crystalline defect. The graphs overlap very well. But the interesting fact can be seen by observing T3: in the WET sample it is possible to ob-

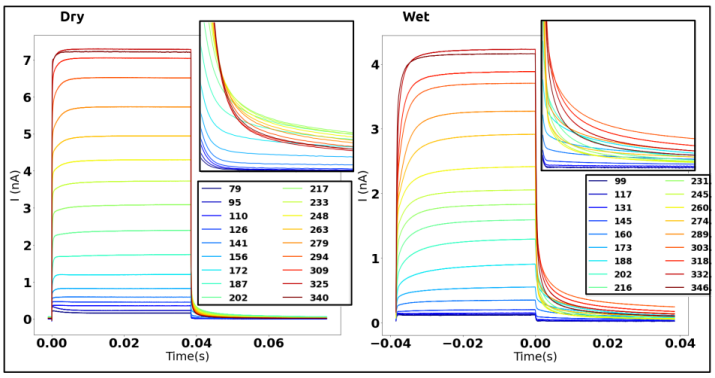

(a)

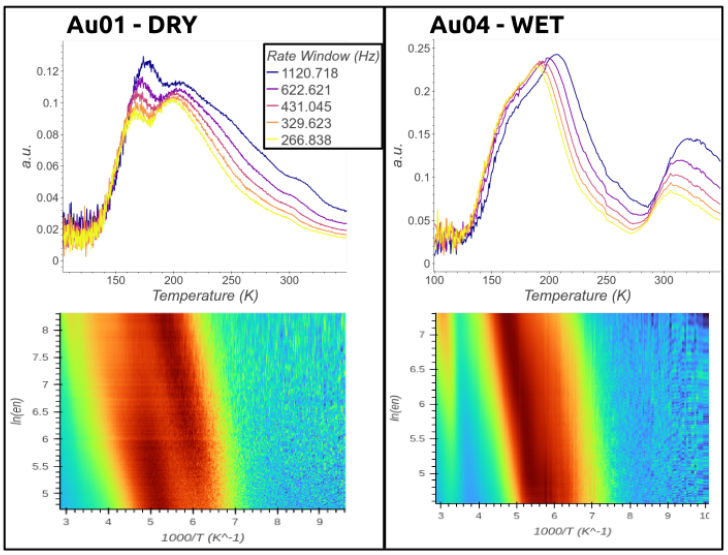

(b)

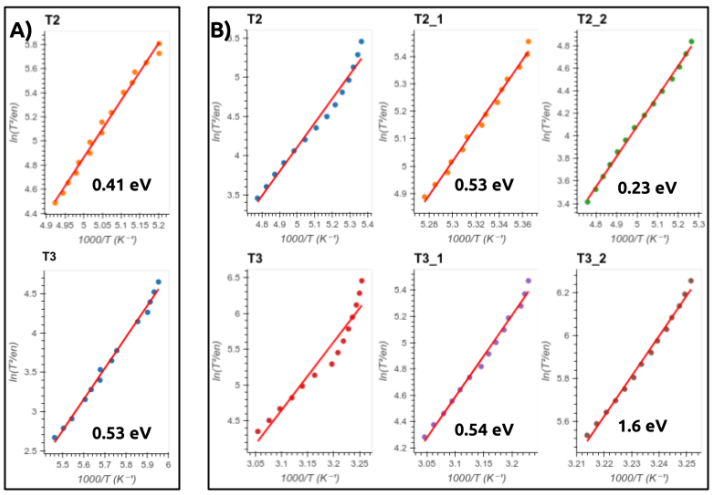

(c)

Figure 35: a): Comparison between current transients at different temperatures for the DRY sample (Au01) and the WET sample (Au04). b) Comparison between PICTS spectra and maps for DRY and WET samples. c): Comparison between the Arrhenius plots. Image A) shows the DRY sample, B) the WET sample. As can be seen, the traps in the WET sample have a segmented trend, where it is possible to clearly see a variation in the activation energy of the trap. To better show this trend, the T2 and T3 traps have been divided into sub-traps.

serve that the trap extends itself into both regions of thermal emission of the T3 trap in the DRY sample before and after being subjected to the X-ray. Similarly, the activation energy of T3 in the WET sample shifts from X-ray pre-exposure values to align with high-frequency post-exposure T3. In our opinion the water in the synthesis solution has highlighted the complexity of the T3 trap, which is modified by exposure to ionizing radiation. Although, therefore, T3 appears different before and after the X-ray bombardment, the trap actually belongs to the same crystalline defect.

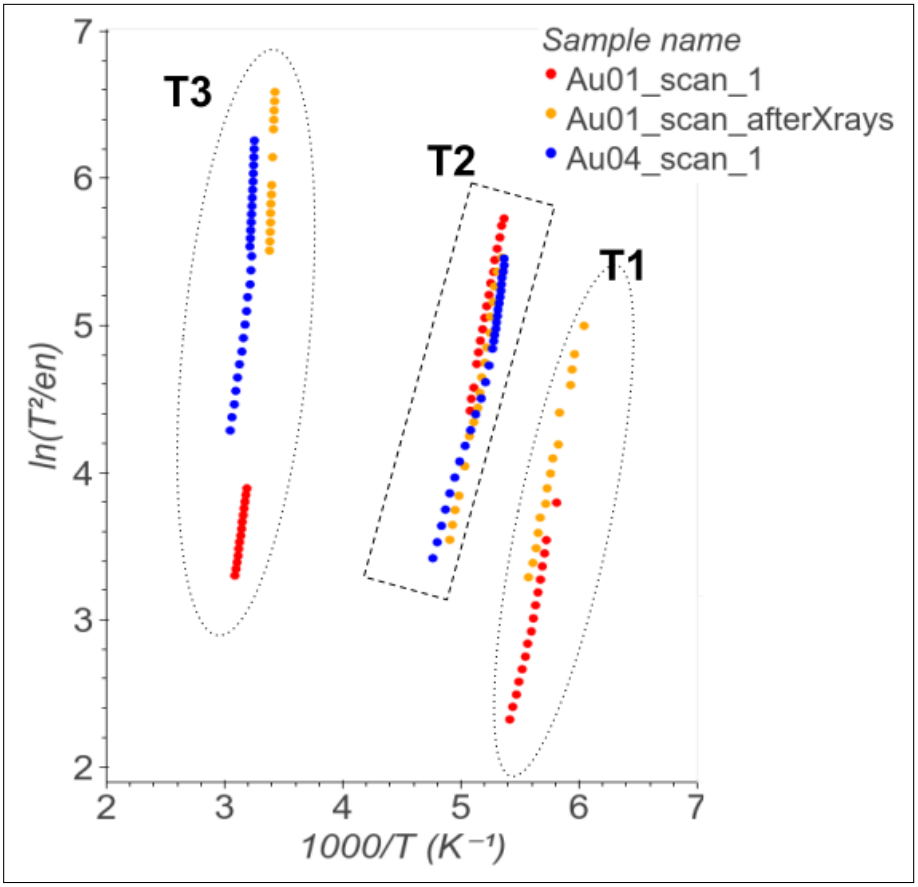

Figure 36: Comparison between Arrhenius plot for Au01 DRY sample (pre and post X-ray) and Au04 Wet sample.

7.4.1 *Evolution of trap concentrations*

Let's see now how the concentrations of traps change both in relative and in absolute values. As can be seen from the figure, it is evident that the introduction of water into the solution has increased the trap concentrations, as could already be guessed by observing the transients. But the increase is within the same order of magnitude. The relative concentrations of trap 2 of the waterless sample Au01 are approximately 40% lower than the Au04 sample, as shown in Figure 37 a). The trap that is most affected by the introduction of water is T3, which is about a factor three greater than the T3 of the DRY sample. The same trend can be observed when we calculate the absolute trap concentrations, as shown in Figure 37 b).

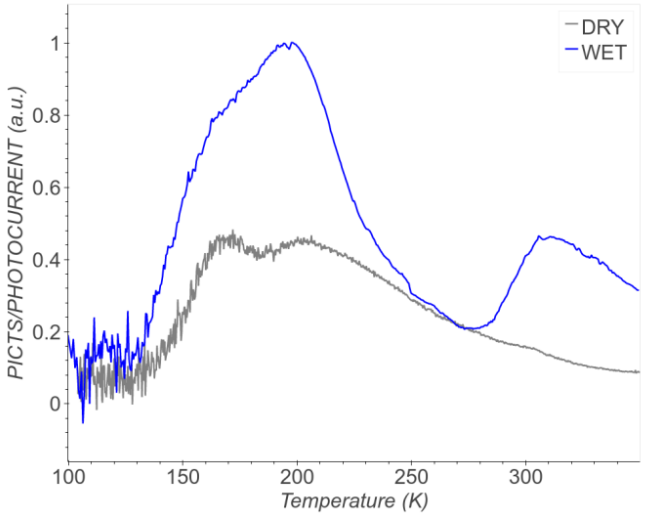

(a)

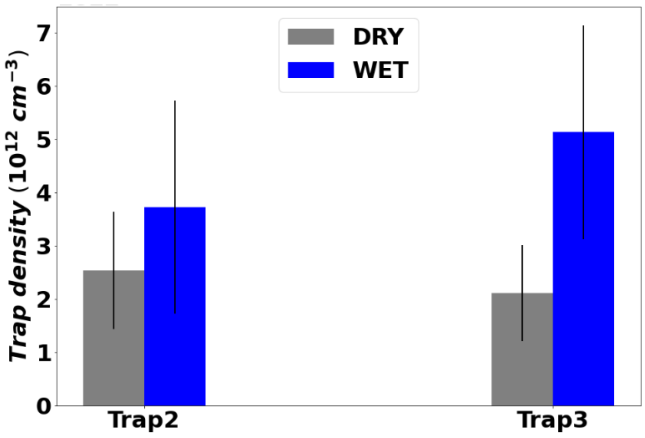

(b)

Figure 37: Trap concentrations compared between the DRY sample and the WET sample. a): normalized relative concentrations. b): Traps concentrations

7.5 WHAT HAPPENS OVER 300K?

A good observer will have been able to observe a pattern that, in one way or another, is repeated in one image after another, always at the same temperature range between 305K and 310K. Let's call this temperature Tc, for simplicity. By observing Figure 19 and Figure 34 it can be seen that the supposed ionic activation occurs precisely at this temperature Tc, which seems to coincide precisely with the maximums of the trap T3. That is the temperature at which the dark current passes from tens of picoampere to microampere within a few tens of kelvin. In Figure 38 we also compared the photocurrents obtained during the various scans. It is precisely at the temperature Tc that a very precise pattern of the photocurrent can be observed.

Although we have observed this curious phenomenon throughout the period of the thesis work, we have not been able to understand what the underlying physical phenomenon is. From the little literature present it seems excluded there is a phase transition. Going deeper into the literature, we see how other research groups have also observed something peculiar to Tc, despite not having paused to investigate the phenomenon more. An example is shown in Figure 39. In their paper, Xie et al. [53] show a detail of the photoluminescence of PEA_2PbBr_4, reported in Figure 39. What we observe is the temperature-dependent X-ray luminescence spectra from 10K and 350 K from undoped $(PEA)_2PbBr_4$ and $Li-(PEA)_2PbBr_4$ 1:1 doped

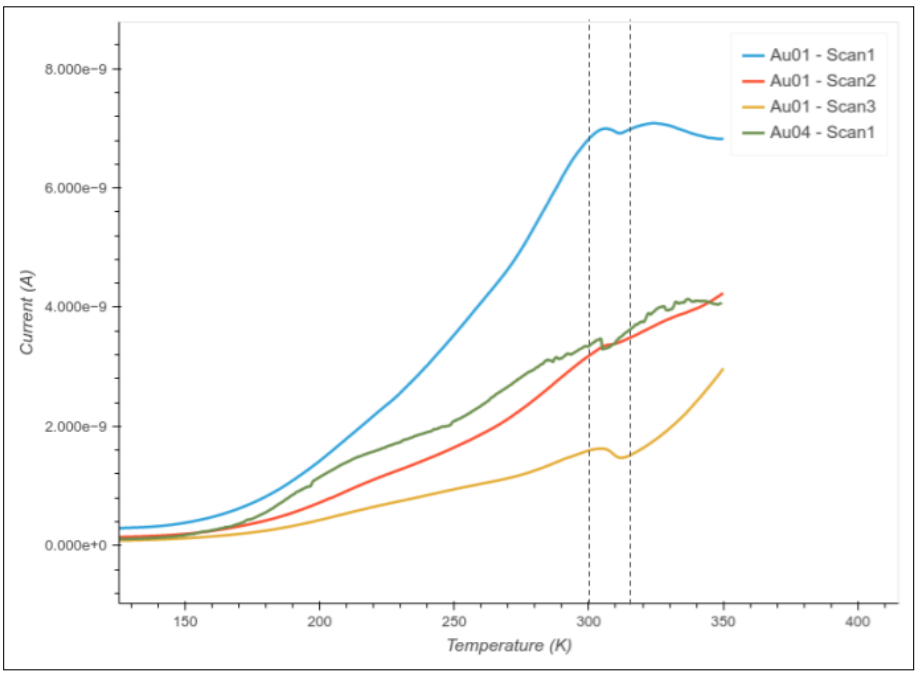

Figure 38: Photocurrent trend in PEA_2PbBr_4.

sample. The intensity of the luminescence abruptly increase up to 300 K, like our current measurements.

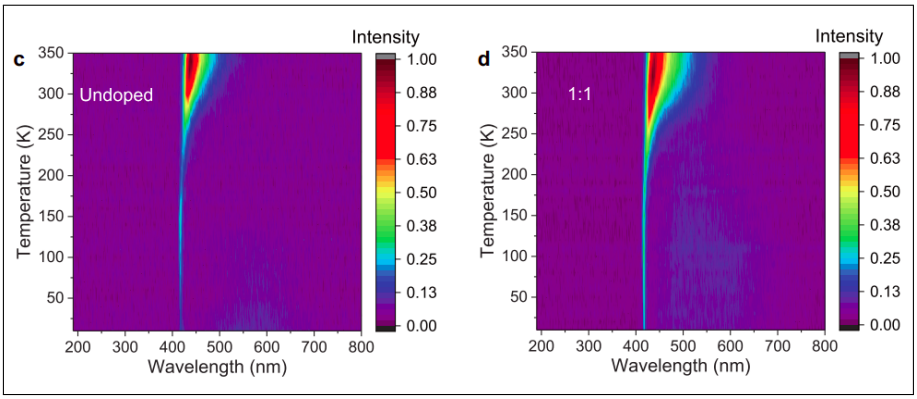

Figure 39: Xie et al. [53]: Temperature-dependent X-ray luminescence spectra from 10 and 350 K from c) undoped and d) 1:1 $Li-(PEA)_2PbBr_4$

7.6 ARE THERE ION MIGRATIONS IN 2D PEROVSKITES?

The DLTS technique has been widely used on 3D HOIPs [54] [55] [56]. $MAPbBr_3$ and $MAPbI_3$ were the most investigated hybrid perovskites. The values of the traps found by the various research teams were in disagreement in some cases. It appeared that there was an high variability according to the sample. The research teams independently led by Futscher and Reichert [45] [57] [58] showed the variability in the expected results and the nature of the traps measured by DLTS technique were due to ionic migration in the materials. Trap values are found to be affected by the stoichiometric starting conditions during the preparation of the synthesis solution. In another study, the presence of ions on the surface of 3D perovskites that diffuse inside the bulk were observed in situ, through SPM [59]. To date there is enough confidence in stating that in 3D perovskites ionic component condition charge transport properties and some of the deep states identified are due to ionic migration. Some studies have gone even deeper by showing how various components such as water, oxygen and nitrogen can passivate this process [60].

Regarding 2D perovskites, however, some studies show that there are no ionic migrations in the material, suppressed by the organic interlayer cations [26] [27]. In our work, by applying Nernst-Einstein equation, we saw an activation energy of about 1.3 / 1.4 Volt in samples with interdigitated gold contacts and in samples with lateral silver epoxy paste. This activation energy was not observed in samples with interdigitated chromium contacts. These results, shown in Figure 19, are in contrast to those found in the literature [44] [26]. We

must therefore try to give an interpretation to data found, taking into account that the presence of an activation energy, alone, is not evidence of ion migration. It is know that metal such as gold and silver can diffuse in semiconductors, and also in 3D HOIPs [49]. In samples with gold or silver contacts, once a certain critical temperature is exceeded, gold or silver ions can diffuse inside the sample, modifying the transport properties and the electrical conductivity. In the literature this process is described as irreversible. Alterations in electrical conductivity should no longer return to their initial values. What we observe in our samples is a completely reversible process, therefore it cannot be the same process.

Considering the Ohmic behavior of the metal-semiconductor junction in dark conditions, it is to be excluded that energy value we found is the energy barrier that charge carrier must overcome to pass from perovskite to metal and vice versa, because otherwise we would see a current pattern similar to that of a symmetrical Schottky barrier. The last hypothesis that remains, excluding any phase transition, even more exotic, which would seem to be excluded at that temperature, remains the kinetics of the gold ions during the evaporation process of the interdigitated contacts. Gold is a much heavier atom than chromium and much less reactive. It is thrown ballistically against the surface of the material and leave surface defects such as vacancies, with which it does not interact and which can be thermally activated. This could be an hypothesis, but further investigation are required. Another hypothesis could could be that the energetically activatable defects are already present on the surface of PEA_2PbBr_4 and chromium is able to passivate them. In the case of a sample with gold interdigitated contacts or without interdigitated contacts, the defects are present and undergo a certain thermal process which is activated around 300 K.

This hypothesis could be satisfactory as it is similar to what happens with 3D perovskites. The difference between the two materials is that in 3D HOIPs the ion activation processes are observed and ionic diffusions are measured, in $PEAPbBr_4$ we have not found any trace of ionic transport phenomena in addition to that presumed activation energy. The characteristic decay time of the current transient, the reproducibility of the I-V measurements made, the reproducibility of PICTS spectra, and the stability to radiation and deterioration due to external conditions and aging stability make the presence of ion migration unlikely. Another supporting clue is that the opto-electronic properties and defect energy activation of the samples with gold and chromium are practically identical, despite the fact that no activation energy is measured in the latter. Other evidence we have indicates that ion transport phenomena are negligible in 2D perovskites. When

a sample of a material with ionic transport is subjected to a bias, the ions diffuse along the induced electric field inside, then reaching an equilibrium phase where the ionic transport is interrupted. This phenomenon, observed in 3D, did not appear in our data. Consecutive scans of PICTS spectra with samples placed at potential differences of about ten volts for several hours, showed no appreciable difference in results. The behavior of the samples during the photocurrent measurements under an electrometer, with potential differences at the ends of the interdigitated contacts of the order of 350 Volt, did not give any trace of appreciable ionic currents. To conclude, therefore, there appear to be no ionic components from our data. The cause of the activation energy that we see in almost all samples, except those with interdigitated chromium contacts, is to be found in other phenomena that remain unexplained for the moment.

CONCLUSIONS

PEA_2PbBr_4 is an hybrid organic-inorganic perovskite (HOIPs) in which a molecular layer of inorganic conducting material alternate with organic layer of dielectric material. This structure, which self-assembles during synthesis by crystallization, makes the material in fact a multiple quantum well with very interesting opto-electronic properties. These class of compound are usually called 2D HOIPs. 2D HOIPs possess several interesting advantages as active layer in direct X-ray detection. The main goal of this work was the study of deep states in PEA_2PbBr_4, their energetic characterization, and the study of the evolution of defective states with aging or after exposure of the sample to high dose of X-ray. The study of deep levels by Photo-Induced Current Transient Spectroscopy revealed three clearly visible traps with reproducible results on a wide range of samples synthesized at different times. For simplicity, we call these traps T1, T2 and T3, respectively. The values turn out to be T1 = (0.32 ± 0.05) eV, T2 = (0.39 ± 0.5) eV and T3 = (0.57 ± 0.08) eV for pristine samples. For T2 and T3 it was possible to estimate the density of the traps, respectively $(3 \pm 1)10^{12}$ cm^{-3} and $(1.5 \pm 0.6)10^{12}$ cm^{-3}. These values, given the complexity of the evaluation of traps density in the PICTS technique, should be considered as indicative of the order of magnitude and are certainly a reliable lower limit. However, the PICTS technique requires stringent conditions for the evaluation of traps density, and systematic errors that could lead to an underestimation of the real value cannot be excluded, even if we are quite confident that the values found are indicative and true.

Radiation hardness was evaluated. A crystal with interdigitated gold contacts was first subjected to two successive PICTS scans, to evaluate the reproducibility of the measurements, and then was subjected to an X-ray bombardment for a total of 200 Gy. Traps T1 and T2 were shown to be stable even after X-ray bombardment, while trap T3 was found to have an activation energy of (2.2 ± 0.3) eV. Traps concentrations after the bombardment with X-ray have slightly reduced, while remaining in the same order of magnitude. It is an unexpected result that shows a great resistance to radiation from this material, and to be sure of the results, traps densities have been evaluated with two different and independents techniques. The evolution of the traps during the aging of the material was evaluated. Three different measurements were carried out, the first of which on the pristine crystal, the second after three months and the third after one year. The sample, during this period, was stored under normal environmental

conditions. Also in this case what can be seen is a good stability of the material to environmental conditions. The concentration of traps increases over time, but remains in the same order of magnitude even after a year.

During the work, we noticed that the synthesis in a humid environment (relative humidity around 70%) allowed us to grow good quality crystals, while a dry environment (relative humidity around 20%) made crystallization too fast and too small crystals grew to be handled. We then tried to investigate the role that water could play in the formation of deep states. Distilled water was added to the synthesis solution and several crystals were grown. The opto-electronic properties of the samples did not show particular differences except a lower dark current of at least an order of magnitude, unfortunately too close to the lower scale of our measuring instruments to have a certain estimate, but we can still say that this dark current did not exceed a few hundred of femto-ampere when at the ends of the crystal there was a bias of 10V. All three traps have increased in concentration. The concentration of T3 increased most of all, a value that would seem to be proportional to the amount of water added. This would suggest that T3 trap is closely linked to water molecules, although the underlying physical phenomena remain unknown for now.

This work could be seen as an important starting point for the investigation of defect states in PEA_2PbBr_4 by Photo-Induced Current Transient Spectroscopy. But many questions remain open and further investigations will be necessary. Given the particular geometry of the interdigitated contacts, it was impossible to discriminate whether the traps we were observing were electrons or holes traps. The experiments should be repeated with a "sandwich contacted" samples, in order to discriminate the charge carriers on the basis of the applied bias, positive or negative. However, the resistivity of the material is so high (about tens of T per centimeter) that it would be necessary to use a laser as a light source and apply a bias of several tens of volts across the crystal. This could bring the signal-to-noise ratio to less than optimal levels. From data we exhibited about radiation hardness, aging stability, PICTS measurement reproducibility and I-V reproducibility, what emerges is that no ionic migrations were detected in the material, or in any case their presence is negligible. Despite this, by applying the Nernst-Einstein relations, an activation energy of about 1.3 eV, at a temperature of just over 300 K was observed in all samples, except those with chromium interdigitated contacts. It is likely that this activation energy is not due to ionic activations, but to interactions between the surface of the 2D perovskite and the metal evaporated on top. More in-depth studies will be needed to unravel the nature of the observed activation energy.

BIBLIOGRAPHY

[1] Haotong Wei and Jinsong Huang. "Halide lead perovskites for ionizing radiation detection." In: *Nature Communications* 10.1 (2019). DOI: 10.1038/s41467-019-08981-w.

[2] Ferdinand Lédée, Andrea Ciavatti, Matteo Verdi, Laura Basiricò, and Beatrice Fraboni. "Ultra-Stable and Robust Response to X-Rays in 2D Layered Perovskite Micro-Crystalline Films Directly Deposited on Flexible Substrate." In: *Advanced Optical Materials* 10.1 (2021), p. 2101145. DOI: 10.1002/adom.202101145.

[3] Congcong Wang, Benjamin R Ecker, Haotong Wei, Jinsong Huang, and Yongli Gao. "Environmental surface stability of the MAPbBr3 single crystal." In: *The Journal of Physical Chemistry C* 122.6 (2018), pp. 3513–3522.

[4] Yvonne J Hofstetter, Inés García-Benito, Fabian Paulus, Simonetta Orlandi, Giulia Grancini, and Yana Vaynzof. "Vacuum-induced degradation of 2D perovskites." In: *Frontiers in chemistry* 8 (2020), p. 66.

[5] Paul Drude. "Zur elektronentheorie der metalle." In: *Annalen der Physik* 312.3 (1902), pp. 687–692.

[6] Arnold Sommerfeld. "Zur elektronentheorie der metalle auf grund der fermischen statistik." In: *Zeitschrift für Physik* 47.1 (1928), pp. 1–32.

[7] Carter W. Craig Balluffi Robert W Allen Samuel M. *Kinetics of Materials*. vol. 10.1002/0471749311. John Wiley & Sons, Inc., 2005 September 23. DOI: 1.1002/047174311.

[8] N. David Mermin Neil W.Ashcroft. *Solid state physics*. Holt, Rinehart and Winston.

[9] J. W. Orton P. Blood. *The Electrical Characterization of Semiconductors: Majority Carriers and Electron States*. Academic Pr., 1992. ISBN: 0125286279; 9780125286275.

[10] WTRW Shockley and WT Read Jr. "Statistics of the recombinations of holes and electrons." In: *Physical review* 87.5 (1952), p. 835.

[11] Re N Hall. "Electron-hole recombination in germanium." In: *Physical review* 87.2 (1952), p. 387.

[12] Thomas M. Brenner, David A. Egger, Leeor Kronik, Gary Hodes, and David Cahen. "Hybrid organic—inorganic perovskites: low-cost semiconductors with intriguing charge-transport properties." In: *Nature Reviews Materials* 1.1 (2016). DOI: 10.1038/natrevmats.2015.7.

[13] Dieter Weber. "CH3NH3PbX3, ein Pb (II)-system mit kubischer perowskitstruktur/CH3NH3PbX3, a Pb (II)-system with cubic perovskite structure." In: *Zeitschrift für Naturforschung B* 33.12 (1978), pp. 1443–1445.

[14] G. De perowskite Rose. "De novis quibusdam fossilibus quae in Montibus Uraliis inveniuntur." In: *Fossili Novo* (1839).

[15] Steven C. Tidrow. "Mapping Comparison of Goldschmidt's Tolerance Factor with Perovskite Structural Conditions." In: *Ferroelectrics* 470.1 (2014), pp. 13–27. DOI: 10.1080/00150193.2014.922372.

[16] W. Travis. "On the application of the tolerance factor to inorganic and hybrid halide perovskites: a revised system." In: *Chemical Science (2016), 7, 4548-4556, doi:10.1039/C5SC04845A* (2016).

[17] George Kakavelakis, Murali Gedda, Apostolis Panagiotopoulos, Emmanuel Kymakis, Thomas D. Anthopoulos, and Konstantinos Petridis. "Metal Halide Perovskites for High-Energy Radiation Detection." In: *Advanced Science* 7.22 (2020), p. 2002098. DOI: 10.1002/advs.202002098.

[18] Xingmo Zhang. "Growth and optimization of hybrid perovskite single crystals for optoelectronics/electronics and sensing." In: *Journal of Materials Chemistry C (2020), 8, 13918-13952, doi:10.1039/D0TC00473A* (2020).

[19] Joshua Maggiora, Feng Li, and Rongkun Zheng. "Charge Transport Properties of Methylammonium Lead Trihalide Hybrid Perovskite Bulk Single Crystals." In: *physica status solidi (RRL) – Rapid Research Letters* 15.1 (2020), p. 2000410. DOI: 10.1002/pssr.202000410.

[20] Bethan Charles, Jessica Dillon, Oliver J. Weber, M. Saiful Islam, and Mark T. Weller. "Understanding the stability of mixed A-cation lead iodide perovskites." In: *Journal of Materials Chemistry A* 5.43 (2017), pp. 22495–22499. DOI: 10.1039/c7ta08617b.

[21] Valerio Adinolfi, Wei Peng, Grant Walters, Osman M Bakr, and Edward H Sargent. "The electrical and optical properties of organometal halide perovskites relevant to optoelectronic performance." In: *Advanced Materials* 30.1 (2018), p. 1700764.

[22] Christie LC Ellis, Emily Smith, Hamza Javaid, Gabrielle Berns, and Dhandapani Venkataraman. "Ion migration in hybrid perovskites: Evolving understanding of a dynamic phenomenon." In: *Perovskite Photovoltaics* (2018), pp. 163–196.

[23] Weike Zhu, Shurong Wang, Xin Zhang, Aili Wang, Cheng Wu, and Feng Hao. "Ion Migration in Organic-Inorganic Hybrid Perovskite Solar Cells: Current Understanding and Perspectives." In: *Small* 18.15 (2022), p. 2105783.

[24] Constantinos C Stoumpos, Duyen H Cao, Daniel J Clark, Joshua Young, James M Rondinelli, Joon I Jang, Joseph T Hupp, and Mercouri G Kanatzidis. "Ruddlesden-Popper hybrid lead iodide perovskite 2D homologous semiconductors." In: *Chemistry of Materials* 28.8 (2016), pp. 2852–2867.

[25] Yani Chen, Yong Sun, Jiajun Peng, Junhui Tang, Kaibo Zheng, and Ziqi Liang. "2D Ruddlesden-Popper perovskites for optoelectronics." In: *Advanced Materials* 30.2 (2018), p. 1703487.

[26] Yanjun Fang Qi Wang Yehao Deng Yun Lin Yang Bai and Jinsong Huang. "Suppressed Ion Migration in Low-Dimensional Perovskites." In: *ACS Energy Lett. 2017.2:1571-1572* (2022).

[27] Lili Gao, Jiaxue You, and Shengzhong (Frank) Liu. "Superior photovoltaics/optoelectronics of two-dimensional halide perovskites." In: *Journal of Energy Chemistry* 57.Un (2021), pp. 69–82. DOI: 10.1016/j.jechem.2020.08.022.

[28] Xiao Han, Yongshen Zheng, Siqian Chai, Songhua Chen, and Jialiang Xu. "2D organic-inorganic hybrid perovskite materials for nonlinear optics." In: *Nanophotonics* 9.7 (2020), pp. 1787–1810.

[29] Himchan Cho, Young-Hoon Kim, Christoph Wolf, Hyeon-Dong Lee, and Tae-Woo Lee. "Improving the stability of metal halide perovskite materials and light-emitting diodes." In: *Advanced Materials* 30.42 (2018), p. 1704587.

[30] Hsinhan Tsai, Wanyi Nie, Jean-Christophe Blancon, Constantinos C Stoumpos, Reza Asadpour, Boris Harutyunyan, Amanda J Neukirch, Rafael Verduzco, Jared J Crochet, Sergei Tretiak, et al. "High-efficiency two-dimensional Ruddlesden–Popper perovskite solar cells." In: *Nature* 536.7616 (2016), pp. 312–316.

[31] Zhiyuan Xu Yixin Dong Xiaofei Ji Di Lu Guangwei Lv and Yongsheng Liu. "Thiophene-Based Two-Dimensional Dion–Jacobson Perovskite Solar Cells with over 15 % Efficiency." In: *J. Am. Chem. Soc. 2020.142:11114-11122* (2022). DOI: .org/10.1021/jacs.0c03363.

[32] Adam H Slavney, Rebecca W Smaha, Ian C Smith, Adam Jaffe, Daiki Umeyama, and Hemamala I Karunadasa. "Chemical approaches to addressing the instability and toxicity of lead–halide perovskite absorbers." In: *Inorganic chemistry* 56.1 (2017), pp. 46–55.

[33] Jian Qiu, Yingdong Xia, Yiting Zheng, Wei Hui, Hao Gu, Wenbo Yuan, Hui Yu, Lingfeng Chao, Tingting Niu, Yingguo Yang, et al. "2D intermediate suppression for efficient Ruddlesden–Popper (RP) phase lead-free perovskite solar cells." In: *ACS Energy Letters* 4.7 (2019), pp. 1513–1520.

[34] Laura Basiricò, Andrea Ciavatti, and Beatrice Fraboni. "Solution-Grown Organic and Perovskite X-Ray Detectors: A New Paradigm for the Direct Detection of Ionizing Radiation." In: *Advanced Materials Technologies* 6.1 (2020), p. 2000475. DOI: 10.1002/admt.202000475.

[35] Yunxia Zhang, Yucheng Liu, Zhuo Xu, Haochen Ye, Qingxian Li, Mingxin Hu, Zhou Yang, and Shengzhong Frank Liu. "Two-dimensional $(PEA)_2PbBr_4$ perovskite single crystals for a high performance UV-detector." In: *Journal of Materials Chemistry C* 7.6 (2019), pp. 1584–1591.

[36] M Ayoub, M Hage-Ali, JM Koebel, R Regal, C Rit, F Klotz, A Zumbiehli, and P Siffert. "Real defect concentration measurements of nuclear detector materials by the combination of PICTS and SCLC methods." In: *Materials Science and Engineering: B* 83.1-3 (2001), pp. 173–179.

[37] Xavier Mathew. "Photo-induced current transient spectroscopic study of the traps in CdTe." In: *Solar energy materials and solar cells* 76.3 (2003), pp. 225–242.

[38] CD Thurmond. "The standard thermodynamic functions for the formation of electrons and holes in Ge, Si, GaAs, and GaP." In: *Journal of the Electrochemical Society* 122.8 (1975), p. 1133.

[39] JA Van Vechten and CD Thurmond. "Entropy of ionization and temperature variation of ionization levels of defects in semiconductors." In: *Physical Review B* 14.8 (1976), p. 3539.

[40] LORENTZ ENGSTROM. "The regulation of liver pyruvate kinase by phosphorylation—dephosphorylation." In: *Current topics in cellular regulation* 13 (1978), pp. 29–51.

[41] M. Tapiero. "Photoinduced current transient spectroscopy in high-resistivity bulk materials: Instrumentation and methodology." In: *Journal of Applied Physics 1988.64:4006-4012* (1988). DOI: .org/10.1063/1.341361.

[42] JC Balland, JP Zielinger, M Tapiero, JG Gross, and C Noguet. "Investigation of deep levels in high-resistivity bulk materials by photo-induced current transient spectroscopy. II. Evaluation of various signal processing methods." In: *Journal of Physics D: Applied Physics* 19.1 (1986), p. 71.

[43] Osamu Yoshie and Mitsuo Kamihara. "Photo-induced current transient spectroscopy in high-resistivity bulk material. II. Influence of non-exponential transient on determination of deep trap parameters." In: *Japanese journal of applied physics* 22.4R (1983), p. 629.

[44] Xun Xiao, Jun Dai, Yanjun Fang, Jingjing Zhao, Xiaopeng Zheng, Shi Tang, Peter Neil Rudd, Xiao Cheng Zeng, and Jinsong Huang. "Suppressed ion migration along the in-plane direction in layered perovskites." In: *ACS Energy Letters* 3.3 (2018), pp. 684–688.

[45] Moritz H Futscher, Ju Min Lee, Lucie McGovern, Loreta A Muscarella, Tianyi Wang, Muhammad Irfan Haider, Azhar Fakharuddin, Lukas Schmidt-Mende, and Bruno Ehrler. "Quantification of ion migration in $CH_3NH_3PbI_3$ perovskite solar cells by transient capacitance measurements." In: *Materials Horizons* 6.7 (2019), pp. 1497–1503.

[46] Patrycja Makuła, Michał Pacia, and Wojciech Macyk. "How to correctly determine the band gap energy of modified semiconductor photocatalysts based on UV–Vis spectra." In: *The journal of physical chemistry letters* 9.23 (2018), pp. 6814–6817.

[47] Jiajun Luo, Shunran Li, Haodi Wu, Ying Zhou, Yang Li, Jing Liu, Jinghui Li, Kanghua Li, Fei Yi, Guangda Niu, et al. "Cs2AgInCl6 double perovskite single crystals: parity forbidden transitions and their application for sensitive and fast UV photodetectors." In: *Acs Photonics* 5.2 (2018), pp. 398–405.

[48] Giovanni Armaroli, Laura Ferlauto, Ferdinand Lédée, Matilde Lini, Andrea Ciavatti, Alessandro Kovtun, Francesco Borgatti, Gabriele Calabrese, Silvia Milita, Beatrice Fraboni, et al. "X-Ray-Induced Modification of the Photophysical Properties of MAPbBr3 Single Crystals." In: *ACS applied materials & interfaces* 13.49 (2021), pp. 58301–58308.

[49] Natalia N Shlenskaya, Nikolai A Belich, Michael Grätzel, Eugene A Goodilin, and Alexey B Tarasov. "Light-induced reactivity of gold and hybrid perovskite as a new possible degradation mechanism in perovskite solar cells." In: *Journal of Materials Chemistry A* 6.4 (2018), pp. 1780–1786.

[50] Jiaxing Song, Jingyu Qian, Leijing Liu, Dianwu Huang, Zaifang Li, Bin Xu, and Wenjing Tian. "Theoretical study on defect properties of two-dimensional multilayer Ruddlesden-Popper lead iodine perovskite." In: *Computational Materials Science* 194 (2021), p. 110457.

[51] A. Cavallini, B. Fraboni, W. Dusi, and et al. "Deep levels and compensation in -irradiated CdZnTe." In: *Appl. Phys. Lett. 2000.77:3212-3214* (2000). DOI: .org/10.1063/1.1324980.

[52] B Fraboni, A Gasparotto, F Priolo, and G Scamarcio. "High Fe2+/3+ trap concentration in heavily compensated implanted InP." In: *Applied Physics A* 73.1 (2001), pp. 35–38.

[53] Aozhen Xie et al. "Lithium-doped two-dimensional perovskite scintillator for wide-range radiation detection." In: *Communications Materials* 1.1 (2020). DOI: 10.1038/s43246-020-0038-x.

[54] Sung Heo. "Deep level trapped defect analysis in CH3NH3PbI3 perovskite solar cells by deep level transient spectroscopy." In: *Energy & Environmental Science (2017), 10, 1128-1133, doi:10.1039/C7EE00303J* (2017).

[55] Thi Kim Oanh Vu, Il-Wook Cho, Jaewon Oh, Dong Uk Lee, Mee-Yi Ryu, and Eun Kyu Kim. "Defect suppression and photoresponsivity enhancement in methylammonium lead halide perovskites by CdSe/ZnS quantum dots." In: *Journal of Colloid and Interface Science* 590 (2021), pp. 19–27. DOI: 10.1016/j.jcis.2021.01.037.

[56] K. Xue. "Defect Investigation in Perovskite Solar Cells by the Charge Based Deep Level Transient Spectroscopy (Q-DLTS)." In: *Advances in Engineering Research and Application, doi:10.1007/978-3-030-04792-428*. LNNS 63 (2019). Ed. by © Springer, Nature Switzerland, AG, H. Fujita, et al., 204–209.

[57] Sebastian Reichert, Qingzhi An, Young-Won Woo, Aron Walsh, Yana Vaynzof, and Carsten Deibel. "Probing the ionic defect landscape in halide perovskite solar cells." In: *Nature Communications* 11.1 (2020). DOI: 10.1038/s41467-020-19769-8.

[58] Sebastian Reichert, Jens Flemming, Qingzhi An, Yana Vaynzof, Jan-Frederik Pietschmann, and Carsten Deibel. "Improved evaluation of deep-level transient spectroscopy on perovskite solar cells reveals ionic defect distribution." In: *arXiv preprint arXiv:1910.04583* (2019).

[59] Collin Stecker, Kexi Liu, Jeremy Hieulle, Robin Ohmann, Zhenyu Liu, Luis K Ono, Guofeng Wang, and Yabing Qi. "Surface defect dynamics in organic-inorganic hybrid perovskites: from mechanism to interfacial properties." In: *ACS nano* 13.10 (2019), pp. 12127–12136.

[60] Roberto Brenes, Christopher Eames, Vladimir Bulović, M Saiful Islam, and Samuel D Stranks. "The impact of atmosphere on the local luminescence properties of metal halide perovskite grains." In: *Advanced Materials* 30.15 (2018), p. 1706208.